NANOPOROUS MEMBRANE BASED BIOSENSOR FOR CELL BEHAVIOUR STUDY VIA IMPEDANCE SPECTROSCOPY

YU JINJIANG

Ph.D

THE HONG KONG POLYTECHNIC UNIVERSITY

2011

The Hong Kong Polytechnic University

Department of Health Technology and Informatics

Nanoporous Membrane Based Biosensor For Cell Behaviour Study Via Impedance Spectroscopy

YU Jinjiang

A thesis submitted in partial fulfillment of the requirements for the degree of Doctor of Philosophy

March 2010

CERTIFICATE OF ORIGINALITY

I hereby declare that this thesis is my own work and that, to the best of my knowledge and belief, it reproduces no material previously published or written, nor material that has been accepted for the award of any other degree or diploma, except where due acknowledgement has been made in the text.

_____

YU Jinjiang

Abstract

A novel poly(ethylene glycol) (PEG) based microchip with nanoporous alumina membrane was developed for the study of human esophageal cancer cells (KYSE 30) *in vitro* behavior with impedance spectroscopy. Nanoporous alumina membrane was successfully fabricated by a two-step anodization technique while the nanopore size was controlled by applying different anodization voltages. The PEG hydrogel microwells were fabricated using photolithography on nanoporous alumina surface modified with a 3-(Trimethoxysilyl)propyl methacrylate (TPM) monolayer. During the photopolymerization reaction, and hydrogel microwell arrays were covalently bonded to the substrate via the TPM monolayer. In the surrounded areas of the microwells where PEG was UV polymerized, solid hydrogel was covalently bonded with silane-modified membrane and the PEG hydrogel covering layer prevented electrolyte flow through the portions underneath the membrane The surface modification effect was characterized by X-ray photoelectron spectroscopy (XPS), water contact angle and protein adsorption experiments to confirm the existence of PEG and silane. The diffusion studies for various biomolecules including bovine serum albumin (BSA), insulin and the anti-cancer drug molecule of cisplatin were carried out with the microfabricated membrane array using a mini-diffusion chamber. The diffusion properties of the nanoporous alumina membrane with nanopore size of 20nm and 100nm were studied by a UV-Vis spectrophotometer. The biocompatibility of nanoporous alumina membrane was demonstrated by using two types of cells, rat bone marrow derived mesenchymal stem cells (RMSCs) and human KYSE-30 esophageal squamous epithelial cancer cells. Then, human KYSE-30 esophageal squamous epithelial cancer cells were successfully

patterned within the PEG microwells and selective cell adherence on the TPM modified alumina surface inside the microwells was realized. Cell morphology changes due to cells adhesion, spreading, and proliferation were detected by nanoporous membrane based impedance spectroscopy in a real time and non-invasive way. The effects of various anti-cancer drugs of retinoic acid (RA), 5-Fluorouridine (5-FU) and Cisplatin (CDDP) were studied using this nanoporous membrane based cellular array with impedance spectroscopy. The initial concentration effects of 5-Fluorouridine (5-FU) on impedance spectra were also studied with concentrations of 0.1 mg/mL, 0.2mg/mL and 0.5mg/mL. Finally, biochemical control experiments for apoptosis enrichment factor detection under the effect of 5-FU with the concentration of 0.1mg/mL was studied at different treatment time points. The apoptosis enrichment factor results were also compared with impedance spectra and the correlation was found between them. This showed that this new nanoporous membrane based morphology-sensitive electrochemical system could be an effective and sensitive platform to indicate the degree of apoptosis.

Acknowledgements

I would like to express my deepest and most sincere gratitude to my supervisor, Dr. YANG Mo. His guidance and support from the first day to the final level enabled me to develop my understanding of research. His understanding, tolerance and encouragement have been of great value for me.

I warmly thank my co-supervisors Dr. ZHANG Ming, Dr. LEUNG Hang Mei Polly and Dr. SURYA Charles for their supervision and guidance, Dr. Johnny Cheuk from ABCT for providing us cancer cell and anti-cancer drug, Mr Man Nin YEUNG from MRC for the help in SEM, Mr. Chao Chen from AP for MEMS fabrication, and HTI postgraduate student office for their valuable help and assistance.

I wish to thank all the colleagues in our lab: Dr. LIU Qingjun, Dr. XU Baojian, Mr. Brian POW Yu Fung, Mr. LIU Zongbin, Mr. TAN Fei, Mr. YUM Kee Him, Miss. Qing Xueshan and all others.

Finally, I owe my loving thanks to my parents and my beloved wife Miss. XIAO Lidan for their continuous support. My wife has lost a lot because we are in two different cities. Without her encouragement and understanding it would have been impossible for me to finish my PhD work.

YU Jinjiang

Table of Contents

List of Figures

Chapter 1 Introduction

1.1 Nanomaterials for Biological Application

Nanoscience and nanotechnology got started in the early 1980s and have changed our daily life as well as the research work in the past decades. Recent studies within the research fields involve a wide range from fundamental sciences (such as physics, chemistry and biology) to applied sciences (such as applications in life science and biomedical engineering) at the nanometer size scale ($1nm=10^{-9}m$). The nano-scale is particularly important and relevant in biological and biomedical applications. As shown in Fig 1.1.1, the diameters of some large bio-molecules such as DNA molecules, antibodies and many other proteins fall into 1~100 nm range. And the dimensions of virus and bacteria (known as smallest prokaryotic cells) are around 100~1000 nm, while the sizes of most sub-cellular compartments such as nucleus, actin filaments within eukaryotic cells are within 1~1000 nm range (Bauer, Birenbaum et al. 2004). In the past twenty years, numerous different types of nano-structured materials were employed for biological applications, such as nanoparticles, carbon nanotubes, nanowires and nanoporous membranes. These common types of nanomaterials were discussed briefly below.

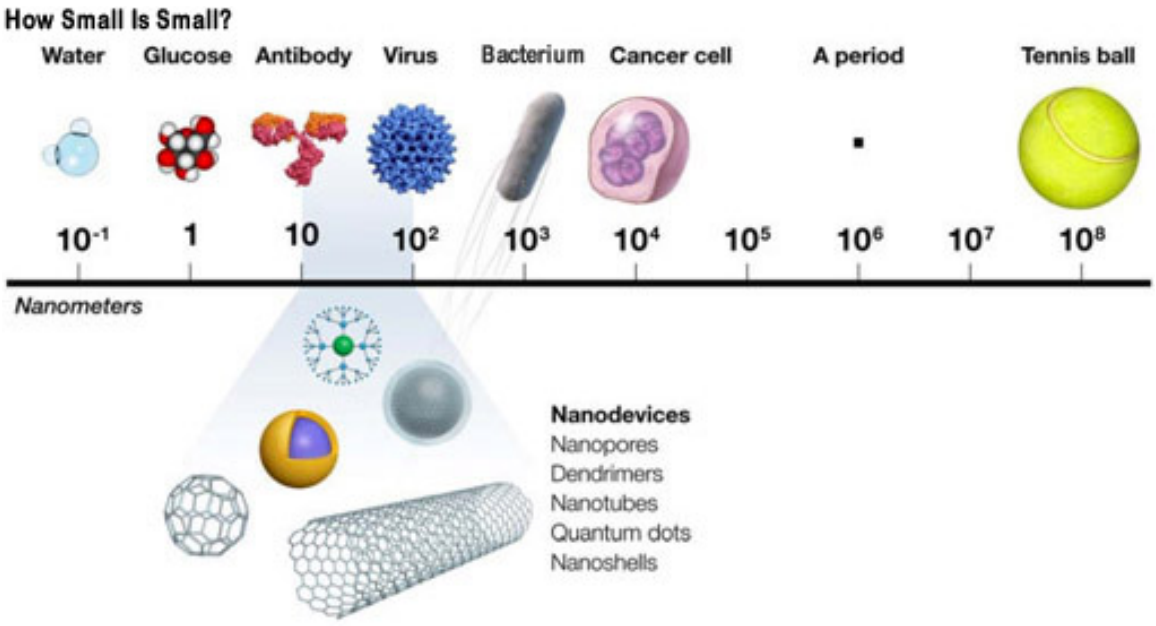

Fig 1.1.1 How small is small?

(http://publications.nigms.nih.gov/chemhealth/cool.htm)

Nanoparticles are studied due to their size-dependent material properties, mainly for physical and chemical properties (Murray, Kagan et al. 2000). Optical properties and magnetic effects are also currently studied as important factors and they have several advantages for applications in biological science (Liu 2006). Some nanoparticles, such as semiconductor nanocrystals, can be utilized as fluorescent probes in biological staining, direct immune-labeling, in situ hybridization, cytometry and diagnostics, because they have a narrow, tunable, symmetric emission spectrum, which are photochemically stable. These optical features can make them superior to existing fluorophores in some cases (Alivisatos 1999). The magnetic nanoparticles-based drug and gene delivery are proposed in the late 1970s by Widder, Senyi and colleagues and there are even some clinical trials with promising results in recent years. Nanoparticles

have potential to be effective tools for treatment of a variety of diseases (McBain, Yiu et al. 2008) .

Carbon nanotubes (CNTs) are well-ordered, all-carbon hollow graphitic nanomaterials with a very high length-to-diameter ratio. In the past years, it has been very hot to conduct research on CNTs and apply them in various scientific areas. The large surface area, high mechanical strength but ultra-light weight, rich electronic properties, and excellent chemical and thermal stability make them the good candidates for biological and biomedical applications since their discovery in 1991 (Baughman, Cui et al. 1999; Yang, Thordarson et al. 2007). Different methods have made it possible to solubilize and disperse CNTs in water or organic solvents by chemical modification and functionalization of their surfaces. The methods help researchers to manipulate and process them in physiological and biological environments (Liu, Zhao et al. 2006). After surface modification, some biomolecules such as proteins, carbohydrates and DNA, RNA molecules can be conjugated with CNTs and play an important role in the potential applications (Cui 2007). These conjugation and integration of biomolecules enable the hybrid systems to become electrochemical biosensors such as enzyme electrodes, immunosensors or DNA sensors etc (Wang 2005). CNTs are also excellent substrates for cellular attachment and growth, and they also affect cell behavior, cell differentiation and induce cellular functions by adsorbing more proteins. The properties recommend CNTs to be a candidate for scaffold material in tissue engineering (Miyawaki, Yudasaka et al. 2008; Usui, Aoki et al. 2008; Li, Gao et al. 2009).

Undoubtedly, CNTs are being considered to be a good substrate for the growth of cells, and also a possible candidate for many biomedical applications. But their toxic effects have become a strong concern for the environment and for human health. Toxicological impacts of nanotubes on a biological system should be studied more carefully. The needle-like fibre shape of CNTs has been compared to asbestos, so CNTs may lead to lung cancer, which are easily caused by exposure to asbestos. These dangerous factors restrict the use and development of CNTs in biomedical field.

While silicon nanowire is the most commonly used one, there are also some other nanowires such as gold nanowires, nickel nanowires, gold-platinum or gold-nickel nanowires. Most of them can be used for biological applications (Reich, Tanase et al. 2003). Semiconductor nanowires exhibit a conductivity change in response to variations of the electric field or potential on the surface, which could be used as field-effect transistors (FETs). The potential applications in biological science include highly sensitive biosensors, tools for drug discovery, detection of DNA & RNA enzymatic processes, multiplexed real-time, label-free detection of proteins, and even detection of single virus (Patolsky, Zheng et al. 2006). The fabrication and production processes of nanowires have attracted much interest by using bottom-up or top-down approaches, which both have their own advantages and shortcomings. For template-assisted fabrication of nanowires, nanoporous materials are very widely used in recent studies.

Among the different types of nanomaterials used for biological applications, nanoporous materials are of scientific and technological importance because of their unique surface,

structural, and bulk properties. They are used in various fields such as ion exchange, catalysis, sensor, biological molecular separation, isolation and purifications etc.

1.2 Nanoporous Materials for Biological Applications

Nanoporous structure material is a kind of porous materials, which usually has pore diameters between 1~500 nm, and have high porosities at nano scale. They are very attractive for many biological applications. The advantages of porous materials and the functionality of the material itself can be combined together, and the physical-chemical-biological properties can be enhanced or inhibited by the nanometer-size porous structure.

The very high surface area to volume ratio is probably the most important property of nanoporous materials. The increased pore surface is able to interact either with adsorbents, with particles embedded into the pores or the flow passing through the materials. The control on pore size, morphology and specific distribution enables enhanced absorption, and ultimately leads to substantial improvements on functional applications such as catalysis, membranes, electrodes, chromatography, separation, and sensing element.

Nanoporous materials can be classified on the basis of their material constituents or their properties. Table 1 shows the available nanoporous materials according to the chemical compositions and technical characteristics. For pore size, following the International

Union of Pure and Applied Chemistry (IUPAC) classification, mesopores are those with 2 to 50 nm in diameter and macropores are pores with 50 to 100 nm in diameter.

Table 1.2.1 Classification of nanoporous materials

	Polymeric	Carbon	Glass	Alumino-silicate	Oxides	Metal
Pore Size	Meso-macro	Micro-meso	Meso-macro	Micro-meso	Micro-meso	Meso-macro
Surface Area/Porosity	Low >0.6	High 0.3-0.6	Low 0.3-0.6	High 0.3-0.7	Medium 0.3-0.6	Low 0.1-0.7
Permeability	Low-Medium	Low-medium	High	Low	Low-medium	High
Strength	Medium	Low	Strong	Weak	Weak-medium	Strong
Thermal stability	Low	High	Good	Medium-high	Medium-High	High
Chemical stability	Low-Medium	High	High	High	Very high	High
Costs	Low	High	High	Low-medium	Medium	Medium
Life	Short	Long	Long	Medium-long	Long	Long

The topography of nanoporous surfaces and the spatial distribution of different functional groups on or inside nanoporous materials can be used to control proteins, cells, and tissue interactions, and also for separation of biological samples. Different applications of nanoporous materials are discussed below.

Separation and sorting of biomolecules are very useful for isolation and purification in many fields including pharmaceutical industry, food industry and biotechnology. Biomolecular separation in nanopores was recently explored for various applications. The nanoporous membrane can act as a scaffold for cells, and as a blood filter that retains serum proteins and allows smaller waste substances out (Fissell, Humes et al. 2007). And also, the nanoporous materials can be used to externally regulate the flow volume and speed through them.

Biosensing device, which combines biological components with physiochemical detection components, is used to detect analytes in biological samples. Nanoporous materials can be used as biosensing devices. The materials immobilize enzymes or antibodies on them for further detection and determination. For example, TiO_2 and ZnO nanoporous thin films are shown to be capable of sensing blood glucose and cholesterol (Li, Luo et al. 2001； Singh, Arya et al. 2007).

Single-molecular analysis is very important for probing biomacromolecules such as DNA, RNA and proteins one by one. When biomolecules are drawn through nanopores embedded in insulating nanoporous materials, it is possible to access information on the concentration, structure, size and sequence of them, by measuring the frequency, magnitude and duration of blockage in ion-current of electrolyte. Individual molecules of single- and double-stranded DNA or RNA can be detected by this new method (Akeson, Branton et al. 1999). The nanopore size, pore surface chemistry, nanoporous topography could be controlled in nano-scale during fabrication process of many materials. It makes possible to regulate analyte - surface interactions and it has the

potential to support the engineered pores for single-molecule detection and analysis (Bayley and Cremer 2001).

Immunoisolation needs encapsulation of implanted cells or drug release system and protects the cells from immune reaction. Small molecules such as oxygen, glucose and insulin can pass the small pores of nanoporous semipermeable membrane, but the passage of much larger immune system molecules such as immunoglobulin can be impeded by the nanopores. For example, nanoporous silicon membrane interfaces were explored to treat diabetes in implantable artificial pancreas (Tsujino, Ako et al. 2007).

Controlled drug delivery is very important for drug release in a chosen way for more effective therapy and to eliminate the possibility of improper dosing. The nanopore size, porosity, permeance, depth and thickness can be well-controlled for many nanoporous materials, especially nanoporous membranes. It provides a promising method for making capsules that may be used for giving controlled release of pharmacologic agents.

Among the different nanoporous materials used in biological applications, nanoporous alumina membranes have attracted lots of interest and effort due to its excellent biocompatibility and well established fabrication process, which makes it a good candidate in many research fields.

1.3 Nanoporous Alumina Membranes

Among the nanoporous materials which are widely used in biological science and other research fields, nanoporous alumina membrane, also known as anodic aluminum oxide (AAO), has raised a great attention due to its excellent biocompatibility and well established fabrication process. Nanoporous alumina membranes can be used as template material for fabrication of other nano-devices such as nanowires and nanofibers, detection and sensing of various biological species, applications in tissue engineering and artificial membrane formation, and also for micro- and ultra- filtration of small biological molecules.

1.3.1 Template for Fabrication of Nanowires

Due to the simple two-step anodization process, controlled pore size and uniform pore distribution, nanoporous alumina membranes are widely used as templates to fabricate nanowires. There is a lot of research for the fabrication of magnetic nanowires that are comprised of different metals or alloy by electro-deposition into nanoporous alumina membranes (Sharma, Pishko et al. 2007).

Whitney has reported fabrication of nickel and cobalt nanowire by electrochemical deposition into nanoporous alumina membrane template, and the system displayed distinctive characteristics because of their one-dimensional structure. Paulus filled nanoporous alumina membranes with different metals by an AC electro-plating procedure at a voltage of 16 V, and controlled the length of nanowires by controlling the

plating time. They successfully produced a series of ferromagnetic nanowires with different length, made of Fe, No or Co (Paulus, Luis et al. 2001). By using similar electrodeposition technology, Fodor fabricated $Co_{1-x}Fe_x$ alloy nanowires with 40 nm diameters and x=0-1.0 and the nanowires showed a highly anisotropic magnetization with the easy axis along the length of the wire (Fodor, Tsoi et al. 2002). Other research efforts include the nanowires fabricated by nanoporous alumina membranes on substrates for device applications and the detailed electrodeposition behaviors of metals on the templates (Wu, Leu et al. 2005; Chong, Zheng et al. 2006).

1.3.2 Detection and Sensing of Biological Species

Nanoporous alumina membranes can be fabricated with a regularly arranged hexagonal pattern of nanopores with controlled diameters. Such nanoporous oxide membranes have high surface area densities and allow binding relatively large amounts of target molecules on each spot of the surface. Especially, when using in fluorescence detection, the nanoporous oxide membranes can afford a substantial increase in the fluorescence signal intensity. Thus it can be used as a convenient substrate detection and sensing application for biological species, such as protein, DNA or RNA, by using fluorescence technology, immune-labeling, or other techniques.

Smirnov demonstrated the application nanoporous alumina membranes as substrates for fluorescence detection of labeled biomolecules (Takmakov, Vlassiouk et al. 2006). They fabricated 450-nm-deep, 60-nm diameter membranes, used biotin covalently bound to the surface to detect streptavidin modified with Alexa Flour 488 dye, which gave out

fluorescent signal. The fluorescence intensity in nanoporous alumina membranes increased by a factor of 5 compared to flat aluminum and enhancement as high as 7 times is observed compared to flat glass surface. The membranes offered significant advantages such as convenient preparation, increased density of binding sites, enhanced amounts of target molecules, and improved collection efficiency of fluorescence (Takmakov, Vlassiouk et al. 2006).

Pan et al. reported the detection approach of DNA (DeoxyriboNucleic Acid) oligonucleotides based on reflection from functionalized nanoporous alumina membranes (Pan and Rothberg 2003). The large surface area in nanoporous materials allowed for a substantial change in refractive index after binding of analyte molecules, enabling relatively high sensitivity to be achieved to detect DNA oligonucleotides. They functionalized the surfaces of the approximately 40 nm diameter membranes with alkanoic acid to spontaneously adsorb proteins from solution onto aluminum oxide. 2 nmol/cm^2 of complementary DNA could be sensed as a 3.4 nm shift in a spectral minimum. This technique could obtain sub-picomole sensitivity straightforwardly with 0.1 mm probe spots. But rinsing and drying are required for the measurement so the binding kinetics could not be real time monitoring (Pan and Rothberg 2003).

1.3.3 Tissue Engineering

Due to its excellent biocompatibility, nanoporous alumina membrane is a good scaffold for cell culture. Pure alumina has already been used as s substrate for tissue constructs due to its chemical and mechanical properties. For nanoporous alumina membrane,

tissue culture and co-culture of cells on the surface also have been investigated. It is known that the surface chemistry including surface topography is one of the important factors to influence the cellular response. The impact of the nanoscale pores on cell response is an important issue which can be investigated by evaluating cell adhesion, cell growth, morphology changes, and extracellular matrix production via different methods. Alumina surfaces incorporated with nanoscale porous features show high biocompatibility. Moreover, the cell response can be improved with nanoscale architecture.

Tejal's research group in Boston University studied osteoblast cells response on nanoporous alumina membranes. A two-step anodization process was optimized for the fabrication of nanoporous alumina membranes with uniform pore dimension and distribution (Swan, Popat et al. 2005). The impact of the nanoscale pores on osteoblast response was studied by evaluating cell adhesion, morphology, and matrix production via different methods. The advantages of using alumina with proved biocompatibility and incorporated nanoporous features for improvement of cell response were demonstrated in their research (Swan, Popat et al. 2005).

Tejal's research group also compared the long term osteoblast cell response to the nanoporous alumina membranes surface with those cultured on amorphous membranes, Anopore^{TM}, glass, latex and aluminum. Cell adhesion was first investigated by counting the trypsinized cells 1 day and 4 days after seeding on different surfaces. The total protein content of the viable cells cultured for 4 weeks was used to determine the amount of protein adsorbed on various surfaces after cell lysis. The cells cultured on the

nanoporous alumina membranes showed higher protein content. Results also indicated osteoblast cells adherent on the nanoporous alumina membranes produced more extracellular matrix protein compared to cells adhered on other surfaces (Popat, Swan et al. 2005). Nanoporous alumina surfaces could also be modified by physically adsorbing vitronectin and covalently immobilizing RGDC peptide to enhance adhesion of osteoblasts (Swan, Popat et al. 2005).

Moreover, the cellular response of adhesive cells can be regulated by modification of the surface chemistry of the substrate. Substrate surface modification with polymer, proteins or peptide could influence cell adhesion and growth on the substrate. Methods of surface modification include physical adsorption, chemical conjugation, mechanical methods, covalent attachment, and biological methods.

1.3.4 Support of Lipid Membrane

A lipid bilayer is an artificial membrane composed of lipid molecules (usually phospholipids). It is an essential component of all biological membranes, including mammalian cell membranes. And it is important for the permeability properties of cell membranes. The functional coupling of lipid bilayer with inorganic solids has become a very attractive topic in the past twenty years (Sackmann 1996). Many labs are focusing on fabricating artificial lipid membrane structures attached to a solid surface to allow for the functional insertion of trans-membrane peptides, measurement and detection of transport activity, which is a prerequisite for biosensor devices (Romer and Steinem 2004).

Steinem reported the application of using nanoporous alumina membrane as support substrates for lipid bilayer to make artificial membrane (Steinem, Janshoff et al. 1996). The nanoporous alumina membranes with different pore diameters were produced by an anodization process. One side of the porous material was covered with a thin gold layer followed by chemisorption of a hydrophobic thiol compound, which was a prerequisite for the formation of suspending membranes with the name of nano-black lipid membranes (nano-BLMs). The bilayer formation process and long-term mechanical stability of the nano-BLMs were tested by electrical impedance spectroscopy. The membrane exhibited high membrane resistances which were suited for single-channel recordings. Gramicidin and alamethicin were successfully inserted into the artificial membranes to demonstrate the functionality of the nano-BLMs (Steinem, Janshoff et al. 1996).

1.3.5 Filter for Biomolecules

Due to the high pore density, fairly well-defined nanopore distribution, and high mechanical strength, nanoporous alumina membrane is popular in membrane filtration and ultrafiltration for biotechnology applications such as detection, separation, diffusion, DNA extraction and purification.

It is possible to combine detection and separation/purification for unmodified target ss-DNA (and RNA) together by using nanoporous alumina membrane as an affinity filter. Vlassiouk demonstrated nanoporous alumina membrane filters modified with DNA for

"label-free" detection and separation/purification of the target ss-DNA. The filter was very promising for development of various ss-DNA (or RNA) detection methods because of the high surface density of DNA, high efficiency of hybridization, and increased effective surface area (Vlassiouk, Krasnoslobodtsev et al. 2004).

After surface modification, nanoporous alumina membranes could be combined with other organic membranes such as polymer monolayers to increase the efficiency of preventing nonspecific protein adsorption. This can finally result in filtration or separation of biological molecules. In Sang's research group, poly(ethylene glycol) (PEG) monolayers were grafted to nanoporous alumina membranes using covalent silane grafting or physical adsorption methods to form hybrid organic-inorganic membranes. The effect of PEG modification on the gas, liquid and protein permeabilities of the membranes were demonstrated. It suggested that hybrid membrane could provide significantly improved functional behavior over existing organic or inorganic membranes (Lee, Shang et al. 2005).

1.4. Electrochemical Impedance Spectroscopy (EIS) for Biosensing

Electrical impedance is the measurement of the material opposition to the flow of electric current, and it is the ratio between alternating voltage and alternating current, described by Ohm's law. Impedance includes both resistance and reactance. The resistance component arises from collisions of the current-carrying charged particles with the internal structure of the conductor. The reactance component is an additional

opposition to the movement of electric charge that arises from the changing magnetic and electric fields in circuits carrying alternating current.

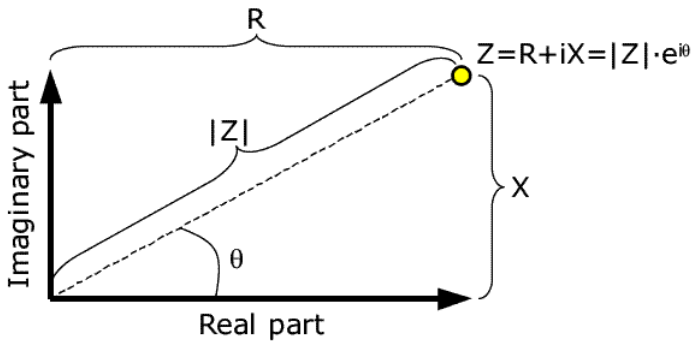

Fig 1.4.1 Plot of the electrical impedance Z

Impedance, Z (Ohm) is a complex measure of the resistance, R (Ohm), and reactance, X (Ohm), as shown in Fig 1.4.1. It contains two parts and can be expressed in the complex impedance plane according to: $\boldsymbol{Z = R + jX}$, where the real part of impedance is the resistance R and the imaginary part is the reactance X. The resistance and reactance together determine the magnitude, |Z| (ohm), and phase of the impedance, θ (deg), through the following relations: $\mathbf{Z = |Z|e^{i\theta}}$, $\boldsymbol{|Z| = \sqrt{R^2 + X^2}}$ and $\boldsymbol{\theta = arctan(X/R)}$.

Impedance biosensors measure the electrical impedance of a system in AC steady state with constant DC bias conditions, by applying a small sinusoidal voltage to the system at a particular frequency and measuring the electrical current go through the system. The measurement procedure can be repeated at different frequencies to get spectra. This is known as electrochemical impedance spectroscopy (EIS). It was used in a variety of electrochemical phenomena over a wide frequency range. When the target biological

sample is captured by the probe, the impedance of the electrode-solution interface or whole measuring system will change in EIS (Daniels and Pourmand 2007).

Impedance biosensors can detect many kinds of target biological molecules by measuring impedance changes of the capture probe layer or the whole system. By using different probes, there are many different types of impedance biosensors including DNA sensors, protein sensors, small molecule sensors, lipid bilayer sensor, cell-based biosensors etc. Overall, impedance biosensor is a simple, rapid, label-free, low-cost detection method for biomolecules detection. Moreover, it does not require special reagents in most applications (Daniels and Pourmand 2007).

1.4.1 Impedance Biosensors for DNA

For DNA impedance biosensors, applied electrochemical potential can induce morphology change such as thickness increase or decrease of a DNA monolayer, possibly due to the interaction between the charged gold electrodes and the charged DNA monolayer (Kelley, Barton et al. 1998). Certain metal ions and/or pH conditions can induce the conformational changes of dsDNA, which can also result in electrical impedance changes (Long, Li et al. 2003; Liu, Bard et al. 2005). Also, ssDNA is relatively floppy and thus tends to lie near the surface while dsDNA is quite stiff, which suggests more ions might have access to the surface after hybridization (Mearns, Wong et al. 2006) The increase in DNA conductivity after hybridization may also induce detectable impedance change, which can be applied for detection of DNA hybridization using redox labels or redox-active intercalators (Mearns, Wong et al. 2006).

Thiol modified DNA can combine with gold surfaces including gold thin film and gold nanoparticles very easily, and this principle can be utilized to fabricate or improve impedance DNA biosensors. Keying et al. reported a simple, sensitive DNA impedance sensor based on gold nanoparticles (Zhang, Ma et al. 2008). They electrodeposited gold nanoparticles on electrode surface, and then immobilized probe DNA on the surface through a 5'-thiol-linker. Impedance spectroscopy was used to detect probe DNA immobilization and hybridization process. The gold nanoparticles modified electrode could improve the density of probe DNA attachment and sensitivity of DNA sensor greatly, compared to the bare gold electrode. This DNA sensor could be reproduced for a few times and had good stability during repeated regeneration and hybridization cycles (Zhang, Ma et al. 2008).

Other nano-materials or micro-materials can also be used to design impedance biosensor for DNA detection. Zhang et al. designed a novel architecture for electrochemical impedance sensing of the immobilization and hybridization of DNA (Zhang, Yang et al. 2009). The membrane integrated the strong adsorption ability of Fe_2O_3 microspheres to the DNA probes and excellent conductivity of self-doped polyaniline nanofibers on carbon ionic liquid electrode. Impedance spectra were used to characterize the resulting conductive microsoheres/nanofibers membrane on the electrode. Immobilization of the probe DNA on the electrode surface was dramatically enhanced, and the sensitivity of DNA hybridization recognition was also improved, both due to the remarkable synergistic effect of microspheres, nanofibers and ionic liquid. The procedure of DNA hybridization was monitored with a label-free EIS spectroscopy. This work suggested a

simple, rapid, specific and label-free EIS strategy to prepare a conductive interface for detection of DNA hybridization (Zhang, Yang et al. 2009).

The impedance biosensors for DNA also have the potential for detection of other samples or elements, which may change the properties of DNA at presence. Cao et al. designed a novel DNA-based biosensor for mercury detection using EIS (Cao, Zhu et al. 2009). Thiol functionalized poly-T DNA was used as gold electrode modifier through formation of Au-S bond between DNA and gold electrode. In the presence of Hg^{2+}, parallel ssDNA can change from linear to hairpin structures because of the specific coordination between Hg^{2+} and thymine bases. This structural change can induce the release of partial DNA molecules from the surface of the gold electrode. The density of DNA on the surface correlated with the concentration of Hg^{2+} in the solution and could be monitored by EIS. In addition, this method showed excellent sensitivity and high selectivity of other metal ions (Cao, Zhu et al. 2009).

DNA aptamer is a very hot concept in protein detection, which can be used as a probe in impedance biosensors for DNA or protein detection. Wang et al developed a novel protein assay method, in which human immunoglobulin E and its DNA aptamer were used as an analytical model (Wang, Xu et al. 2009). The target protein was captured by the aptamer in homogeneous solution and then the resulted complex was hybridized onto probes self-assembled on the DNA array. By impedance spectroscopy, the charge transfer resistance of electrode before and after hybridization could be compared. The result showed that the complex could be hybridized and detected on the modified electrode.

1.4.2 Impedance Biosensors for Protein

EIS is widely explored for detection of various proteins due to its high sensitivity. It provides accurate mechanistic and kinetic information from repeatable adsorption and desorption measurement on the sensor transduction surface of an electrode. The antibody-based reaction allows for direct and label-free electrochemical impedance sensing, which may speed up detection and analysis of biomarkers, also with high sensitivity (Vestergaard, Kerman et al. 2007).

EIS, combined with bioaffinity reactions, can be used for accurate and rapid detection of the binding events on the surface of modified electrodes. Sadik et al demonstrated an experimental approach for monitoring the interfacial biomolecular reaction using the novel differential EIS. The reaction between immobilized antibody and the antigen binding partner was used as the base for the approach, but it may be also applicable for monitoring other biomolecular reactions such as DNA-DNA interaction, DNA-protein interactions, and DNA-small molecule interactions. An ion displacement model was described as a theoretical approach to explain this antibody-antigen binding process (Sadik, Xu et al. 2002).

EIS and cyclic voltammetry (CV) are utilized in a combined framework, for many studies of impedance protein biosensors. Hennessey et al investigated the associative interactions of C-reactive protein (CRP) with CRP antibody (aCRP) immobilized on a gold electrode surface. They used EIS and cyclic voltammetry to obtain differential

pulse voltammetry and charge transfer resistance. It was demonstrated that the impedance spectroscopy was an efficient method to detect the interactions (Hennessey, Afara et al. 2009).

By utilizing different detection and characterization methods including EIS, very low concentration proteins can be detected. Jie et al developed a novel label-free biosensor for the detection of low-density lipoprotein by using self-assembly and gold nanoparticle amplification techniques. The gold nanoparticle layer was first assembled onto a cysteamine monolayer and then conjugated on the gold electrode surface. After treatment with cysteine and reaction with CdS nanocystals, ligand for the lipoprotein's receptor was covalently bound to the biosensor. Impedance spectroscopy was used to characterize this modification procedure with excellent sensitivity, good reproducibility, rapid response, and long-term stability (Jie, Liu et al. 2007).

In order to increase detection efficiency, the detection surfaces may be modified before protein capture and EIS measurement. Huang et al developed a reagentless electrochemical impedance biosensor for detection of a peanut protein, using a gold substrate to immobilize an antibody film. After the immobilization of antibody by amide bond formation, stable impedance spectra could be obtained for the biosensor substrate at different stages of substrate preparation. The relationships between charge transfer resistance/the differential capacitance and protein concentrations were investigated separately by fitting the impedance spectra to a Randles equivalent circuit (Huang, Bell et al. 2008).

The thiol monolayer may also be used for capturing protein before EIS measurement in the impedance protein biosensor. Tlili et al investigated a new immobilization procedure for biological molecules that was based on the formation of reactive ω-functionalized-self-assembled thiol monolayers onto a gold electrode. Impedance spectroscopy was used to characterize the homogeneous self-assembled monolayer (SAM). These SAMs could immobilize biotin hydrazide by covalent binding, and impedance spectroscopy was used to examine the interaction between biotin and avidin, as a typical protein-ligand model system for an affinity biosensor. The impedance data were fitted and described with a Randles equivalent circuit (Tlili, Jaffrezic-Renault et al. 2008).

1.4.3 Impedance Biosensors for Other Species

EIS is also widely used for sensing other samples, such as glucose, virus, bacteria, cells or even tissues. Glucose is a very important carbohydrate in biology. Glucose sensing has attracted a lot of interests both in research and clinic fields. EIS was also used for glucose sensing in the past years. Kang et al fabricated a new sensitivity-enhanced glucose biosensor with impedance spectroscopy to measure the properties of resulting biosensor (Kang, Mai et al. 2008).

Avian influenza virus H5N1 is of global concern as a potential pandemic threat which has killed millions of poultry in a growing number of countries throughout Asia, Europe and Africa. Detection of H5N1 is very helpful to decrease the global threats. Wang et al developed an impedance immunosensor as a new application for sensitive, specific and rapid detection of avian influenza virus H5N1. Target H5N1 viruses were captured by

the immobilized polyclonal antibodies immobilized on gold microelectrode surface. The impedance change induced by the virus was correlated to the concentrations of virus in the solution. Target AI H5N1 virus at a high titer could be detected by the impedance immunosensor within 2 hours. Equivalent circuit analysis of the impedance data indicated that the double layer capacitance were responsible for the impedance change due to protein A modification, antibody immobilization and bovine serum albumin (BSA) blocking (Wang, Wang et al. 2009).

Fast detection and sensing of bacteria is the first step for rapid treatment or removal of pathogens to reduce the risk for humans. Impedance spectroscopy was widely used for fast detection of bacteria. Yang et al presented a new, simple, rapid, inexpensive, and label-free impedance method to detect bacterial cells by making use of the impedance properties of bacterial suspensions (Yang 2008). It was found that bacterial cell suspensions in deionized (DI) water with different cell concentrations could generate different electrical impedance spectral responses, but cell suspensions is phosphate buffered saline (PBS) solution could not produce any significant differences spectra in response to different cell concentrations. Impedance at a fixed frequency decreased with the increasing cell concentrations in DI water suspensions, which was due to the cell wall charges and the release of ions or other osmolytes from the cells. This study demonstrated that bacterial cell concentration could be inferred by measuring the impedance of cell suspensions in DI water. This new detection mechanism could be an alternative to current impedance methods for quantifying bacterial cells (Yang 2008).

The electrical properties of the biomaterials are very important for the applications in biomedical field. Tissue structure and chemical composition of one biological material may correlate with its electrical properties such as its frequency characteristics. EIS which measures the impedance properties of tissues can be utilized in tissue engineering. Dean et al investigated the electrical impedance properties of rat lung and other tissues ex *vivo* using EIS. The relationship between the structure and the functional characteristic was confirmed by the results. Both conductivity and relative permittivity varied for different biological tissues. The values of impedance magnitudes were higher at low frequencies compared with those at high frequencies. This study is of practical interest for some biological applications of electrical pulses including electroporation, whose efficacy depends on the cell type and its electrical impedance characteristics (Dean, Ramanathan et al. 2008).

1.5 Electrochemical Impedance Spectroscopy (EIS) for Cell Based Sensing

Electrical impedance spectroscopy is one of the best electrochemical methods for fast detection of cellular activities. Cellular activities can be monitored in a non-invasive way by measuring the impedance of culture medium, buffer solution, or interfacial impedance between electrodes and cells. The impedance changes are caused by the release of metabolic products, which finally change the composition of culture medium and magnitude of dielectric forces at the interface (Katz, Lioubashevski et al. 2004). The impedance changes have provided researchers with a direct method to study the

mechanisms of regulating cell growths and the effect of various chemicals on cell adhesion, proliferation and viability (Yang, Li et al. 2004; K'Owino and Sadik 2005)

1.5.1 Electric Cell-substrate Impedance Sensing (ECIS)

Recent development of micro fabrication technologies and the lab-on-a-chip concept have encouraged researchers to design and miniaturize electrical impedance spectroscopic sensing devices to measure small-sized samples rapidly, stably and to be integrated with other analytic methods (Han, Han et al. 2006). There are many references describing the applications based on the measurement of cell-electrode impedance with serveral types of sensing mechanisms.

There is an established technique widely known as electric cell-substrate impedance sensing (ECIS). In ECIS the cells are cultured and spread on small gold film electrode. Information related with the morphology of the cells on the gold electrode surface could be extracted and analyzed quantitatively by measuring the electrical impedance of the electrode (Keese, Wegener et al. 2004). In operation, the sensor devices with cultured cells are connected to device station placed inside a CO_2 incubator. An impedance analyzer was connected with the device station using electrical cables. Cells were seeded into the devices and attached to the gold electrode surfaces. The presence and absence of cells, and also the change of cell morphological properties such as cell density on the electrode, cell shape and cell adhesive properties, affect the electronic and ionic passage on the gold electrode sensor surfaces. Information about biological status and properties of cells cultured on the surfaces could be acquired by measuring the impedance between

or among electrodes. Electronic impedance data are measured automatically in real time, which were converted to digital signals for more detailed processing and analysis (Wegener, Keese et al. 2000).

ECIS was successfully applied to monitor cell shape changes in various cell types under different experimental conditions. For instance, Tiruppathi et al. have used ECIS to detect the cell shape change of bovine endothelial cells in real time, which was modulated by activation of second messenger pathways (Tiruppathi, Malik et al. 1992). The high sensitivity of the ECIS measurement was demonstrated by detecting the periodic morphology changes of cultured cells caused by PH changes, which was resulted from the periodic injections of CO_2 in ordinary cell culture incubators (Lo, Keese et al. 1994). ECIS was also used to monitor the fast changes in cell shape associated with elevated cAMP levels in human orbital fibroblasts after addition of prostaglandin E (Reddy, Wang et al. 1998).

The attachment and spreading of mammalian cells on different protein coatings, the influence of divalent cations on spreading kinetics were investigated by using ECIS. Wegener et al described the optimization of ECIS to monitor cell adhesion, cell attachment and spreading of mammalian cells on the surfaces quantitatively and in real time. Small gold-film electrodes deposited on a culture dish were used as growth substrate and AC impedance amplitude was altered as the cells attached and spread on the electrode surface. They demonstrated that high-frequency capacitance measurements (f = 40 kHz) were well suited to serve as a direct measurement for the degree of cell spreading and surface coverage of the electrode. The excellent time resolution of this

technique and computer-controlled measurement of several samples at the same time allowed an in-depth analysis of cell spreading kinetics under various experimental conditions. The detachment of confluent fibroblastic cell layers after addition of soluble peptides that mimic the recognition sequence of fibronectin and other extracellular matrix proteins (RGDS) was also detected by ECIS technique (Wegener, Keese et al. 2000).

Different types of cells are also investigated by ECIS techniques. Xiao et al. studied the attachment and spreading of fibroblast V79 cells cultured on a small gold electrode surface coated with fibronectin or ovalbumin by a modified ECIS sensor (Xiao, Lachance et al. 2002). The sensor device equipped with a detecting gold electrode and a counter gold electrode was used to culture cells. The impedance data between electrode-electrolyte interface and a cell monolayer was accurately obtained for frequency spectra ranging from 1 to 10 kHz. The linear relationship between resistance of the electrode-electrolyte interface and the number of fibroblast cells attached on the detecting electrode was observed. And the slope of the linear relationship was dependent on the types of coating proteins. The resistance change was proportional to the area covered by the cells (Xiao and Luong 2003) (Xiao, Lachance et al. 2002).

ECIS was also utilized to monitor cells other than mammalian cells. John monitored the behaviors of insect cells such as attachment, motility, and mortality. An array of eight small gold electrodes deposited on the bottom of tissue culture wells was used to culture adherent cells and the cells were immersed in a culture medium. The impedance data increased after the cell attachment and spreading on the gold electrode because of the

cells acted as insulating particles to restrict the current flow. Con-canavalin A is proved to be the best promoter to accelerate the rate of cell attachment since impedance data shows differences form that insect cells interacted with various proteins used to precoat the gold electrode. The measured impedance data still fluctuate to reflect the constant motion and metabolic activity of the cells even after the cells were fully spread on the surface. As the cell behavior was sensitive to external chemicals, three chemicals were used as model systems to demonstrate the applicability of ECIS. Better than other conventional assays, the quantitative data obtained from impedance spectroscopy are taken continuous and in real time to depict cell motility and mortality of cells (Luong, Habibi-Rezaei et al. 2001).

1.5.2 Other EIS Techniques for Cell Based Sensing

ECIS utilize electrode, mostly gold electrode as platform for cell based sensing, there are also many other types or derivatives of cell based impedance biosensors.

Planar microelectrode arrays were used as an improvement and replacement of sensing electrode. Jung developed a cell-based biosensor consisting of a planar microelectrode array to detect extracellular potentials and their modulation when some toxins or other active agents applied. The microelectrodes were electroplated with platinum black to improve cell-electrode coupling. Impedance measurement was used as one of the methods to assess the effectiveness of the procedure. The total electronic coupling of cellular biopotentials to the microelectrodes was demonstrated by recordings obtained

from two different excitable cell types, myocytes and neurons cultured on microelectrode arrays (Jung, Cuttino et al. 1998).

Monitoring of cellular behavior by impedance measurements on interdigitated electrode structures was also reported. Ehret described a new method for on-line and real-time monitoring of concentration, growth and physiological state of cells in culture. The biosensor was based on impedance measurements of adherently growing cells on interdigitated electrode structures (IDES). Cell attachment, cell spreading, cell growth and killing of the cells were tested. Since there was no detectable electrical influence on the cells, the impedance measurements could be performed for several days. Impedance spectroscopy data could be changed by cell density, growth and long-term behaviors of cells on the electrodes. The influence of serum components (deprivation of fetal bovine serum) was used to indicate morphological changes and the toxic effects of heavy metal ions (cadmium) could be visualized from impedance signals (Ehret, Baumann et al. 1997) (Ehret, Baumann et al. 1998).

In cell related biomedical field, EIS is also an important technique. Edwin presented the development of a cell clinic by using EIS.A micromachined cavity, which could be closed with a lid. It was used to perform impedance studies on single or a small number of cells. Impedance measurements on Xenopus leavis melanophores were reported. Impedance changes could be detected after cell spreading and identify intracellular events also could be monitored, such as the aggregation of pigment granules. The measured impedance changes could be correlated with the optically visible movement. (Jager, Immerstrand et al. 2002)

Overall, EIS is an important tool for cell related sensing and many cell based impedance biosensors were developed successfully. ECIS was widely used for monitoring cell morphology changes, and were developed and utilized as one of the most promising label-free technique for studying cell behaviors in recent years.

1.6 Cancer Cell Morphology Change during Apoptosis

Cancer is a class of diseases or disorders characterized by uncontrolled division beyond the normal limits of cells, and the cells have ability to invade other cells or tissues, either by direct growth into adjacent normal tissue through feet invasion or by migration of cells to distant sites through metastasis (Wikipedia). Cancer was the leading cause of death in Hong Kong for decades. In 2003, it claimed about 12,000 lives, or one in every three deaths. The proportion of lung cancer patients is the highest among all cancer patients. In 2001, among the 21,000 cases of cancer, 3,800 or 18% were cases of lung cancer. (The Hong Kong Anti-Cancer Society, HKACS) Actually that's one of the most important reasons why the HKSAR government extends the no smoking areas from Jan 1st, 2007.

Apoptosis is one of the main types of programmed cell death, but evasion of apoptosis is an essential capability of cancer cell. Apoptosis is a strictly regulated and genetically controlled cellular 'suicide' program. It could be induced by cytokines, absence of growth factors, radiation, chemicals or some physical conditions. Cancer cells have the special ability of avoiding apoptosis and continue to proliferate, and this is one of the

fundamental and important steps in cancer development. Actually almost all cancer cells have mutations which enable avoiding of apoptosis. Cancer cells bypass apoptosis utilizing a wide variety of mechanisms including dynamic interplays between oncogenes and/or mutated tumor suppressor genes. Tipping the subtle balance between cell death and proliferation in favor of cell survival may result in uncontrolled proliferation or excessive cell loss, and finally induce tumor formation.

In drug-curable cancers, apoptosis is a primary mechanism associated with the induction of cancer remission (Hanahan and Weinberg 2000). Thus, a drug that activates apoptosis might achieve significant efficacy in treatment of cancer. (Sellers and Fisher 1999) Currently, many therapies used for treatment of cancer kill cancer cells mainly depends on activation of apoptosis programs in cancer cells (Fulda and Debatin 2004). Because the initial definition of apoptosis was based on morphological grounds, identification of apoptotic cells also could be morphology-based (Rodriguez and Schaper 2005). A cell undergoing apoptosis can be characterized by typical morphological and biochemical hallmarks including cell shrinkage and rounding, irregular projections blebs on the cell membrane, cell detachment, nuclear DNA fragmentation, disassembly into apoptotic bodies and disintegration of cell–cell contacts etc. (Hacker 2000) The images observed and captured by a microscope are mainly structural properties of the cells or the tissue, such as size, shape and orientation of the cells, amount of intra and extra cellular water, and structure of the cell membranes. These structural properties are to a high degree reflected in the impedance spectra (Glamann and Hansen 2006).

Morphological investigation with common features of apoptosis are present in the specific drug treated cells suggests the drug might be an efficient anti-cancer regimen *in vitro*(Chui, Gambari et al. 2006). One standard for the identification of cells undergoing apoptosis is ultrastructural evidence of chromatin condensation, which is the earliest characteristic morphological feature. But the process is extremely labor intensive and the costs of electron microscopy for this purpose are prohibitive, it is not recommended for routine work although it is an excellent parameter with high reliability (Rodriguez and Schaper 2005).

Many existing methods to monitor apoptosis *in vitro* are based on fluorescence probes or by flow cytometry. The probes are always invasive and designed to specifically label relevant molecules in apoptotic cells. Some biochemical assays also measure the activity of apoptosis-related enzymes or determine the degree of DNA fragmentation to detect apoptosis (Yin, Wang et al. 2007). The microscopic techniques were widely used to study cell morphology such as cell attachment and spreading, but the direct results are images described only in qualitative terms. Although these events can be quantified by microscopic techniques coupled with image analysis, it is still a time-consuming work to assess changes of cell morphology (Giaever and Keese 1993; Wegener, Keese et al. 2000). So, a real-time and label-free method for monitoring cell morphology is of special interest in anti-cancer drug screening procedure.

1.6.1 ECIS for Detection Morphology Changes During Apoptosis

ECIS is very useful for monitoring cell morphology changes during apoptosis. In ECIS the cells are cultured directly on the surface of small gold-film electrode. It is possible to deduce alternations in cell-cell and cell-substrate contacts, by measuring the electrical impedance of the cell-covered electrode, performed with non-invasive, low amplitude sensing voltages.

Arndt applied ECIS in order to monitor the apoptosis-induced changes in cell shape in an integral and quantitative way with high time resolution. Endothelial cells derived from cerebral micro-vessels were used as cellular model systems to improve the sensitivity of this impedance assay, because of these cells are well known to express electrically tight intercellular junctions. Apoptosis induced by chemicals could be verified by biochemical and cytological assays. The relationship between time courses and cell shape changes was followed with unprecedented time resolution by impedance measurements at 1 kHz and it was correlated with biochemical parameters. The observed impedance changes could be assigned to alternations on the sub cellular level from the impedance measurements along a broad frequency range or $1 – 10^6$ Hz. The disassembly of barrier-forming tight junctions preceded changes in cell-substrate contacts and it correlated strongly with the time course of protease activation (Arndt, Seebach et al. 2004). Besides of endothelial cells, the apoptosis of cancer cells were also investigated by ECIS. Hongying applied ECIS to monitor apoptosis-induced changes in human colon cancer HT-29 cell shape also with high time resolution and the apoptosis was verified by transmission electron microscope. The capability of ECIS for monitoring the dynamics of aspirin-induced apoptosis was demonstrated. The ECIS technique could be applied as a whole-cell biosensor both in cytotoxicity studies and in the course of drug

development because of the non-invasive performance and the quantitative nature of the method (Yin, Wang et al. 2007).

Not only apoptosis, ECIS also can be used as a monitoring tool even for viral-induced cell death. Campbell has recorded the dynamics of viral infection in cell culture. Dramatic impedance changes were recorded because of infection inducing cytopathic effect, and the changes were mainly due to cell death. In their study, two different fish cell lines and one virus were used. The impedance changes caused by cell response to virus were easily measured and converted to resistance and capacitance. The impedance data suggested an approximate linear correlation between log of virion concentration and time of cell death (Campbell, Laane et al. 2007).

1.6.2 Our Improvement of ECIS

When used for detecting cell morphology changes, ECIS also has some limitations. If the cell concentration is relatively low, the size of electrodes may need to be decreased, but the impedance caused by the small electrode polarization is increased at the low frequency range (Connolly, Clark et al. 1990). While the impedance related with cell morphology changes is much smaller than this high electrode impedance, it is not easy to extract the impedance information of cells from total measured impedance data. So it is necessary for us to develop a new morphology-sensitive electrochemical micro-system with nanopore structures which can detect the small cancer cell morphology change induced by anti-cancer drugs even in trace quantities.

When the electric fields are applied in the cell culture medium through the nanopores on the insulated membrane, ionic current are generated through the nanopores. After cell cultured on the surface for many days, the nanopores are covered by the adherent cells formed monolayer, the current is partially blocked and the impedance will change to reflect the effect. After treatment of specific anti-cancer drug and the cell morphologies having been changed by certain drugs, electric current can go through many more pores and changes in impedance changes may occur. These procedures can be monitored by EIS. During the entire process, the non-conductive nanoporous membrane could avoid the electrode polarization effects during the impedance monitoring compared with the traditional gold or other metal based electrode impedance biosensor.

As described before, nanoporous alumina membrane are non-conductive and has good bio-compatibility for cell culture, it can be a suitable candidate as electrochemical platform for detection of cancer cell morphology change during apoptosis.

Chapter 2 Methodology

2.1 Fabrication of nanoporous alumina membrane

Nanoporous alumina membrane is generally prepared by two-step anodization technique. Two-step anodization is considered to be the most successful technique to make a nanoporous surface with aluminum foil. It has gained importance due to particular characteristics such as controllable pore diameter, periodicity of patterns on surface and extremely narrow distribution of pore size, which offers a promising route to synthesize a large surface area and ordered nanostructure with high aspect ratio. The two-step anodization method was first introduced by Masuda and Fukuda and was improved in the past several years (Masuda et al. 1997).

Nanoporous alumina membrane was fabricated from pure aluminum (Al) foil (99.99% purity, thickness = 0.5 mm, Alfa Aesar) by the standard two-step anodization technique. Pure Aluminum foil was cut into small pieces of 5 cm by 5 cm dimension. After washed in ultrasonic bath with deionized water, acetone and deionized water again, it was dried with nitrogen jet. The first anodization process was taken in 0.25M oxalic acid and the aluminum was used as anode while copper (Cu) sheet was used as cathode. The oxidation layer was characterized by numerous defects, originally caused by defects in the aluminum surface. Owing to the decreasing current with the increase of the thickness of the barrier layer, the formation of pores was initiated at defect positions. Supported by electric field, aluminum oxide and hydroxide at the pore walls were preferentially

dissolved by the acidic electrolyte which consists of 4% (w/w) chromic acid and 8% (w/w) phosphoric acid in the etching step. The second anodization step was taken followed using the same conditions. When the electric field increased, the dissolution process was accelerated, and nanopores with larger diameters were formed. An ice bag was attached on the beaker to keep the temperature of the electrolyte around 10 °C during the anodization. Finally, the amorphous barrier layer of alumina was etched away using a solution of 8% (w/w) phosphoric acid and 0.1 M copper chloride ($CuCl_2$).

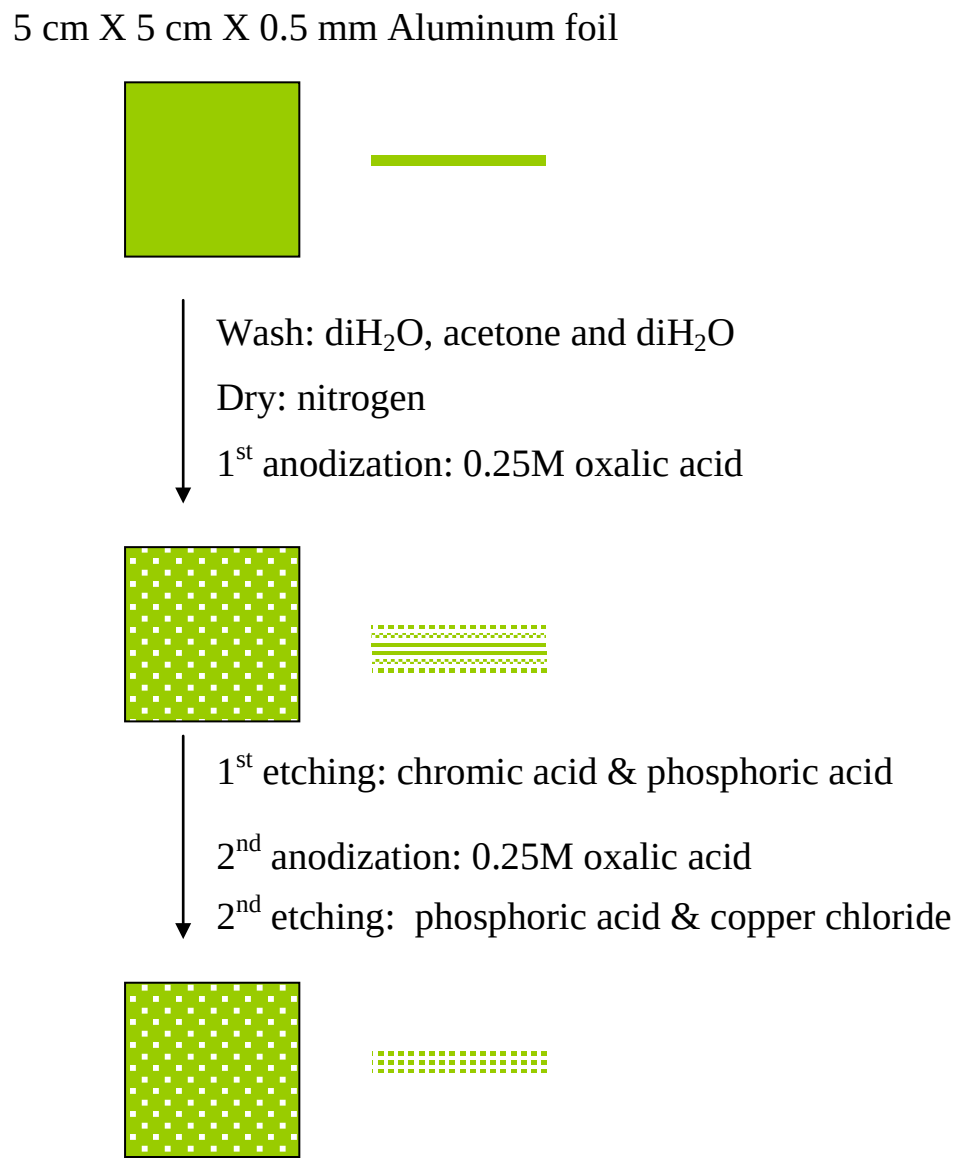

Fig 2.1.1 Fabrication of nanoporous alumina membrane with two-step anodization

This process was capable of fabricating nanopores in the range of 30–200 nm depending on the anodization voltage used for oxidation. In order to control the sizes of the nanopores and find the realistic relationship between anodization voltage and nanopore diameter, different voltages between 40 V to 120 V were chosen to apply for different experiments. Membranes fabricated could be characterized using scanning electron microscopy (SEM) and atomic force microscopy (AFM) analysis. The SEM images could be analyzed by the image analysis software (Metamorph analysis software, Nikon) to examine the nanopore sizes.

2.2 Surface modification and characterization

2.2.1 Silane Treatment and PEG micropatterning

To precisely define sensing area, Polyethylene glycol (PEG) hydrogel, an organic polymer layer, was used to fabricate micropatterning on the surface of nanoporous alumina membrane. With the goal of improving PEG hydrogel adhesion on nanoporous alumina membrane by covalent binding, the substrate surface was firstly silanized with 3-trimethoxysilyl-propyl-methacrylate (TPM) (Aldrich).

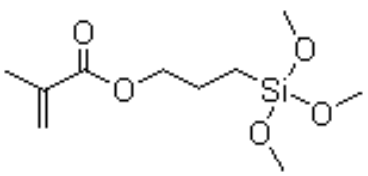

Name: 3-trimethoxysilyl-propyl-methacrylate (TPM)
Molecular Formula: $C_{10}H_{20}O_5Si$
Molecular Weight: 248.35

Fig 2.2.1 Information of TPM, the silane used to do surface modification

The nanoporous alumina membrane was treated in 10mL 30% boiling hydrogen peroxide (H_2O_2) for 30 minutes at 158℃, in order to clean the surface and introduce -OH group on the surface, which will facilitate subsequent modification by silane. Then it was boiled in deionized water for additional 15 minutes for cleaning. After completely dried with air in oven, it was soaked into a 5% (V/V) solution of TPM in anhydrous toluene (1 mL TPM and 20mL anhydrous toluene) at 50℃ in the incubator for about 48 hours. Then the membrane was washed in toluene, followed by methanol, and finally water, to eliminate unreacted silane. At last membrane was gently dried and stored in nitrogen.

Polyethylene glycol diacrylate (PEG, 500Da, Sigma-Aldrich, Inc., louis, MO 63103 USA) was dissolved in PBS (1:3, v/v) solution, while Irgarcure 2959 in ethanol (1:10, v/v) was used as photoinitiator to initiate the polymerization procedure. A UV lamp (EXFO, OmniCure Series 1000) was used to supply the necessary UV light for the procedure. After mixing with PEG and the initiator, about 20uL solution was deposited on the TPM modified surface in the SU-8 chamber confined area. A glass slide was covered on the chamber tightly, and then a photomask with desired pattern was put on the glass surface. UV exposure with energy 10 mW/cm2 was then taken and the exposure time was 90s. The exposed parts became insoluble and the desired micropatterns such as microwell arrays were achieved by washing away the unreacted regions with deionized water. The exposure energy and exposure time were optimized for many different parameters, and the pattern was formed while there was no remained PEG solution in the micro-holes, finally the nanoporous alumina membrane surface with

silane treatment was revealed in the microwells. PEG with other molecular weight was also tested for fabrication. In order to make sure that there was no remaining PEG solution after the procedure, a green fluorescence dye fluorescein diacetate (FDA) was added for observation.

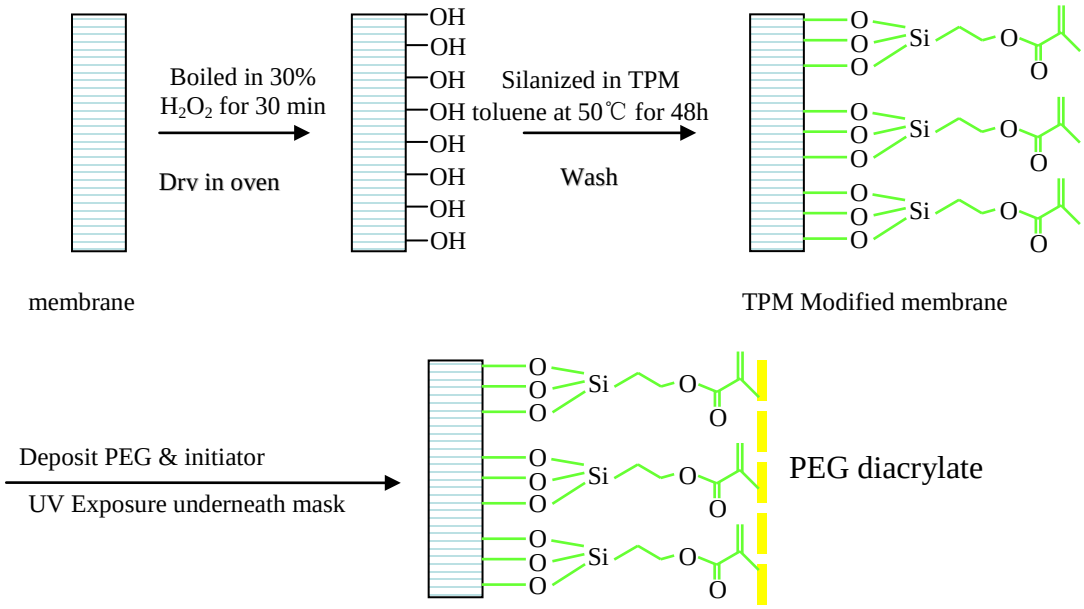

Fig 2.2.2 schematic illustration of surface modification and micropatterning

2.2.2 X-ray photoelectron spectroscopy, water contact angle measurement and protein adsorption

The TPM graft on nanoporous alumina membranes was studied by X-ray photoelectron spectroscopy (XPS) measurement. The XPS used in the experiment was a Shenyang SKL-12 electron spectrometer equipped with a VG CLAM 4 MCD electron energy analyzer while X-ray source was a dual anode source from VG (type XR3E2). Mg Kα radiation (1253.6 eV) at a current of 15 mA was used.

Static water contact angles were measured with a goniometer (Rame-hart 250-F1 standard goniometer with dropimage advanced 2.1, NJ, USA) equipped with a video camera before and after silane treatment or surface modification. Drops of about 30 µl distilled water were deposited onto the glass surfaces, and then the static contact angles after 20 s were recorded. The reported values were averaged based on 20 independent measurements.

To see the efficiency of protein adhesion and adsorption on the different surfaces, Rhodamine-labeled bovine serum albumin (BSA) (Sigma) were dissolved in phosphate-buffered saline (PBS) (Sigma) at a final concentration of 50µg/ml. To test for BSA protein adhesion, a few drops of the protein solution was evenly distributed onto the surfaces and stored at room temperature for 30 min. The samples were then washed and analyzed under a fluorescent microscope (Nikon Eclipse 80i fluorescence microscope, Nikon, Japan). The fluorescent images were quantified using the image analysis software (Metamorph analysis software, Nikon). The overall and average intensities of the whole image or interested areas were calculated and analyzed.

2.3 Diffusion experiments

A mold made of stainless steel was used for the fabrication of a PDMS chamber, then a nanoporous alumina membrane was placed horizontally on the device and the inside of the chamber was sealed with glue. The chamber has two holes on its two ends, for adding medium into the chamber and inserting of electrodes.

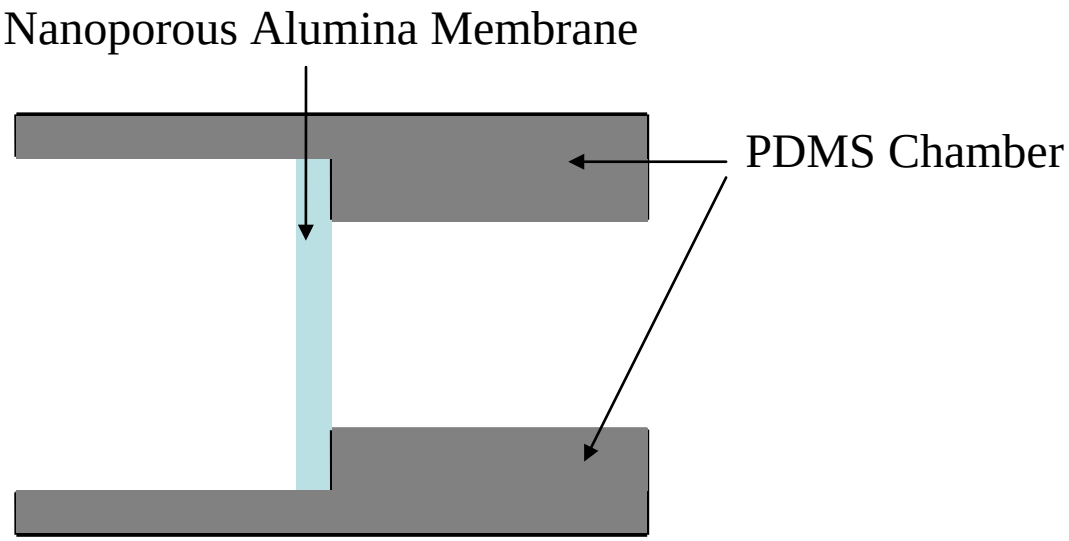

Fig 2.3.1 Demonstration of device incorporated with nanoporous alumina membrane

In order to show the diffusion property of nanoporous alumina membranes, 1 mL protein solution with concentration C_1 was added in one part of the device while the other part of the device filling with 500 uL distilled water. After a specific time interval which allowed the solutions in one part diffuse to the other, 100 uL of solutions with final concentrations C_2 in the other part was taken out for measurement. The solutions were mixed fully before measurement to make it homogenous. Ultrospec 2100 Pro UV/Visible Spectrophotometer (Biochrom, England) was used to measure absorbance of the solutions for a given wavelength range. The wavelength between 190 nm and 500 nm was scanned at the scan speed 750 nm/min. Peaks could be read at 206 nm and 280 nm. The value of the peak at 280 nm was used to calculate the concentrations of the solution by a standard curve of measured peaks versus known concentrations acquired before the measurements.

2.4 Cell Culture

Different types of cells were employed in our project. Human esophageal squamous epithelial cancer cell line KYSE30 and human osteoblast-like cell line Saos-2 were purchased from American Type Culture Collection (ATCC, USA). Rat stem cells were obtained from the marrow of 7-month-old Sprague-Dawley rats.

The cells were cultured on a 35mm diameter tissue culture dish (Nunc GmbH & Co. KG, Germany) in a humidified incubator at 37^{o}C with 5% CO_2/ 95% air. They were maintained routinely in Dulbecco's Modified Eagle Medium (DMEM) with 4,500mg/L glucose (Invitrogen) as basic medium supplemented with 5% Fetal Bovine Serum (FBS, Invitrogen) together with 50U/ml penicillin and 50g/ml streptomycin (Invitrogen). The culture medium was refreshed every 2~3 days. The medium was removed and the dish was washed by sterile phosphate buffered saline (PBS) (Zymed) three times before culture medium refreshment or subculture into new dishes or nanoporous alumina membranes.

The subculture was done at a ratio of 1:3 when they reach confluence. Trypsin is a proteolytic enzyme which can be used to detach adherent cells from the surface of a cell culture vessel. This procedure is called trypsinization and performed whenever the cells need to be subcultured or to be harvested. The concentration of Trypsin/EDTA was 0.25%.

SEM was applied to analyze the detailed status and morphology of cells cultured on nanoporous alumina membranes. After cell culture for some days on membranes, the

membranes were washed with PBS for three times, then fixed in 2.5% glutaraldehyde in 0.1 M PBS (pH 7.4) for around 1 hour at room temperature, then they were washed thoroughly in 0.1 M PBS for three times, 15 minutes each. After that, the samples were dehydrated in graded series of ethanol in PBS for 15 minutes each: 70% ethanol, 80% ethanol, 90 % ethanol, 95% ethanol, 100% ethanol. After drying by nitrogen gun, the samples were carefully mounted on studs using double stick carbon tapes or silver paint , then put into chamber of the sputter coater and coated with a layer of gold before SEM observation (JEOL 6490 and Leica 440).

Fluorescent staining was performed to observe the concentrations or morphology changes of cells cultured on surfaces, mainly on nanoporous alumina membranes. Phalloidin-TRITC (Sigma-Aldrich) was used to stain the cells by binding to actin in the cells. Phalloidin has the ability to bind to F actin in live cells, and as a result of binding phalloidin, actin filaments become strongly stabilized. DAPI (4', 6-diamidino-2-phenylindole) was used to stain nucleic acid since it could easily enter live cells and bind tightly to DNA. The sample was finally viewed using a fluorescence microscope (Nikon, ECLIPSE 80i)

2.5 Impedance spectra with electrolytes

AC impedance analysis was performed using the impedance analyzer controlled by a personal computer. An Ag/AgCl counter electrode was placed in the lower chamber and a Pt wire was immersed into upper chamber as the working electrode. The whole system had been connected with an impedance analyzer VersaSTAT3 (METEK), and the

impedance data had been recorded by using V3-Studio (Princeton Applied Research) during the whole procedure of cell adhesion. The absolute values of the impedance |Z| (f) and the phase angle φ (f) between voltage and current were recorded within a frequency range of 0.1-10^6 Hz, which took ~5 min.

To testify whether the nanopores are open and ions could go through nanopores, a series of NaCl solutions in different concentrations (from 0.001 M to 1 M in distilled water) were applied to perform impedance measurement and analysis. The temperature was kept around 25 °C and all other conditions were remaining the same during the whole measurement process, to ensure the system is stable enough.

After data recording with V3-Studio, Excel 2003 (Microsoft) was used to sort and analyze the data, plot images. ZSimpWin (EChem Software) was used to fit circuit model.

2.6 Micropatterning of cells in the microwells

After PEG micropatterning on TPM modified nanoporous alumina membranes, PEG could not interact with any protein but silane can combine with protein tightly. Before cell seeding, fibronectin, a type of extracellular matrix proteins which can enhance cell adhesion during cell culture process, was used to treat the whole surface then followed by briefly washing. There was no fibronectin left on the surface areas with PEG hydrogel binding but the surface areas with silane modification but no PEG hydrogel has fibronectin.

The cells were seeded on the patterned surface treated with fibronectin and cultured for a specific time. Fluorescent staining was performed to observe the cells constrained in the microwells.

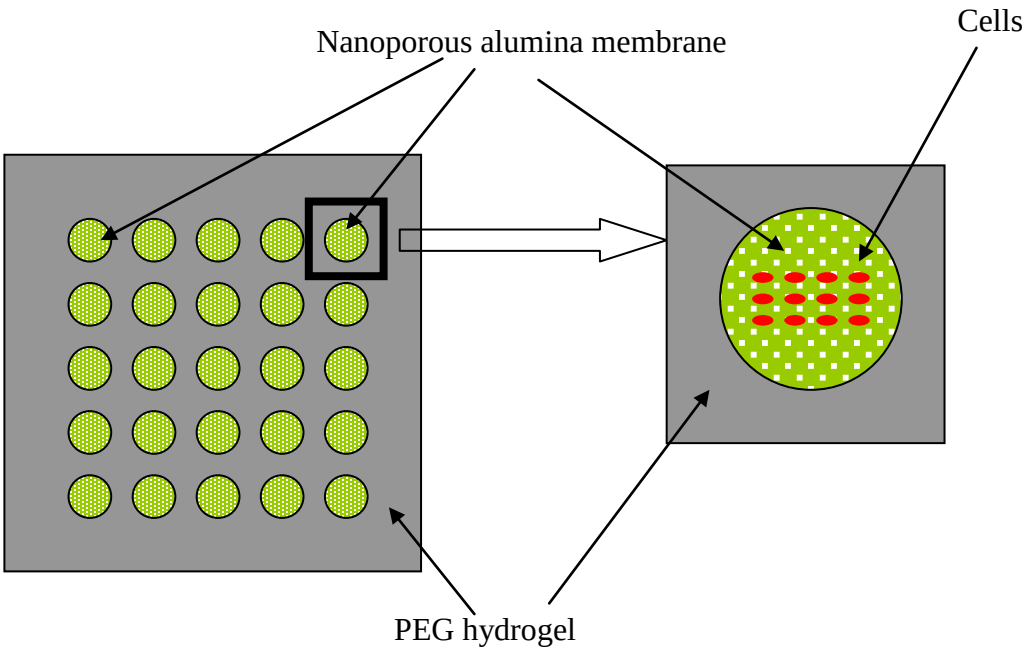

Fig 2.6.1 Schematic diagram of cell micropatterning

2.7 Impedance measurement of cells cultured on membranes

The impedance properties of the cells cultured on the nanoporous for different days were investigated after cell seeding on the surface, to observe cell adhesion and proliferation.

When the cell concentration reached confluent monolayer, the different effect of three different anti-cancer drugs is tested. During the treatments of the anti-cancer drugs, the impedance data is measured and collected.

Cisplatin (CDDP, Sigma-Aldrich) is a platinum-based chemotherapy drug used to treat various types of cancers and it can induce morphological changes of cancer cell lines. CDDP is dissolved in cell culture medium and the final concentration of 0.5mg/ml was applied.

Retinoic acid (RA, Sigma-Aldrich) is an immunomodulator and both a preventive and chemotherapeutic anticancer agent; and its derivatives were used to treat many cancer and tumor types. The anti-cancer effects of retinoic acid are in part due to their ability to inhibit proliferation of cancer cells and it can interfere with the growth and development of cells. RA inhibits the cell-substrate adhesion and motility, and it also induces morphological and functional terminal differentiation of a cell line. It was reported that the modulation of proliferation and adhesion in epithelial cells and fibroblasts of human skin by RA is associated with changes in the extracellular matrix production of Ca^{2+} metabolism. RA is dissolved in absolute ethanol at the concentration of 0.01M (3 mg/mL). Subsequent dilutions were made in cell culture medium with a final ethanol concentration of 0.1% (v/v) and the final concentration of RA is $1X\ 10^{-5}M$.

5-Fluorouridine (5-FU, Sigma-Aldrich)is also used for chemotherapeutic treatment of certain cancers because it is a potent inhibitor of the incorporation of formate into DNA thymine both *in vitro* and *in vivo*. 5-FU is dissolved in cell culture medium and the final concentration is $1X10^{-5}$ M

2.8 Detection of Cell Apoptosis

Besides of impedance measurements, cells were also analyzed for apoptosis by a cell death detection ELISA (Roche Applied Science) after treatment with 5-Fu (0.1mg/mL) for different time. The mono- and oligonucleosomes in the cytoplasm fraction of cell lysates was specific determined by anti-histone antibody and anti-DNA-peroxidase (POD) respectively. And it is calculated by using the following formula: Enrichment factor = absorbance of the sample (dying/dead cells)/ absorbance of the corresponding control (viable cells). Enrichment factor was used as a parameter of apoptosis.

$$E = \frac{A_{sample}}{A_{control}}$$

E: Enrichment factor

A_{sample}: absorbance of the sample (dying/dead cells)/

$A_{control}$: absorbance of the corresponding control (viable cells)

Fluorescent staining also was performed after treatment with 5-Fu for different time, then fluorescence images were acquired and analyzed to find out average covered areas per cell. The relationships between measured impedance data, fitted parameters for equivalent circuit model, enrichment factors from ELISA results and cell covered areas from fluorescence images were evaluated.

Chapter 3 Results

3.1 Fabrication of Nanoporous Alumina Membranes

Nanoporous alumina membrane is known for its self-assembled periodic pore structure with the size of nanometers and is widely used as a template for various nanostructures and nanosystems, as well as an important component in many biomedical applications.

3.1.1 Characterization of nanoporous alumina membranes

The two-step anodization technique is the mainly adopted method to form highly ordered arrays of nanoporous alumina membrane. Masuda and Fukuda are the first researchers who reported the two-step anodization electrochemical procedure to prepare alumina with highly ordered nanopore arrays (Masuda et al. 1997). During the fabrication process, the nanoporous layer is stripped out by an acid etching solution after the first anodization is performed. Then the second anodization produces a highly-ordered, hexagonal close-packed pore array. This method is cheaper and easier to obtain a regular array of nanopores comparing to electron beam lithography method. The nanopores have a uniform pore diameter in the range of 4-400 nm, high pore density in the range of $10^9 – 10^{11}$ cm^{-2} and an aspect-ratio of over 100 is easily obtained.

In this project, we fabricated nanoporous alumina membranes at different voltages with the temperatures of 10 °C. Under these conditions, the ordered nanoporous arrays were acquired. Scanning Electron Microscopy (SEM) was the primary tool used to observe the nanoporous structure of nanoporous alumina membranes surface, as well as the pore diameter and membrane thickness. Fig. 3.1.1 illustrates the top surface view of the fabricated nanoporous alumina membrane by SEM. It demonstrates the micrograph collected with sample anodized at 120 V. It showed that alumina nanoporous membranes were successfully fabricated by two-step anodization method.

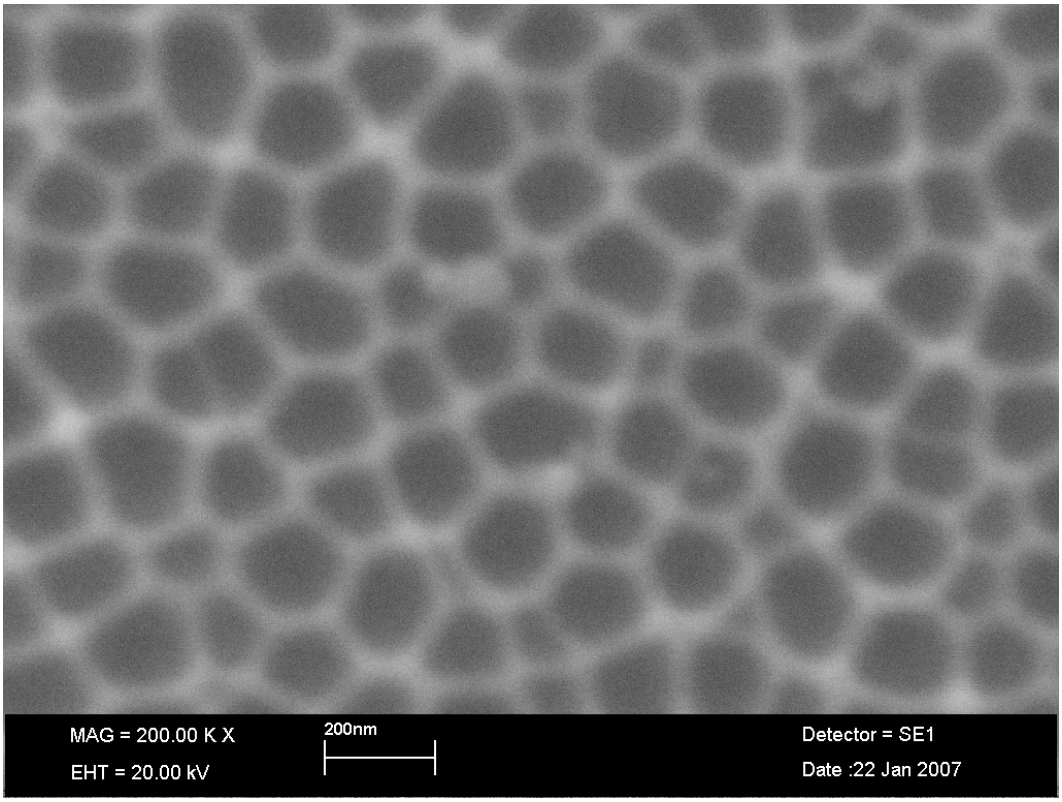

Fig 3.1.1 SEM image of nanoporous alumina membrane

In order to find the best conditions for highly ordered nanoporous pattern, analysis of the geometrical properties such as shape, pore size and density was explored by MetaMorph Offline software (Molecular Devices). Most of the nanopores have the similar values for width and length. But a few of them are rectangular and hexagonal which have many

sides with different width and length. Even for the rectangular and hexagonal nanopores, they also can be considered as circular while calculating the diameter and sizes by using mathematical method. From the analysis of Fig 3.1.1, the average nanopore diameter is 142.8 ± 34.0 nm while the smallest one is around 48.3 nm, and the largest one is around 204.5 nm. The width of the frameworks between adjacent nanopores is around 21.0 nm, so the interval between nanopore centers was around 163.8 ± 34.0 nm. The pore density is 38 pores/μm^2 (~3.8×10^9 pores/cm^2), which agrees with the earlier report by Le & Martin et al (Martin et al. 2003). Le & Martin changed the anodization parameters while controlling the expansion factor and prepared ordered pore structures with interpore distances of 50, 60, 100, 150, and 420 nm, which corresponded to a nanopore density range of 6×10^8 to 5×10^{10} pores/cm^2.

As we described in the introduction part, the nanopores should be fully open to allow the passage of ion current during the impedance spectra measurement. We compared the top and bottom views of the surfaces of different nanoporous alumina membranes to make sure the fabricated nanopores are fully exposed on both top and bottom surfaces.

Generally, comparing the differences of the surfaces from SEM images is an effective method to distinguish types of nanopores on the membranes. (Hoess et al. 2007). Fig 3.1.2 shows three SEM micrographs of nanoporous alumina membranes from different fabrication sources with the same magnification. Fig 3.1.2 (a) shows one sample fabricated in our lab with the conditions mentioned before. The nanopores are black and dark while the framework is white and bright, and the contrast between nanopores and framework is very obvious. The darkness of all the nanopores is at the same level, which

was shown by measuring the grayscale intensity values of nanopores using MetaMorph. It indicates that the nanopores are uniform in depth due to the similar darkness level. And they are completely exposed and fully open on both top and bottom surfaces of the membrane, comparing with other membranes. Fig 3.1.2 (b) shows another nanoporous alumina membrane purchased from United States. The framework is also white and bright, but some of the nanopores are black and with higher gray value while the others are not black and with lower gray value, which indicates there are height differences between these regions. The reasonable explanation is that some of them are exposed on both surfaces but the others of them are just exposed on one of them, either the top surface or the bottom one. This situation happens when the fabrication time is not enough since the fabrication processes may begin from either of the surfaces. If anodization time is not enough, some of the nanopores could not be fully opened, and the differences could be directly observed through SEM micrograph. Fig 3.1.2 (c) shows another nanoporous alumina membrane purchased from a lab in China. Only in part of the surface nanopores and framework can be observed, and in other parts only very small holes or even ripples can be found. And the contrast between the small ripples and surface is not obvious, and it may be defined as “closed” nanopores. Actually it indicates the anodization process only happen on some areas but not through the whole membrane. This shows that the lab-made nanoporous membrane in our lab has good uniformity and periodic structures with the optimal conditions. By comparing the differences of nanoporous alumina membranes from three sources, we concluded the fully open nanopores were successfully fabricated in our lab, which is useful for other experiments after fabrication such as ion diffusion and impedance measurements.

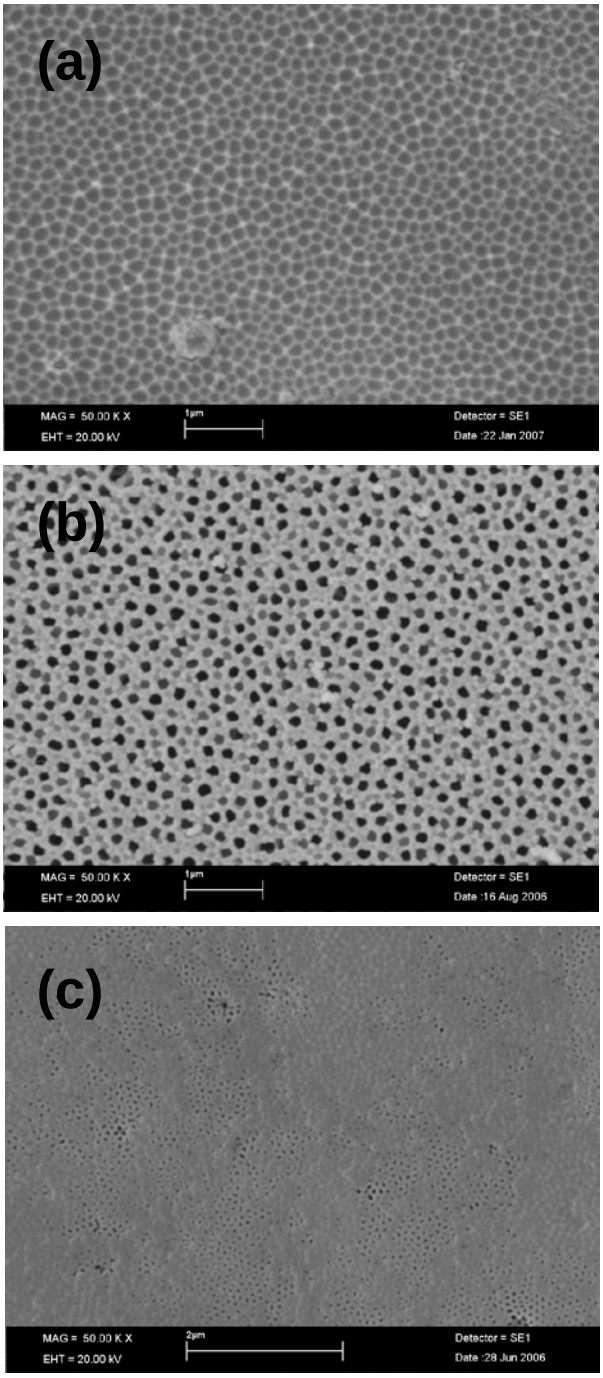

Fig 3.1.2 Top views of different nanoporous alumina membranes (a) Fabricated in our lab, indicating fully open nanopores; (b) Bought from the US, indicating fully open and half open nanopores (c) Bought from China, indicating open and closed nanopores

Tapping mode Atomic Force Microscopy (AFM) is another tool used to determine surface topography and uniformity of nanoporous alumina membranes. Fig. 3.1.3 shows two- and three-dimensional 1.25-µm scans for the membranes with fabrication voltage 60 V. It can be seen from the AFM image that the membrane surface is very uniform, and nanopore diameter is around 95 nm, but the value is not very accurate because of the view angle is not 90°. The pore density can be calculated by counting the numbers of nanopores on the scanned area in the two-dimensional image. The result is 44 pores/um^2, which also can be written as around 4.4×10^9 pores/cm^2.

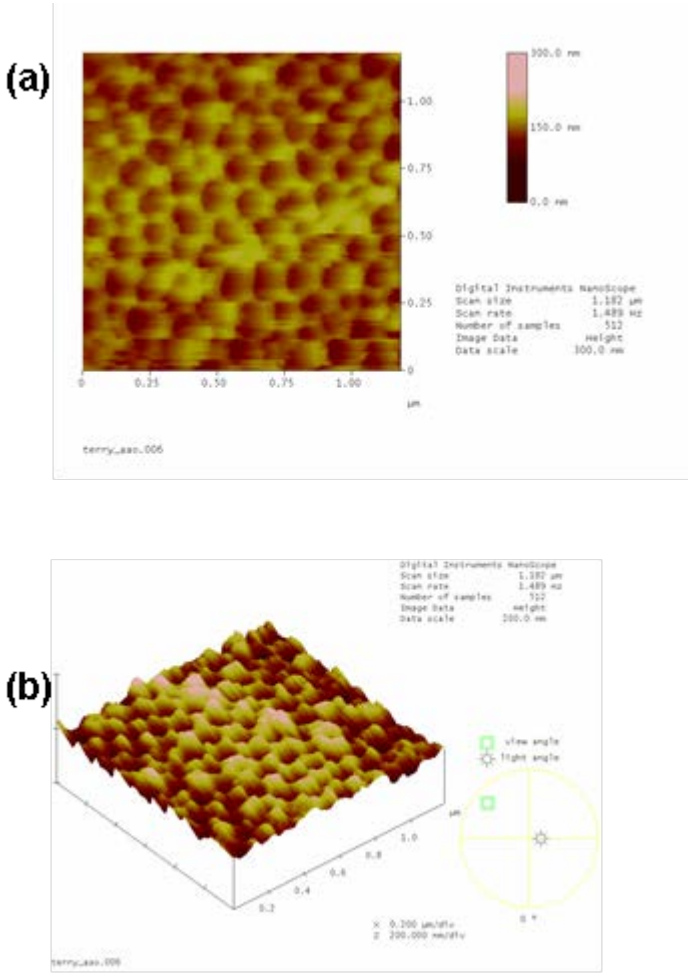

Fig 3.1.3 AFM images of nanoporous alumina membranes (a) Two-dimensional, 1.25-µm (b) Three-dimensional, 2-µm

Since AFM is a surface analysis tool which is mainly used to detect surface topography, the nanopores appear to be as valleys in the thee-dimensional image. The depth of the valleys can be measured from the image to be around 40~50 nm. Actually, these nanopores extend through the membranes and it is concluded that the real depth of nanopores is more than 50 nm. From the references, the thickness of nanoporous alumina membranes could range from 21 nm ~1000nm. (La Flamme et al. 2007, Marsal et al. 2009, Ran et al. 2008, Sharma et al. 2007)

3.1.2 Control of nanopore diameters by adjusting anodization voltages

The nanopore sizes have dominating effects on diffusion rate for ions through the nanoporous membrane during the impedance spectra measurement. We could control the nanopore sizes by adjusting anodization voltages. After optimization, membranes with nanopore sizes ranging from 20nm-200nm were achieved by modulating the voltage from 15V to 150V. Fig 3.1.3 shows the different nanopore diameters under different anodization voltages. For Fig 3.1.3 (a), the anodization voltage is 60 V. The distribution of nanopores is very uniform and the diameter of nanopores is 76.3 ± 14.5 nm. For Fig 3.1.3 (b), the anodization voltage is 80V. No big difference can be seen from the image with bare eyes. By software image analysis, the diameter of nanopres is 91.7 ± 13.5 nm, which is about 20% larger than the one under 40 V anodization voltages. For Fig 3.1.3 (c) the anodization voltage is 100V. The nanopores are obvious larger than the two samples fabricated under lower voltage with the diameter of 119.8 ± 11.3 nm, which is about 57% and 31% larger than the previous two samples, prospectively. For Fig 3.1.3 (d), the anodization voltage is 120V, we can see easily that the nanopores are much larger than

the ones before and the diameter of nanopres is 162.8 ± 22.8 nm, which is 113%, 78% and 36% larger than the pervious two membranes, respectively.

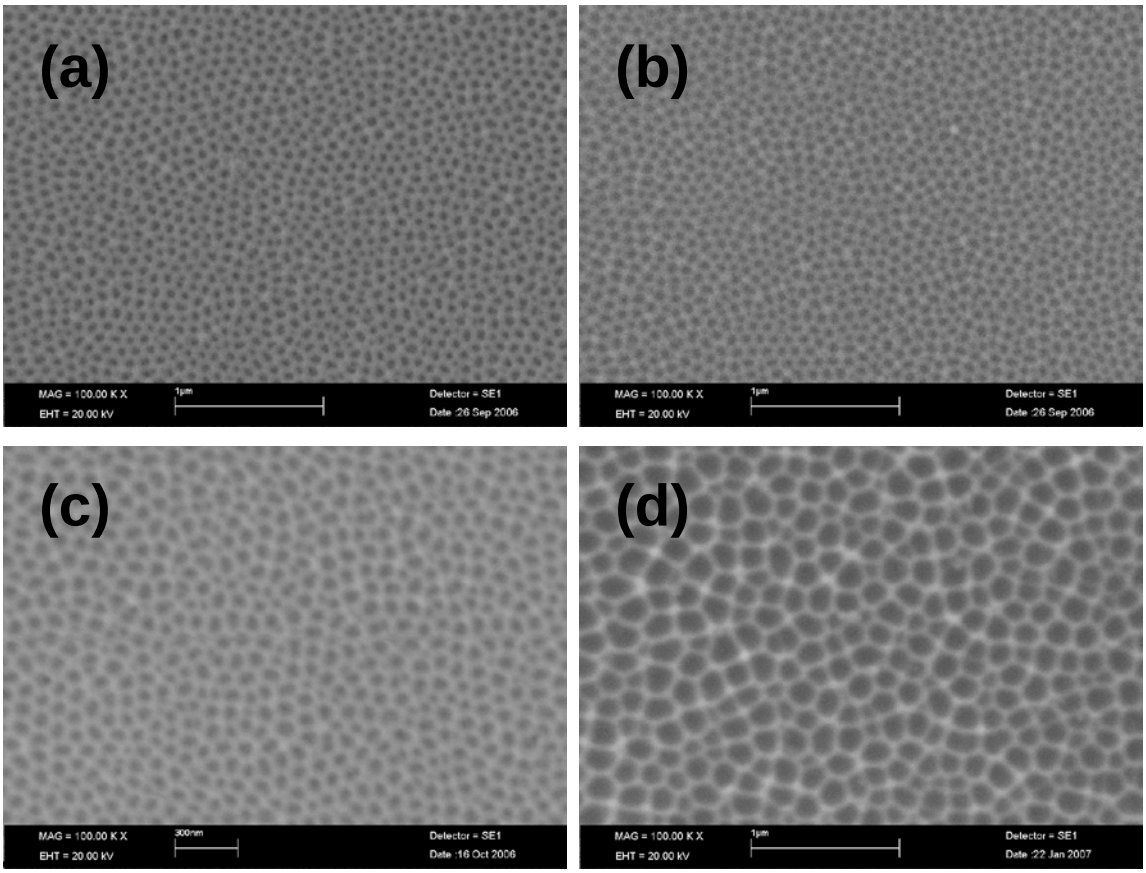

Fig 3.1.4 Effect of anodization voltages on nanopore size (a) V=60V, d=76.3 ± 14.5 nm (b) V=80V, d=91.7 ± 13.5 nm (c) V=100V, d= 119.8 ± 11.3 nm (d) V=120V, d=162.8 ± 22.8 nm

A theoretical linear relationship between anodization voltages and pore diameter of 1.29nm/V was described. (Losic and Simovic 2009) The four nanopore sizes under different anodization voltages were plotted in Fig 3.1.5. A linear trendline for the curve was fitted while intercept was set as 0 to simplify the rules. The equation is y = 1.2625x when R^2= 0.9408, which means the theoretical linear relationship between anodization

voltages and pore diameter is 1.2625 nm/V for the two step anodization process. In our experiments, the two-step anodization method were successfully setup and the nanopore sizes could be controlled by monitoring anodization voltages while other conditions keep unchanged.

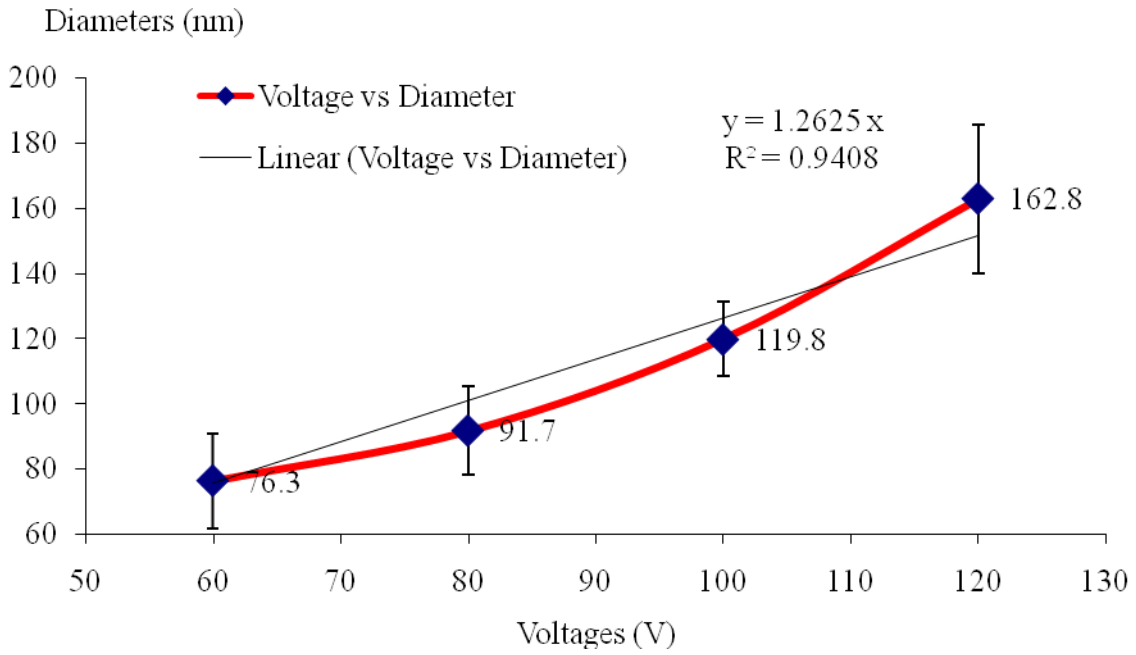

Fig 3.1.5 Relationship between anodization voltage and nanopore diameters

3.1.3 Distribution of nanopore sizes for different average diameters

Fig 3.1.6 shows the nanopore size distribution for different nanoporous alumina membranes which were fabricated by applying different anodization voltages. From the images, when anodization voltage is 60 V, the nanopore sizes are mainly between 60 nm and 80 nm, which occupy 65%. of all the nanoores. At the same time there are also 21% of the nanopore sizes which are between 80 nm and 100 nm. When the anodization voltage is 80V, 65% of the nanopore sizes are between 80 nm and 100 nm, which is larger than the previous one. And only 17% are below 80 nm while 13% are between

100 nm and 120 nm. When anodization voltage is 100V, the diversity is not high and the nanopore sizes are very uniform since most of the nanopores are between 100 nm (data not shown) and 130 nm. They are nearly 23% between 100 nm and 110nm, 33% between 110 nm and 120 nm, and 27% between 120 nm and 130 nm, respectively. When the anodization voltage is 120V, the nanopore sizes are much larger than the previous ones. 42% of the nanopores are between 160 nm and 180 nm, while the previous three samples only have a very few nanopores in this range. And 19% of the nanopores are even larger than 180 nm while 24% are between 140 nm and 160 nm.

From the distribution of the nanopore sizes, it can be concluded that the nanopores diameter can be controlled by adjusting the anodization voltages, because the higher anodization voltage can increase the dissolution speed. And the theoretical linear relationship mentioned before can be used to predict the average nanopore sizes during the two-step anodization. However, not all the nanopores have the same size or within in a very narrow range. It may be due to the non-uniform conditions of the surface properties before anodization since the aluminum is not a 100% pure metal, and the purity is around 99.9%. There must be impurity on some sites of the surface as well as inside of the aluminum, and this may lead to the differences among the nanopores. The nanopore size distribution condition also has an important effect on the ion diffusion rate of the whole membrane, although the average value of the nanopores diameters is the main parameter.

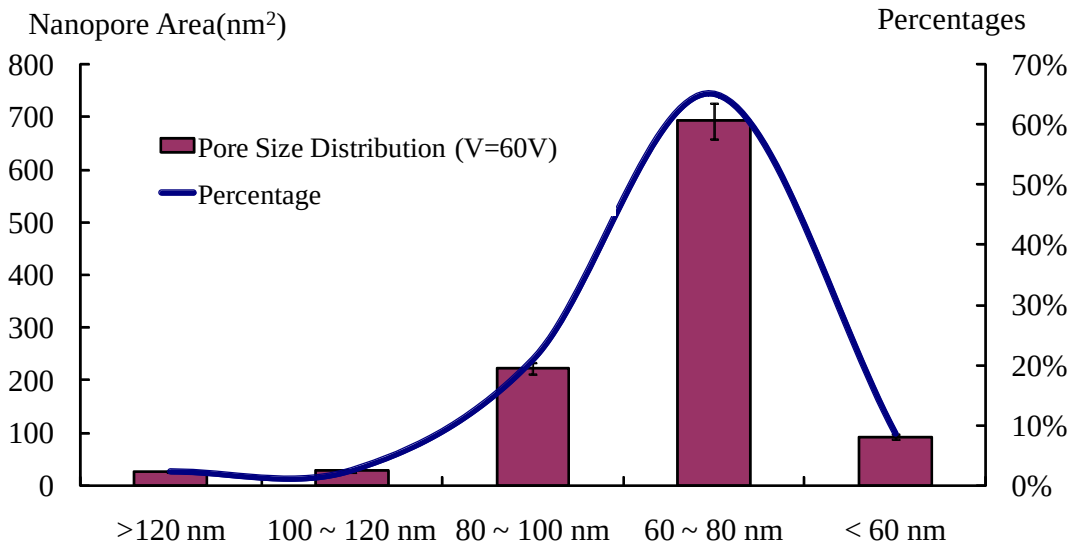
Nanopore Area(nm²)
Percentages
800
700
600
500
400
300
200
100
0
70%
60%
50%
40%
30%
20%
10%
0%
Pore Size Distribution (V=60V)
Percentage
>120 nm
100 ~ 120 nm
80 ~ 100 nm
60 ~ 80 nm
< 60 nm

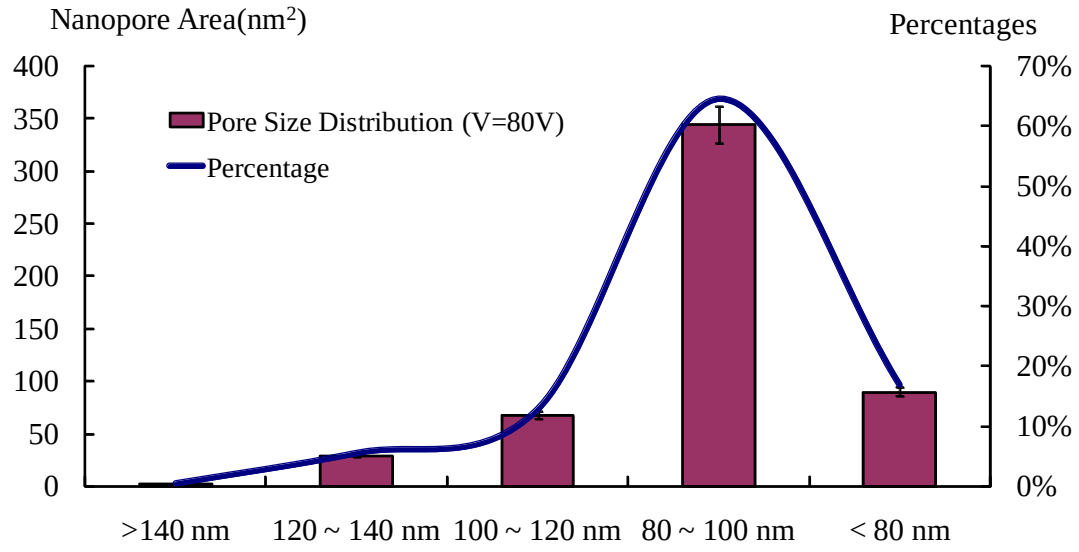
Nanopore Area(nm²)
Percentages
400
350
300
250
200
150
100
50
0
70%
60%
50%
40%
30%
20%
10%
0%
Pore Size Distribution (V=80V)
Percentage
>140 nm
120 ~ 140 nm
100 ~ 120 nm
80 ~ 100 nm
< 80 nm

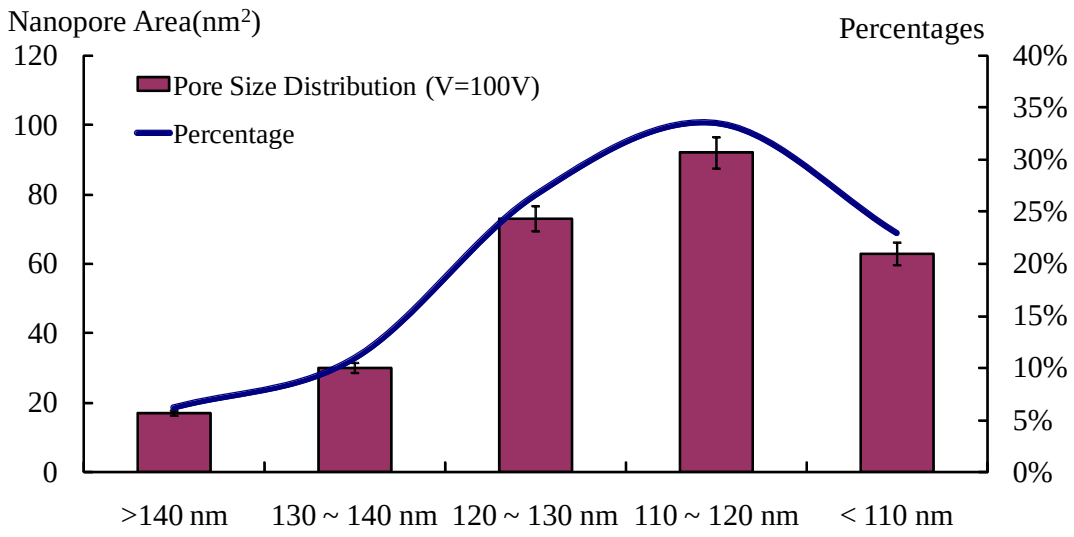

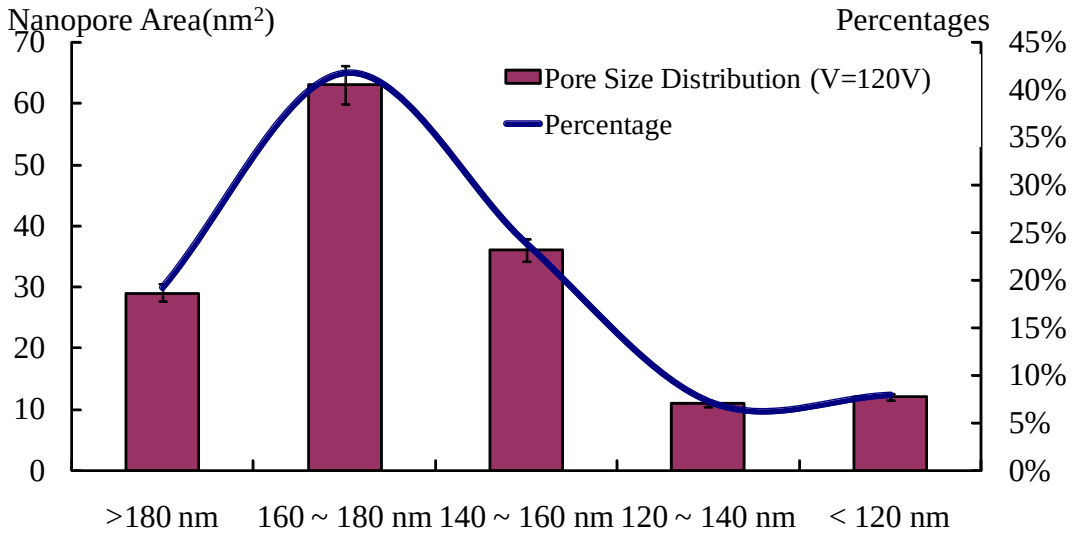

Fig 3.1.6 Pore size distribution under different anodization voltages

3.1.4 Anodization results when high electrical current applied

As we described before, anodization voltage is the main factor to control nanopore diameters and nanopore size distribution. The anodization voltage needs to be controlled during the two-step anodization fabrication while electrical current is less important. Fabrication process may change the temperature of the solution or the ion concentration

of oxalic acid, which may finally result in higher electrical current and change the surface properties.

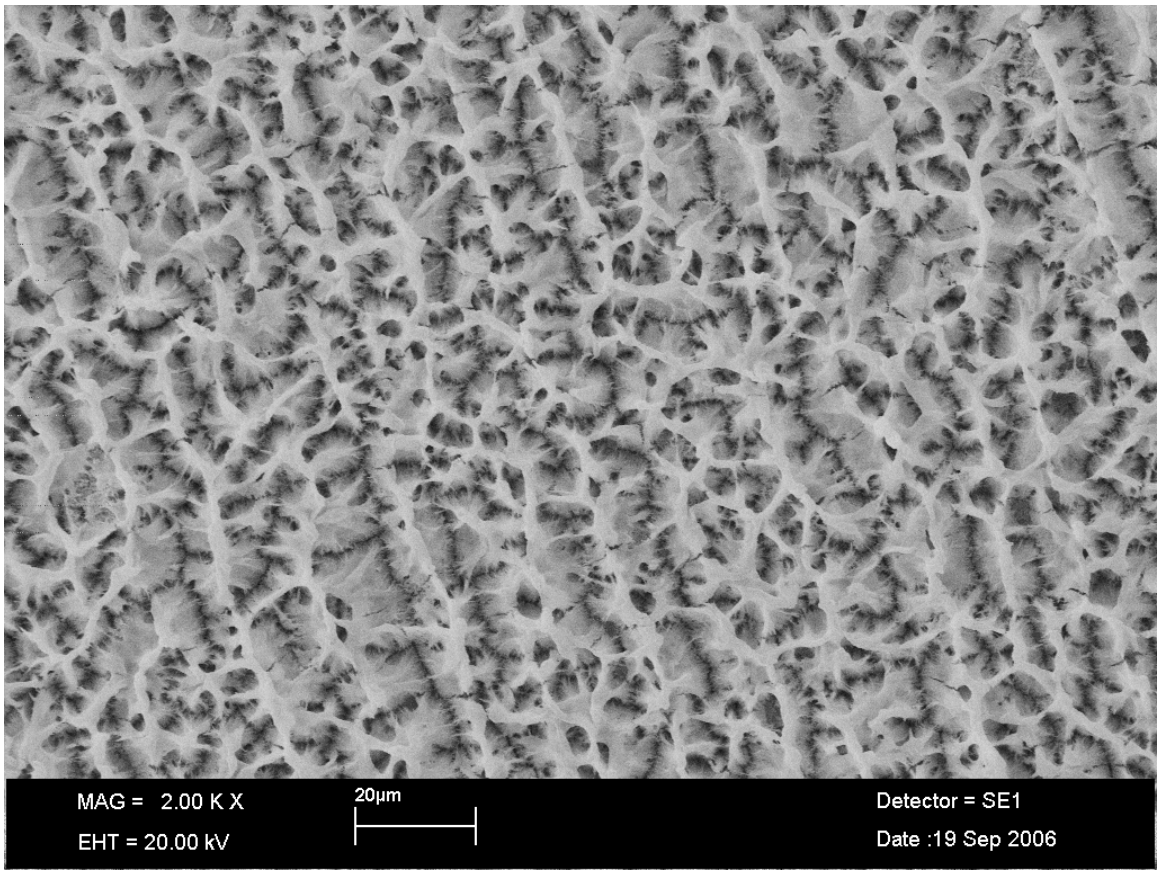

Fig 3.1.7 SEM image of fabricated alumina membrane when V=120V, I>500mA.

Fig 3.1.7 shows a SEM micrograph of fabricated alumina membrane when voltage is 120 V but current is above 500 mA after 2 hours anodization. No nanopores can be found and only topography like mountain chains and valleys appears on the surface. Too high current may etch the surface heavily and connect all the nanopores together to form this mountain and valley like topography, which was far from the nanopores topography. So, the electrical current should be kept less than 200 mA during the whole fabrication process. If higher current is noticed during the process, the fabricate process should be

paused, the oxalic acid solution should be replaced with new one, and the environment should be cooled down to the initial one to ensure the conditions recovery. This may be helpful to acquire nanopores with uniform pattern and similar sizes. Other researchers also reported a stable high-field anodization method. In that case, they controlled the nanopore sizes by changing acid electrolytes without raising the anodization voltages (Li et al. 2006). From the above results and analysis, the nanopores were successfully fabricated by the two-step anodization method and the average nanopore sizes could be controlled by adjusting anodization voltages.

3.2 Surface modification and micropatterning

Alumina surfaces show significant biocompatibility for cellular ingrowth (Swan et al. 2005b) (Wang and Liu 2009). However, the biocompatibility of the nanoporous alumina membranes may be different from the alumina, since surface topography were shown to influence cell adhesion, spreading, attachment, orientation and migration. Surface properties are important for long term biocompatibility, reliability, and durability for cells cultured on nanoporous alumina membranes. (Popat et al. 2005)

Adhesion of cells to biomaterials is an important prerequisite for the successful incorporation of implants or the colonization of scaffolds for tissue engineering (Marquis et al. 2009). Conventional biomaterial surfaces such as those formed by different biopolymers may possess a large degree of surface heterogeneity due to many different factors including the type and distribution of functional groups, presence of hydrophilic and hydrophobic domains, and surface roughness etc (Faucheux et al. 2004).

To prevent protein adsorption and cell adhesion, surface modification using hydrophilic polymers is one of the most effective methods (Jo and Park 2000). It was successfully used to change the properties of material surfaces to obtain controlling over the molecular composition and the resulting integral properties (Faucheux et al. 2004). Recent studies have used surface modification to evaluate the effect of surface charge, wettability and topography on protein adsorption and cell behavior using *in vitro* assay systems. Different molecules are used to modify the biomaterial surfaces, such as albumin, heparin, poly(ethylene glycol) (PEG), self-assembled monolayer (SAM), and phospholipids.

Among these different molecules or chemicals which can be used to change surface properties, PEG is most widely for surface modification because of its excellent properties such as hydrophilicity, flexibility, high exclusion volume in water, no toxicity, non-immunogenicity, and good biocompatibility. There are mainly two different methods for surface modification by PEG: simple physical adsorption and chemical bond formation, such as chemical coupling and graft polymerization. For research of long-term effect about PEG on the surface, it should not be removed easily from the surface, so covalent grafting is most preferred. A most widely used approach for covalent grafting is to introduce functional groups either to the surface or to the hydroxyl (-OH) group of PEG for chemical reaction between PEG and the surface.

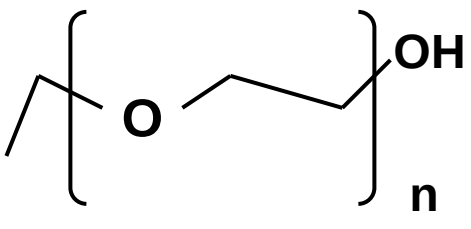

Fig 3.2.1 Chemical structure of PEG

Silane is commonly used as a function group coupled to the surface and PEG, to immobilize and graft PEG on the nanoporous alumina membranes. In this project, self-assembly of silane was used to create modified surfaces capable of covalent bonding with PEG-DA during the photo-initiation of polymerization. A dense work of Al–O–Si bonds was formed during the silanization process and the hydrophobic silane monolayer was formed on the surface. When there was no silane treatment before PEG hydrogel deposition, it was hard for the hydrogel to adhere on the surface firmly but very easy to detach.

The nanoporous alumina membranes were treated with one kind of silane, 3-trimethoxysilyl-propyl-methacrylate (TPM). TPM has the chemical group MeO-Si-O- which can react with the –OH group. The OH- group is introduced on the surface by boiling in H_2O_2. TPM molecule also has vinyl group -C=C-, which can polymerize with vinyl group of PEGDA. Therefore, the PEG hydrogel can attach to the surface of nanoporous alumina membranes by covalent bonding.

To ensure the presence of PEG on the nanoporous alumina membranes, the modified surface was characterized by X-ray photoelectron spectroscopy (XPS), water contact angle and protein adsorption.

3.2.1 Analysis of XPS spectra for different surfaces

The unmodified and silane modified nanoporous alumina membranes were characterized by XPS measurement. XPS is a powerful tool to measure the elemental composition of materials, especially for the top 1-10 nm surface. Though the quantitative accuracy of XPS depends on many factors such as signal/noise ratio, peak intensity, surface volume homogeneity etc, it is still an effective quantitative spectroscopic technique.

Fig 3.2.1 shows XPS spectra of unmodified nanoporous alumina membrane. The general band including all the elements on the surface can be observed during the binding energy range from 0 eV to 1100 eV. The highest peak between 500 eV and 600 eV shows the existence of O 1s. The peak between 26 eV and 36 eV shows the existence of Al 2p. The existence of O 1s and Al 2p approves that the sample is made of alumina. But it is also noted that there is a peak between 279 eV and 300 eV, which is the peak of C 1s. It may be due to the remaining of oxalic acid (HOOC-COOH) on the surface. It is reasonable that the anodization process may introduce some carbon elements by using oxalic acid. The distribution of sulfur elements in nanoporous alumina membranes prepared by sulfuric acid electrolyte was investigated carefully by XPS and other methods (Ozao et al. 2003).

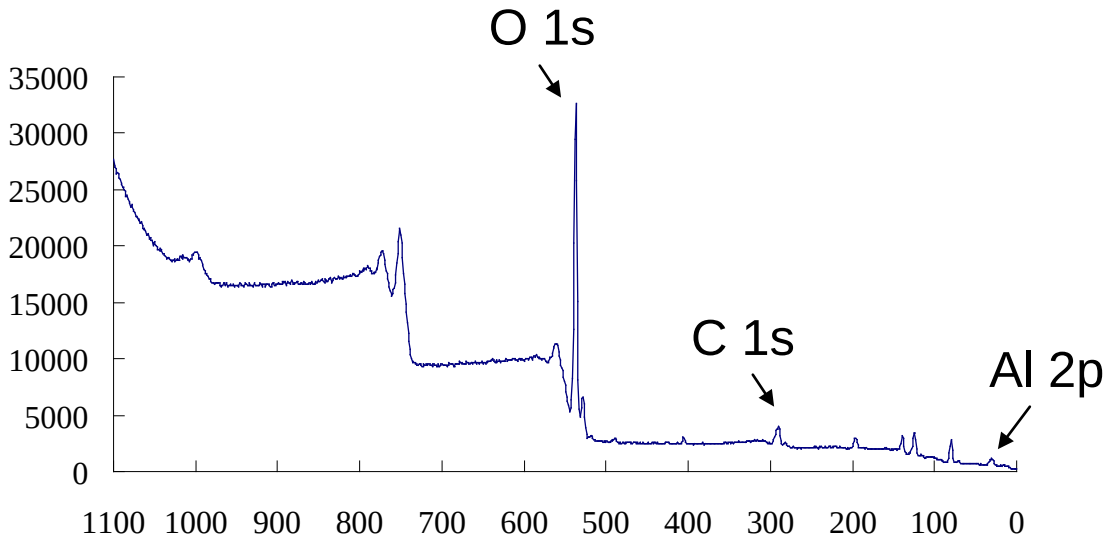

Fig 3.2.1 XPS spectra of unmodified nanoporous alumina membrane

Fig 3.2.2 shows XPS spectra of silane (TPM) modified nanoporous alumina membrane. Similar to the previous one, O 1s, C 1s and Al 2p peaks can be found from the spectra and a small peak between 106 eV and 110 eV shows the existence of Si 2p. Si element only exists in silane during the whole modification process, so it can be concluded that silane has been modified on the surface. Since it is only combined on the surface, so the amount of Si element is much less than other elements. And the amplitudes of O 1s and C 1s peaks are dramatically decreased. The amplitude of C 1s peak is much higher than the previous one, which also indicates the existence of silane since there is high C element in TPM ($C_{10}H_{20}O_5Si$). The XPS spectra measurements of different unmodified and modified alumina surfaces are consistent with the previous report. (Lee et al. 2005)

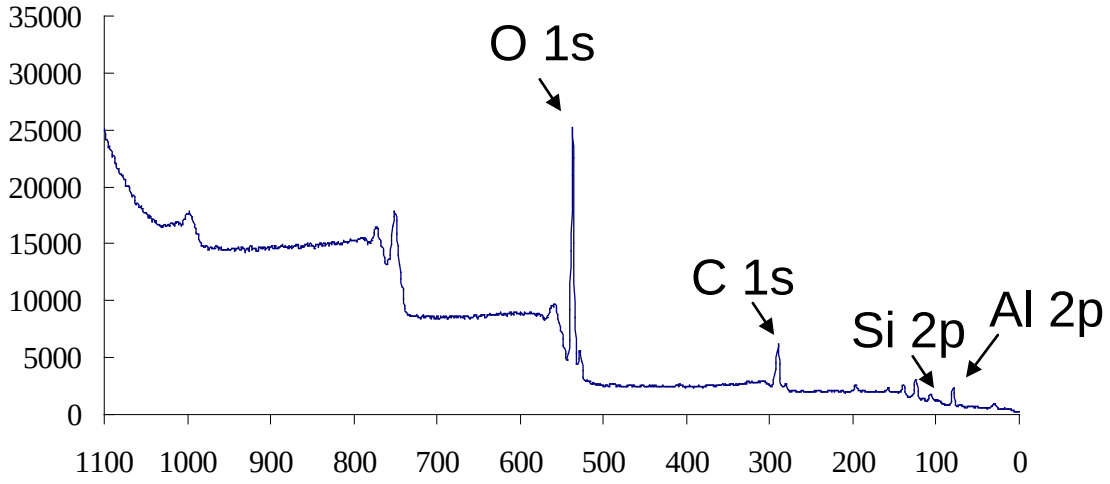

Fig 3.2.2 XPS spectra of silane modified nanoporous alumina membrane

3.2.2 Water contact angle measurements for different surfaces

Contact angle analysis measures the surface energy and ability of liquid, usually deionized water, to "wet" the surface, which is known as wettability. Surface energy is the free energy per unit area for creating new surfaces and is proportional to tendency of molecules to adsorb. Wettability gives information about whether a kind of material is hydrophilic or hydrophobic. A liquid droplet is first put on a solid surface. If the liquid droplet is very strongly attracted to the solid surface (for example water on a strongly hydrophilic solid), the droplet will completely spread out on the solid surface and the contact angle will be close to 0°. Less strongly hydrophilic solids will have a contact angle up to 90°. On many highly hydrophilic surfaces, water droplets will exhibit contact angles of 0° to 30°. If the solid surface is hydrophobic, the contact angle will be larger than 90°. On highly hydrophobic surfaces, the surfaces have water contact angles as high as ~120° on low energy materials e.g. on fluorinated surfaces. However some materials

with highly rough surface may have water contact angle greater than 150°. These are called super-hydrophobic surfaces.

The contact angle of water was measured on unmodified nanoporous alumina membrane, silane modified membrane and PEG grafted membrane. Images of water droplet on different nanoporous alumina membranes were captured. Fig 3.2.3 (a) shows the water droplet on the nanoporous alumina membrane without any modifications. When water droplet contacted the surface, it elongated and expanded on the surface very quickly and finally the height of the droplet is too short to be observed using eyes. The contact angle measured by software shows the angle is 6.25 ± 0.76º (N=20), which indicates the nanoporous alumina membrane is highly hydrophilic. Fig 3.2.3(b) shows the water droplet on the nanoporous alumina membrane after silane treatment of the surface. When a droplet of water is placed on the silane modified surface, the droplet tends to "bead up" and finally the contact angle exceeds 90º. The angles are 109.45 ± 9.89º (N=20), which indicates the silane modified nanoporous alumina membrane is hydrophobic. Fig 3.2.3 (c) shows the water droplet on the nanoporsou alumina membrane with PEG grafting after silane treatment. The water droplet also expands on the surface, but the speed is relatively slow and finally it still forms a droplet which can be observed by eyes. The water contact angles are measured to be 55.33 ± 4.40º (N=20), which indicates the surface property is hydrophilic which is different from the surface after silane treatment.

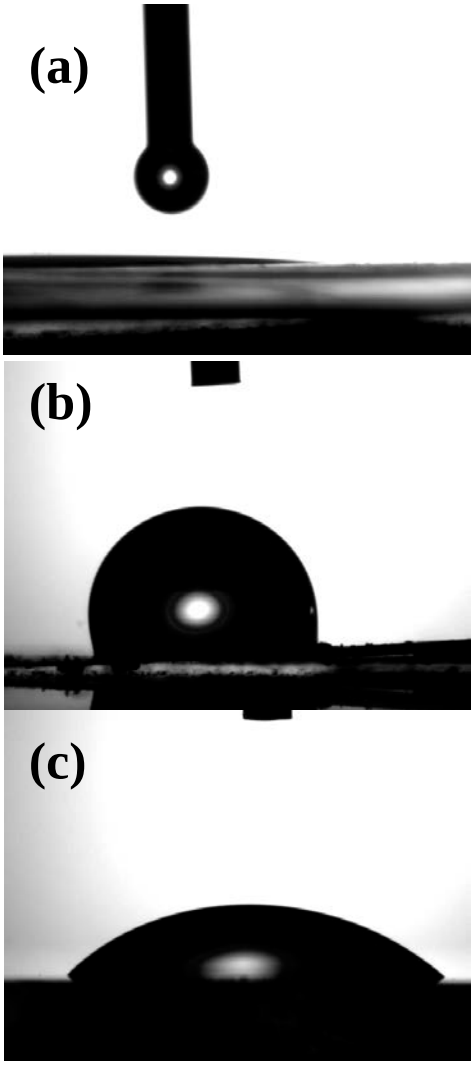

Fig 3.2.3 Images 10 μL water drops deposited on different surfaces (a) without silane modification (b) after silane treatment (c) after PEG modification

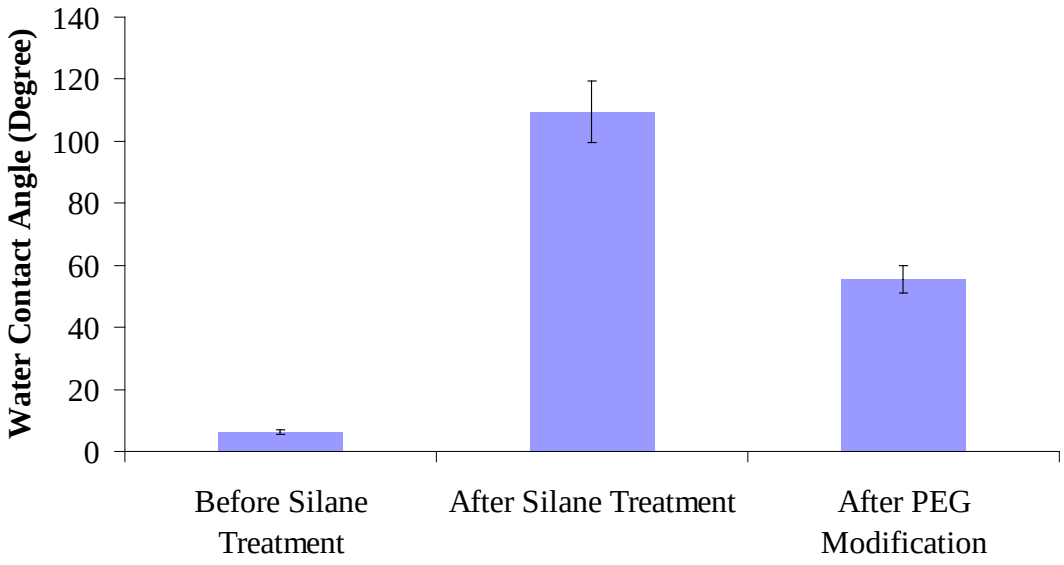

Fig 3.2.4 Water contact angle measurement on different surfaces

The water contact angles measured are plotted in Fig 3.2.4. It shows the values are 6.25 ± 0.76º (N=20), 109.45 ± 9.89º (N=20) and 55.33 ± 4.40º (N=20), respectively. From the results, nanoporous alumina membrane is hydrophilic, and it became hydrophobic after silane treatment, finally it became hydrophilic after PEG modification on the silane treated membrane. From other references (Ran et al. 2008), different nanopore sizes may also have influences on the surface properties. In this project, we use the nanoporous alumina membranes with nanopore sizes around 50 nm, which should be hydrophilic from earlier report, which is also approved in our experiments.

The big difference between the properties of surfaces before and after silane treatment indicates the technique is effective to change surface properties. The nanoporous alumina membranes are hydrophilic and become hydrophobic after silane treatment. which is good for protein adsorption and cell adhesion. Then, PEG can be covalently grafted to the silane treated surface and make it hydrophilic, which can repel protein

adsorption and cell adhesion. If only specific areas are covered by PEG, the differences between these coved areas and the left uncovered areas can show different protein adsorption behaviors. Thus, either making cell micro-pattern on the surface or microholes to confine cells can be acquired by this technique.

3.2.3 Effect of protein adsorption on different surfaces

After surface modification, the nanoporous alumina membrane surfaces without PEG covering become hydrophobic, which is suitable for protein adsorption. The PEG grafted surface is hydrophilic and it could repel protein adsorption. In order to testify the properties of different surfaces, protein adsorption experiments were taken.

The interaction of unmodified and modified membranes with rhodamine-labeled albumin (BSA) in solution was studied. Unmodified and silane-modified membranes were incubated with fluorescence labeled albumin in PBS (1mg/ml) for 1h. The albumin-adsorbed membranes were observed under a fluorescence microscope. PEG hydrogel is known to have resistive effects on proteins and cells due to its hydrophilic properties. Fig.3.2.5 (a) shows protein adsorption on unmodified nanoporous alumina membranes. The whole image is nearly black, which indicates there's even no protein on the surface. The surface of unmodified nanoporous membrane is highly hydrophilic and little protein is adsorbed on it. Fig 3.2.5 (b) shows protein adsorption on silane treated membrane. Since the surface has become hydrophobic and suitable for protein adsorption, the surface is red and it indicates lots of BSA were adsorbed on the surface. Fig 3.2.5 (c) shows protein adsorption on PEG modified surface. PEG is hydrophilic and

has shown to be effective in prevention of protein adsorption. It can be seen from the image that only some areas are a little red, which indicate that only few protein has been adsorbed on the surface. Fig 3.2.5 (d) shows BSA adsorption pattern on PEG/silane modified nanoporous alumina membrane with micropatterns. The microwells are silane treated membrane while the other areas were covered by PEG after silane treatment. It can be seen in the microwells there are lots of protein, but there was only few protein adsorbed on the other areas. The total protein adhered on the silane-modified microwells is much higher than that on PEG coated areas. The big difference in fluorescence intensity indicated the different protein adsorption capabilities. It can be concluded that the micropatterns with different capabilities of protein adsorption has been fabricated successfully.

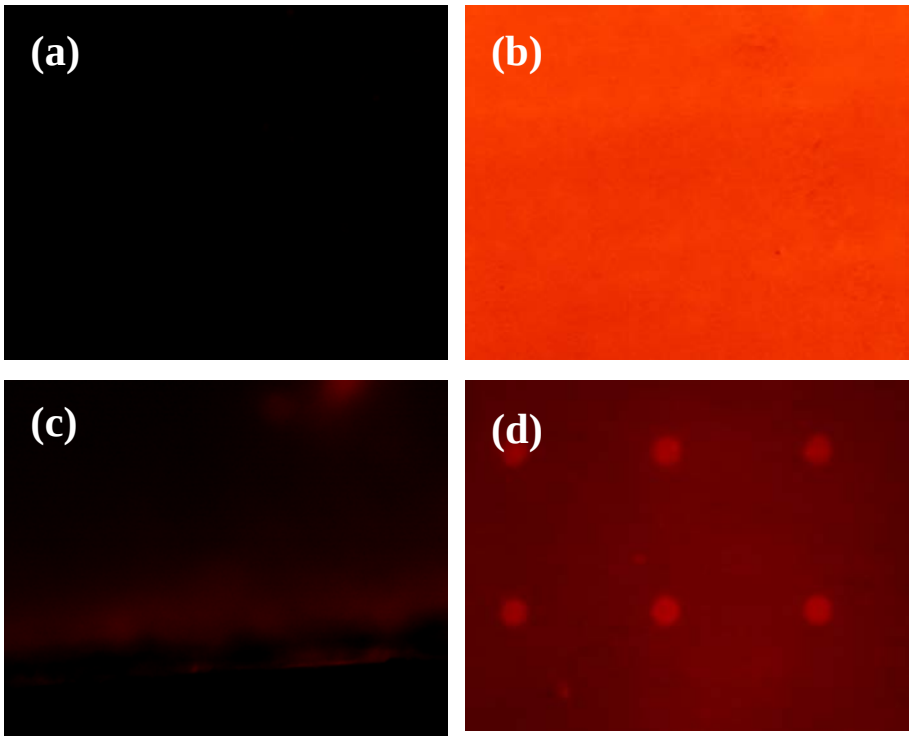

Fig.3.2.5 The images of fluorescent BSA adsorption (a) Fluorescence graphs of BSA on nanoporous alumina membrane without silane treatment, (b) silane-modified membrane (c) PEG coated membrane (d) protein adsorption patterns

The average fluorescence intensity for the entire images can be analyzed by MetaMorph. Data was normalized using silane treated membrane and plotted in Fig 3.2.6. Comparing with the silane treated surface, the surface without treatment could not adsorb any proteins while the surface with PEG modification can have only a little adsorbed protein. This data also can approve that the silane and PEG modification is effective to change the surface properties of nanoporous alumina membrane. It is much easier to absorb proteins on silane modified areas than PEG modified areas. And this will also enhance cell attachment when cells cultured on the Ectracellular Matrix Protein (ECM) pretreated surfaces.

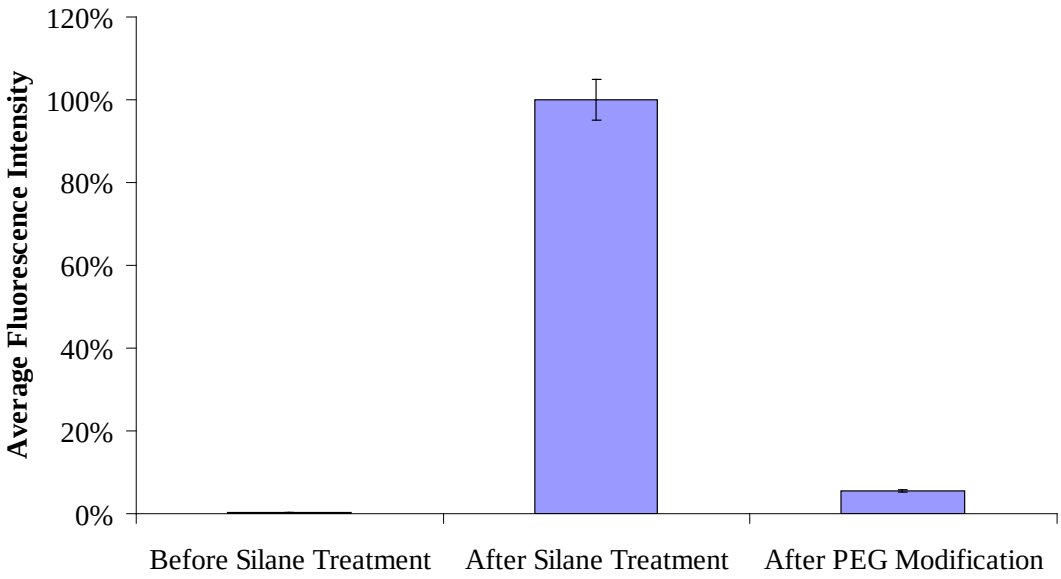

Fig.3.2.6 Average fluorescence intensity for different surfaces (Data was normalized using silane treated membrane.)

Our results have showed that surface modification was taken successfully using silane treatment, and the surface was hydrophobic after the treatment while the protein

adsorption was increased. This will finally induce better cell attachment, spreading and proliferation. Further grafting PEG on the surface after silane treatment makes the surface hydrophilic which can decrease the protein adsorption. This will finally make the surface effective in prevention of cell adhesion. By covering the selective areas of the nanoporous alumina surface with PEG , micropatterns could be achieved to confine the cultured cells and define sensing areas.

3.2.4 PEG Microwells on nanoporous alumina membranes

For the sensing purpose, the nanopores of the membrane should be open, and thus the nanopore structures after PEG grafting during the fabrication was explored. In our experiments, nanoporous alumina membranes with the size of 50 nm were fabricated with the DC voltage of 40V. Based on the SEM images, the fabrication process did not change the pore structure of the membrane and the “open” pores are exposed outside. No obvious changes were observed for the nanoporous alumina membrane structures with non-clogged pores on the bottom of the microwells. In the surrounding areas where PEG was UV polymerized, solid hydrogel was covalently bonded with silane-modified membrane, and this covering prevented the flow through portions underneath nanoporous membrane. This is very important for the microarray sensing applications. So each microwell is functionalized with the open nanopores for the sensing purpose independently and the impedance signals will not interfere with other microwells.

PEG hydrogel microwells were successfully fabricated on the functionalized nanoporous alumina membrane. A 20×20 array photomask of 100 um diameter was used to fabricate the negative patterns by UV initiated polymerization. The PEG micropatterns were anchored by silane monolayer on the nanoporous alumina membrane which was more stable than the physical adsorption methods. Before SEM analysis, the residual unreacted PEG was washed away by water and the clear spatial distribution of hydrophilic PEG and hydrophobic nanoporous alumina membrane was created. Fig 3.2.7(a) shows SEM image of four microwells in the array. For all the microwells, the white edges show the PEG hydrogel layer, the thickness of PEG hydrogel can be measured on the images and is approximately 10 μm. Nanoporous surfaces modified with silane was within the PEG hydrogel microwell. The diameter of the microwell is about 100 μm while the distances between microwells are 250 μm. Fig 3.2.7(b) shows a microwell on the modified nanoporous alumina membrane. The round microwell could be observed clearly in the image with a cleave in the edge area, which shows that region of PEG hydrogel was broken. Actually PEG hydrogel is fragile, and it is easy to be ruptured when it is dried. After the fabrication, the devices were always stored in distilled water. But before SEM analysis, all samples needed to be dried with nitrogen gun. So some indentations or gaps caused by the nitrogen gun could be found in some of the microwells.

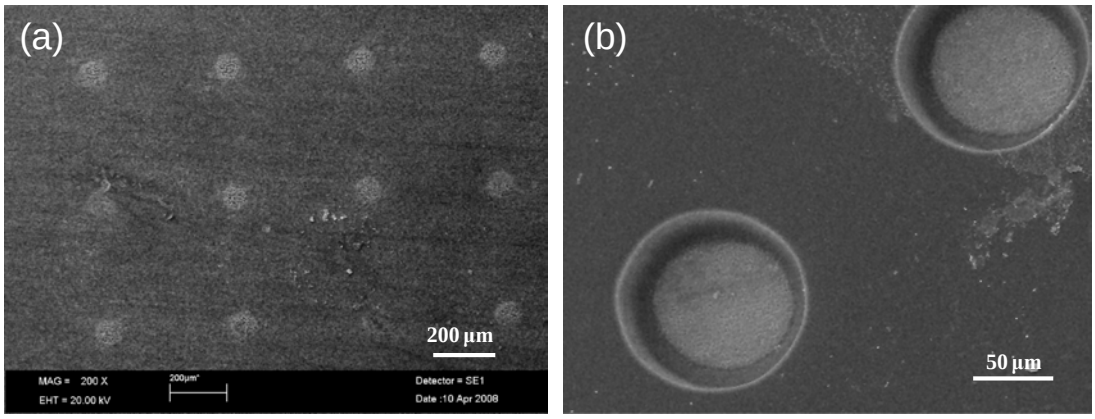

Fig 3.2.7 SEM image of microwell on nanoporous alumina membrane

In order to observe differences between PEG covered areas and areas without covering, an image with higher magnification was taken. Fig 3.2.8a shows a SEM micrograph of the edge area of a microwell. The left white region shows PEG hydrogel cover layer on the edge surface, and the right part shows nanoporous alumina membrane in the bottom. The nanopores are clearly shown in the right part while PEG is fully covered on the left part, which indicates the micro fabrication is successful to fabricate PEG microwells on the nanoporous surface. Fig 3.2.8b shows the bottom nanoporous membrane area where no obvious change is observed for the nanopore structures.

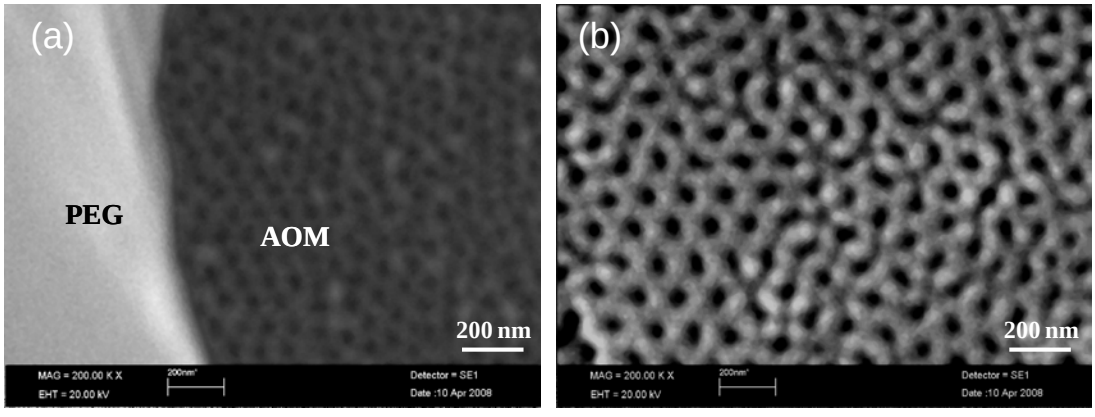

Fig 3.2.8 SEM micrograph of PEG and nanoporous alumina membrane

These results show that PEG micropatterns can be fabricated on the nanoporous alumina membranes after silane modification, which can be used to control spatial distribution of cells and define sensing area in the following experiments.

3.3 Diffusion Property of Nanoporous Alumina Membranes

Diffusion property allows ions or molecules to travel from higher concentration area to lower concentration areas. It is important to study the effects of nanopore size effects on diffusion properties of nanoporous alumina membranes. In this part, a chamber that uses nanoporous alumina membrane as filter membrane to separate solutions with different concentrations is built to conduct the experiments of diffusion study. Fig 3.3.1 is the schematic diagram of the chamber. A piece of nanoporous alumina membrane was adhered in the middle of a PDMS chamber in order to separate solution with different concentrations C_1 & C_2 in two compartments. In our experiment, the initial value of C_2 is 0, which is pure distilled water.

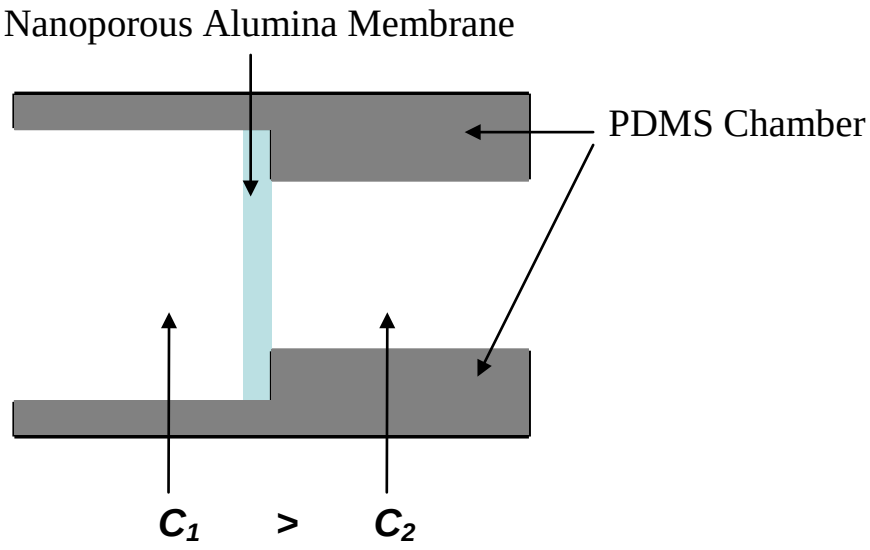

Fig 3.3.1 PDMS chamber with nanoporous alumina membrane as filter to separate solutions with concentrations C_1 and C_2

Nanoporous membranes with three different kinds of nanopore sizes of 20 nm and 100 nm are chosen. Three kinds of molecules with different concentrations are used in our experiments, including bovine serum albumin (BSA), insulin, and Cisplatin (cis-Diaminedichloroplatinum, CDDP). The concentration of molecule concentration can be measured by a UV-Visible spectrophotometer. It is based on the near absorbance of UV- light by the aromatic amino acids tryptophan and tyrosine, including small amount of protein residues such as cystine (disulfide bonded) and phenylalanine. The measured absorbance at wavelength 280 nm (A_{280}) of the protein sample was acquired. For Cisplatin, intensities of the maximum absorbance of cisplatin $\lambda = 301$ nm was acquired. To calculate the concentration, the absorption peak was compared to the curve from standard protein solutions, whose peak values were measured with UV-Vis before with known concentrations.

3.3.1 BSA diffusion using membranes with 100 nm nanopores

Bovine serum albumin is a serum albumin protein that has numerous biochemical applications, because of its stability, its lack of effect in many biochemical reactions, and its low cost. We would investigate the diffusion effect of (a) different BSA concentrations with same pore size; (b) the BSA solutions at the same concentration with different pore size; (c) diffusion rate of BSA in different pore size. We prepared BSA solutions in six different concentrations C_1: 0.1 mg/ml, 0.5 mg/ml, 1 mg/ml, 5 mg/ml, 10 mg/ml, and 20 mg/ml (all in w/v). 100 μL solutions in the right part of the chamber are taken out and the concentration are measured at different time points. Two types of nanoporous alumina membranes with different nanopore sizes of 20nm and 100nm are used.

When using the membranes with 100 nm nanopores, the data was plotted in Fig 3.3.2. Y axis represents the final concentration of the solution in the right part of the chamber (C_2, w/V), and X axis means the different time points (t, min) when the 100 μL solutions are taken out and measured. For every initial concentration C_1, it is observed that all the curves show the similar trend. The concentrations of C_2 increased over time, which shows the protein diffusing process from the left compartment to the right compartment through the nanopores over time.

The slopes of the lines between every two points indicates the diffusion rates in the time interval between the points. For the first 30 minutes, the slopes are obviously larger than

the following time, which means the diffusion rate is highest at the beginning. After 90 minutes, the slopes are close to 1, especially for the high initial concentration ones, which means the final concentrations nearly remain unchanged after 90 minutes. The slopes of the lines between 30 minutes and 60 minutes, and the ones between 60 minutes and 90 minutes, are similar to each other.

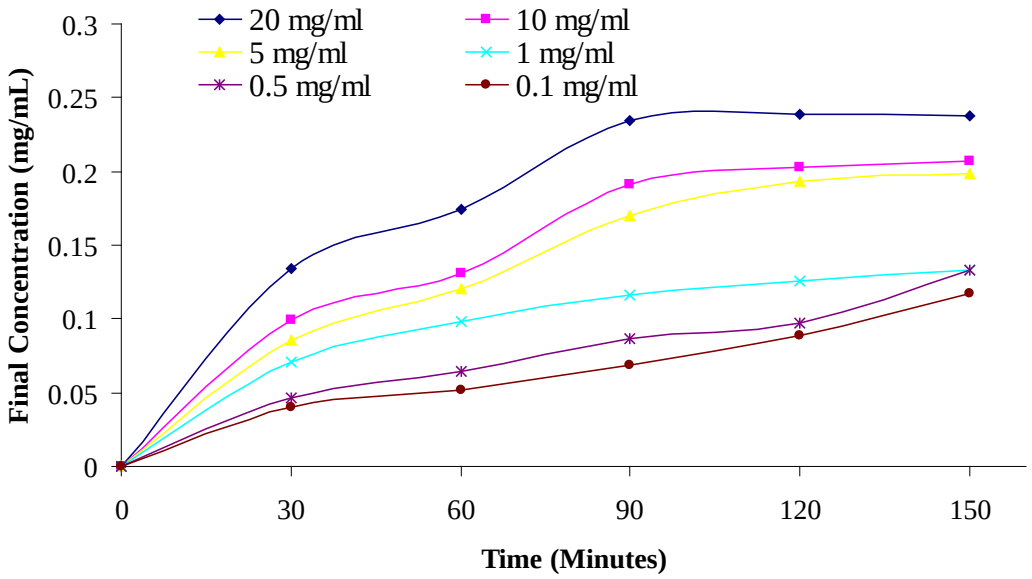

Fig 3.3.2 Final concentration of C_2 for BSA diffusion experiments at different time points (average nanopore diameters D=100 nm)

For initial diffusion stage analysis, final concentration data C_2 between 30 minutes and 90 minutes is taken out for further analysis which is plotted in Fig 3.3.3, to find out the relationship between the final concentrations of the solution in the left part and time points for every initial concentration. Y axis is the final concentration C_2 by subtracting the data at 30 minutes, X axis is the time points starting from T= 30 minutes. Data was fitted and the equations were shown.

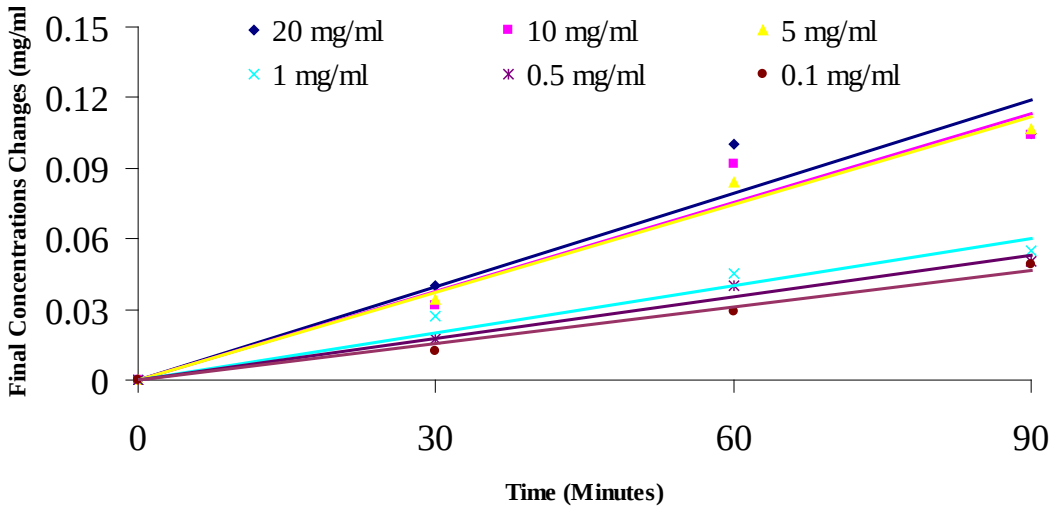

Fig 3.3.3 Final concentration changes between 0 minutes and 90 minutes

For C_1= 20 mg/ml, the equation between C_2 and t is C_2=0.0016 t, where R^2= 0.9842

For C_1= 10 mg/ml, C_2=0.0014 t, where R^2=0.9641.

For C_1= 5 mg/ml, C_2=0.0013 t, where R^2=0.9857.

For C_1= 1 mg/ml, C_2=0.0008 t, where R^2=0.9842.

For C_1= 0.5 mg/ml, C_2=0.0007 t, where R^2=0.9923.

For C_1= 0.1 mg/ml, C_2=0.0005 t, where R^2=0.9882.

The slope of the lines can be described by the coefficients, which reflects the diffusion rate over the time change, R^2 is close to 1, shows the final concentration is linear related with diffusion time.

The diffusion rates for higher initial concentrations are obviously higher than the lower ones. A solution with higher initial concentration C_1 would create a higher concentration gradient between two compartments of the chamber, so the molecules from a high concentration region will migrate to a low concentration region. The larger gap of the

concentration gradient, the faster of the molecules move. Therefore in this case, when a higher concentration of BSA is applied, the higher rate of diffusion will appear. But the diffusion rates are not proportional to the initial concentrations. For the 20 mg/ml concentration solutions, its diffusion rate is around 0.0016 mg/(ml*min), and for the 10 mg/ml the value is 0.0014 mg/(mg*min). The concentration for the first one is two times than the second one while the diffusion rate for the first one is only 14% higher than the second one. Similar relationships can also be found for other concentrations. The highest initial concentration is around 200 times to the lowest one, but the diffusion rates for the highest ones are only three times than the lowest one. The diffusion constant can be calculated and it can be concluded even for the nanoporous alumina membranes with average diameter 100 nm, not all the nanopores are the same sizes and open fully for the protein. The conclusion corresponds to the pore size distribution analyzed before.

3.3.2 BSA diffusion using membranes with 20 nm nanopores

When using the membranes with 20 nm nanopores, data is plotted in Fig 3.3.4. The meanings of Y and X axis are similar to Fig 3.3.3. For every initial concentration, the final concentrations also increase over time and the protein diffuses through the nanopores over time. But the final concentrations at every time points are smaller than the ones for 100 nm membranes, which indicates the diffusion rates for 20 nm membranes are smaller than 100 nm ones. For the first 30 minutes, the slopes are also obviously larger than the following time, which means the diffusion rate is higher at the beginning than the other times. But even after 150 minutes, the slopes are not close to 1, which means the concentrations hasn’t reached equilibrium after 150 minutes. For every

initial concentration, the slopes of each line between 30 minutes and 150 minutes are similar to each other.

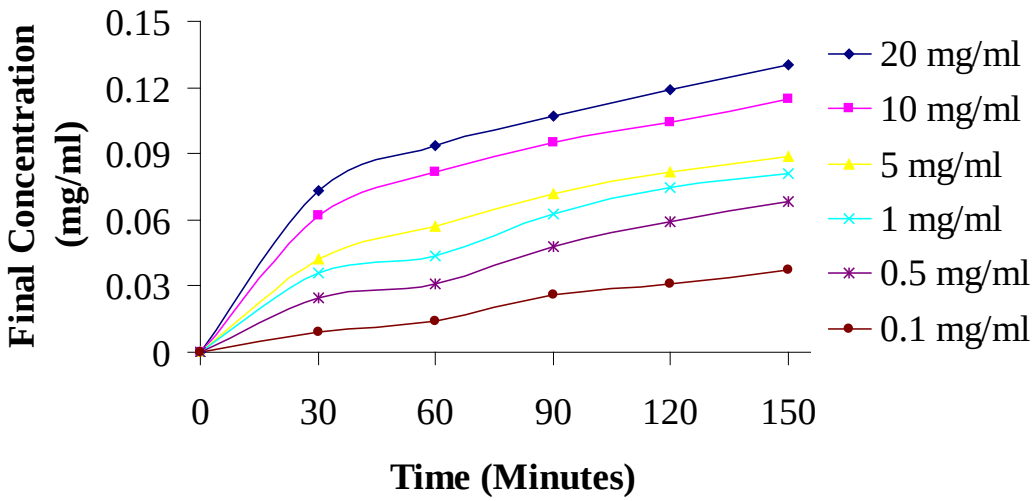

Fig 3.3.4 Final concentration of C_2 at different time points (average nanopore diameters D=20 nm)

For initial diffusion stage analysis, data of C_2 between 30 minutes and 150 minutes were plotted and fitted as six lines in Fig 3.3.5. Using the same methods for 100 nm membranes analysis, data was fitted with lines and the equations are shown.

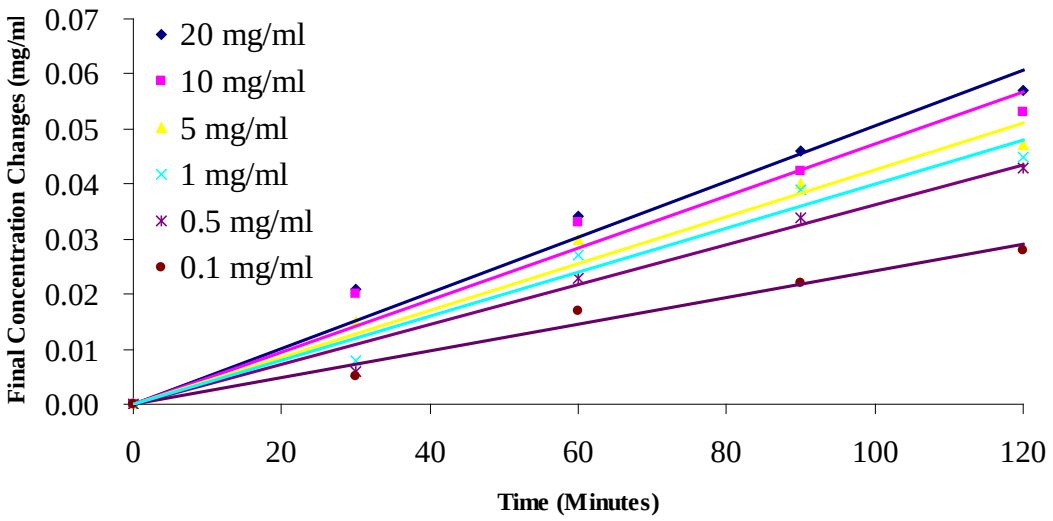

Fig 3.3.5 Final concentration changes between 30 minutes and 150 minutes

For C_1= 20 mg/ml, the equation between C_2 and t is C_2= 0.00049t, where R^2= 0.9684.

For C_1= 10 mg/ml, C_2=0.00045 t, where R^2= 0.9590.

For C_1= 5 mg/ml, C_2=0.00040 t, where R^2= 0.9694.

For C_1= 1 mg/ml, C_2=0.00036 t, where R^2= 0.9715.

For C_1= 0.5 mg/ml, C_2=0.00032 t, where R^2= 0.9792.

For C_1= 0.1 mg/ml, C_2=0.00021 t, where R^2= 0.9773.

Different from the 100 nm membranes, the diffusion rates for higher initial concentrations are not much higher than the lower ones for 20 nm membranes. For the 20 mg/ml concentration solutions, its diffusion rate is around 0.00049 mg/(ml*min), and for the 10 mg/ml the value is around 0.00045 mg/(mg*min). The concentration for the first one is two times than the second one while the diffusion rates for the two concentrations are very close to each other. Similarly, the diffusion rate for concentrations 5 mg/ml, 1mg/ml are around 0.00040 and 0.00036 mg/(ml*min),

respectively. For the solution with concentration 0.5 mg/ml, the diffusion rate is around 0.00032 mg/(ml*min). Only for the lowest concentration 0.1 mg/ml, the diffusion rate was decreased as 0.00021 mg/(ml*min). The highest concentration we measured is around 200 times to the lowest concentration, but the diffusion rates for the highest ones are only 2.5 times than the lowest one. It can be concluded even for the nanoporous alumina membranes with average diameter 20 nm, it is harder for protein diffusion through the nanopores, maybe only a few of nanopores allow the protein diffusion, which make the higher concentration solution could not diffuse quicker than the lower concentration ones.

The size of nanopores may have the influences on the diffusion of proteins when the diameters are comparable with the size. The relationship between the two sizes was studied during BSA diffusion procedure. In the diffusion experiments with different nanopore sizes, other conditions are kept unchanged. To compare the different diffusion rate of 20 nm and 100 nm nanopores, the values of coefficient for different initial concentration were plotted in Fig 3.3.6. Y axis represents values of coefficient for the equations which are the diffusion rates for the nanoporous alumina membranes between 30 minutes and 90 minutes, or 150 minutes, respectively. X axis represents the initial concentrations, the bars with purple color are data for 100 nm membranes, and the bars with red color are data for 20 nm membranes. For every initial concentration, the diffusion rates with 100 nm membranes are significantly higher than the ones with 20 nm membranes. For 20 mg/ml initial concentration, the diffusion rate for the 100 nm membrane is 3 times larger than the 20 nm one, but for 0.5 mg/ml solutions, the diffusion rate for the 100 nm one is only 2 times larger than the 20 nm ones. For every

initial concentration, the coefficient value for 100 nm nanopores is larger than 20 nm nanopores, which suggests that 100 nm pore size has a higher permeability of BSA than 20 nm pore size. This shows that the diffusion rate is larger for nanoporous membranes with larger pore size if other conditions are the same (i.e. room temperature, normal pH and pressure).

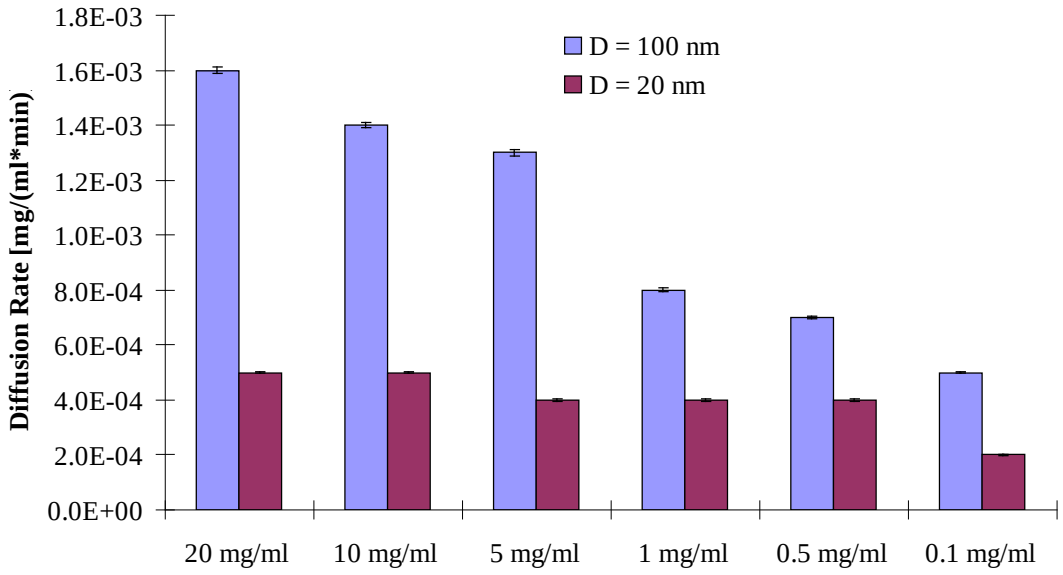

Fig 3.3.6 Comparison of diffusion rates between nanoporous alumina membrane with different nanopore diameters (purple: 100 nm, red: 20 nm)

Similar experiments with two other biomolecules, insulin and CDDP, were also explored. For all these biomolecules, it is illustrated that there are more diffusion taken place in a relative larger nanopores. Furthermore, the relationship between molecular weight and size of the testing molecules should also be considered. The molecular size should be much smaller than the nanopores, to ensure the passage of them through the nanopores. Those molecules with large molecular size may be constrained by the nanoporous alumina membrane. Therefore, only suitable size of the molecules will be transported in

the appropriate size of the alumina membrane. The nanoporous membrane with appropriate nanopore sizes has a controlling function which can restrict the transport of relative large molecules.

3.3.3 Diffusion properties for different molecules

To demonstrate particular characteristics of the nanoporous membrane, it is proposed that the controlling system is based on the alumina nanoporous membrane with different pore size. The diffusion of BSA, insulin and CDDP with same concentrations of 0.01, 0.05, 0.1 mg/ml was used. They are tested in a testing device with 20 nm and 100 nm, respectively. The diffusion rate with respect to its concentration was plotted in Fig 3.3.7

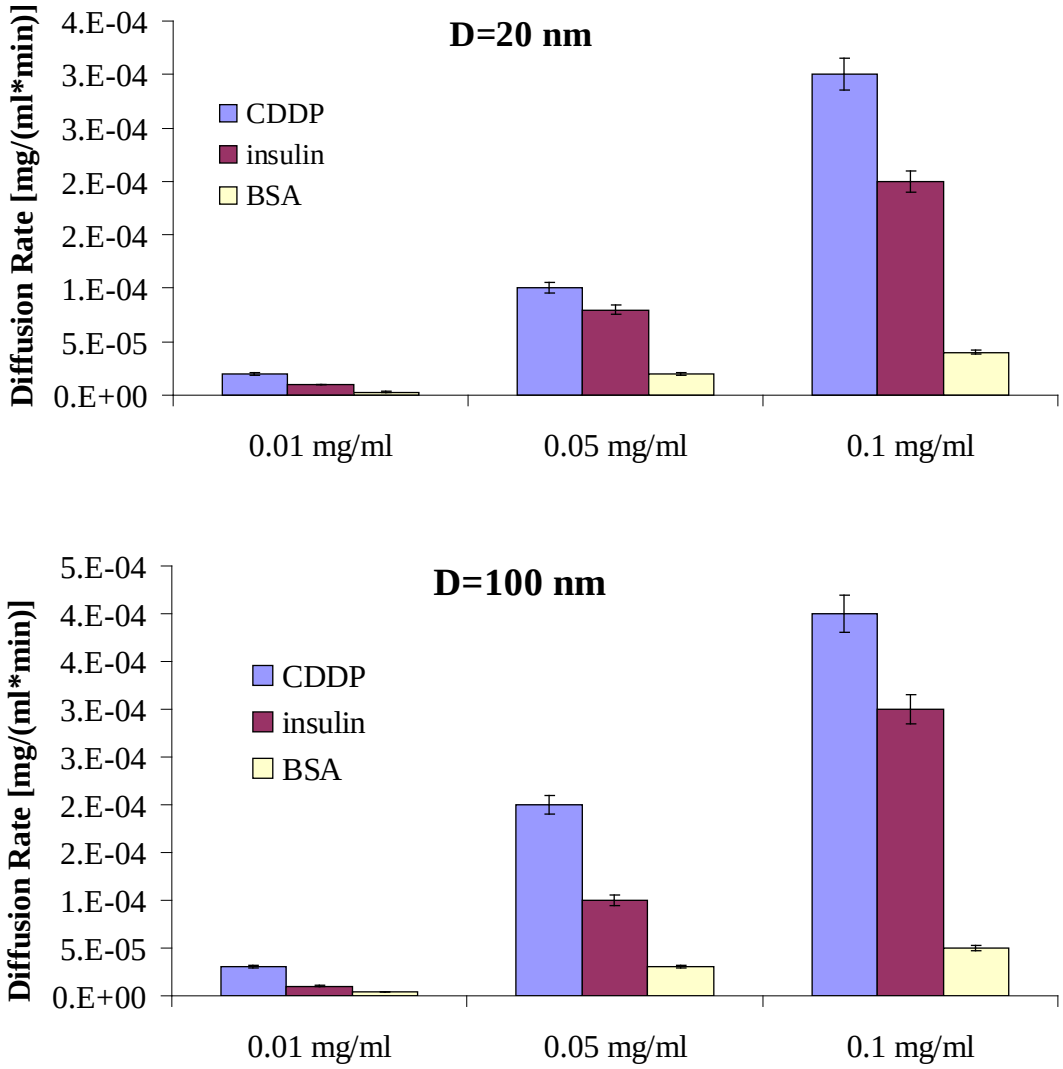

Fig 3.3.7 Diffusion rates of different proteins of nanoporous alumina membranes (upper) average nanopores diameter D=20 nm (lower) average nanopores diameter D=100 nm

The measured diffusion rate in both membranes showed a descending order as below: CDDP> insulin > BSA. For both 20 nm and 100 nm membranes, the measured diffusion rate of CDDP is the highest. Based on the result obtained, it is suggested that the diffusion rate is dependent on the molecular size of the molecules. The molecular weight of the above molecules was shown in an ascending relationship with the

increasing of molecular weight: CDDP (MW=300), insulin (MW=5808) and albumin (MW=67000). As the nanopore size increases, each of the molecules diffusion rate become larger. However, the diffusion rate of CDDP leads while those of other molecules are far behind. The reason is that CDDP has a quite small molecular size that can diffuse very freely in the two membrane pore size and the diffuse rate is even faster in a larger membrane. The small molecules always move faster than the bulky molecules. In addition, it is observed that the diffusion rate of CDDP measured using membranes with 20 nm nanopores is substantially less than that of membranes with 100 nm nanopores. This data suggest the diffusion rate of the molecules is constrained by the nanopore size when a specific molecule is chosen, result in a slower efflux through nanopore membrane.

The curve shows an inversely proportion relationship between the diffusion rate of the molecules. Herein, in extreme case, if the molecular dimensions are closer or larger than the nanopores, there is only few or even no diffusion. Thus, when a specific molecular was chosen, membranes with larger nanopores should be used to do the diffusion. For nanopores which are much larger than the molecular dimensions of the solute, the diffusion rate increase and the relationships are fitting to the Fickian diffusion model. The diffusion rate is proportional to the concentration differences. Linear relationships were found between 30 minutes and 120 minutes. For nanopore size that is slightly higher or close to the molecular dimensions of the solute, the diffusion rate is constrained; non Fickian diffusion model is observed.

The diffusion effect of three protein molecules through a nanoporous membrane was identified. The solution of bovine serum albumin (M_w = 67000 Da), insulin (M_w = 5808 Da) and CDDP (M_w = 300) in different concentrations were studied. The final concentration is increasing over time. In the three testing solution, BSA also shows the highest final concentration when the same initial concentration is applied. Although both 20 nm and 100 nm membranes allow proteins to diffuse and transport, the 100 nm membrane always shows a higher diffusion rate than 20 nm membranes. So we choose 100 nm in the following experiments which need ions diffusion. Higher molecular weight results in lower diffusion rate when other conditions kept unchanged. When a protein or drug is chosen to be a potential candidate for drug delivery, nanoporous alumina membranes with larger nanopores than the size of the molecules should be applied.

3.4 Cell behavior and biocompatibility of nanoporous alumina membranes

The two step anodization technique to fabricate nanoporous alumina membrane proves to be a reliable and repeatable method. Surface modification was shown to be effective to change the surface properties to induce or prevent protein adsorption on specific areas of the surface. The nanopores are fully open and allow the diffusion and transport of proteins, which was confirmed by diffusion experiments. The next question is cell biocompatibility of nanoporous alumina membranes. The impedance measurement can be applied only if the cell behaviors are normal when cultured on the membranes. The surface directly contacts with cells. Both chemical and topographical properties of the

material surface can play an important role in determining cell behavior. For biomedical applications, controlling cell responses to a bio-material is of interest with regard to tissue culture. (Tan and Saltzman 2002) In our project, cells were successfully cultured on nanoporous alumina membranes and monitored to testify the biocompatibility.

3.4.1 Stem cells cultured on nanoporous alumina membranes

Mesenchymal stem cells (MSCs, purchased from ATCC) were cultured on nanoporous alumina membranes. The cells were visualized by fluorescence microscopy after staining. Fig 3.4.1 shows the fluorescence images of MSCs cultured on nanoporous alumina membranes after 4 days of cell culture. Fig 3.4.1(a) shows cells stained with phalloidin-TRITC, from which we can see the cell cytoskeleton. Fig 3.4.1(b) shows the same cells stained with DAPI, from which we can see the cell nucleus. The cells spread on the surface very well while the cell nucleus were kept intact which could tell us the cell status are normal after they were cultured on the nanoporous alumina membranes surfaces for more than 4 days.

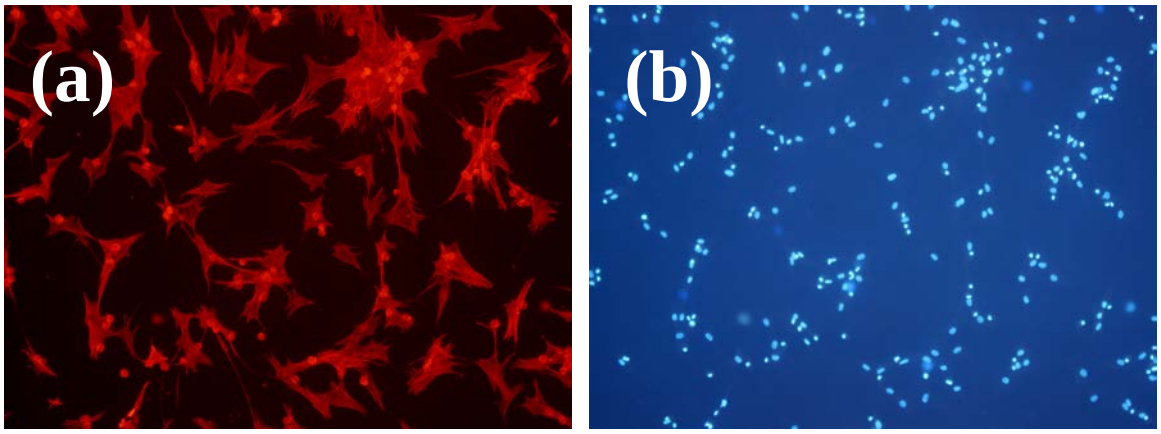

Fig 3.4.1 Fluorescence images showing mesenchymal stem cells (MSCs) cultured on nanoporous alumina membranes

MSCs are multipotent stem cells and they have ability to differentiate into specific cell lineages including fibroblast, osteoblast, chondrocyte or other cell types by providing different differentiation media. Recent studies have investigated the influence of nanoporous alumina membranes on MSCs proliferation and differentiation up to 3 weeks. The surfaces demonstrated much better results than control surfaces. (Popat et al. 2007)

3.4.2 Cancer cells cultured on nanoporous alumina membranes

KYSE30, a type of human esophageal squamous epithelial cancer cell line, is well differentiated human squamous cell carcinoma from esophageal cancer. It is widely used to determine the role and mode of inactivation of some important genes such as p15, p16 and p53 in human esophageal tumors. We cultured KYSE30 on different surfaces for

many days, especially on nanoporous alumina membranes, and SEM and fluorescence staining was used to observe the cells.

Fig 3.4.2 shows SEM micrograph of KYSE30 cancer cells cultured on nanoporous alumina membranes. Fig 3.4.2 (a) shows that cells maintain the morphology and spread on the surface very well. Many cells could be observed on the surface. Fig 3.4.2 (b) shows one cell in larger magnification. The cell is covered on the surface and it is spreading very well. It shows high degree of spreading and normal morphology on the surface. The length of cell cytoskeleton is many times larger than the cell diameters and it indicates that many nanopores under the cells have already been covered.

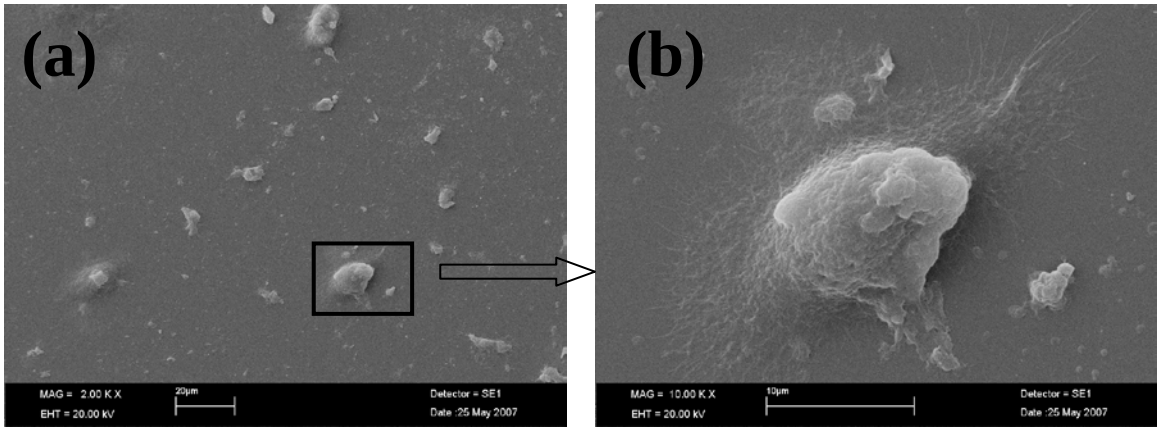

Fig 3.4.2 SEM micrographs of KYSe30 cultured on nanoporous alumina membranes (a) three cells shown (b) one cell shown in larger magnification

.

Fig 3.4.3 shows a KYSE30 cell in contact with the nanoporous membranes. The cell also shows spreading morphology and it has covered many nanopores of the membrane. It can be concluded that when ions intend to pass through the nanopores, they would only go the nanopores which are not been covered. The nanopores been covered by cells

would block the ions, hence the electrical current caused by the ions would decrease but the impedance would increase at the same time. Any cell morphology changes would change the numbers of nanopores covered by the cells, then to change the impedance. It is possible for us to monitor cell morphology changes by measuring impedance spectra.

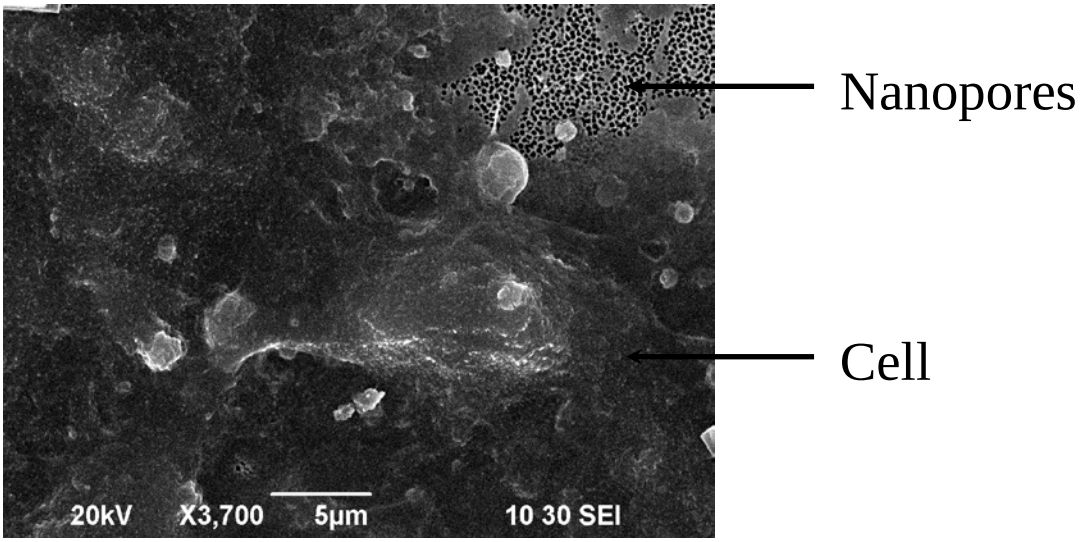

Fig 3.4.3 SEM images showing KYSE30 cells after 7 days in culture while covering many nanopores

3.4.3 Cancer cell proliferation on nanoporous alumina membranes

During 9 days of culture, different cells were stained with phalloidin-TRITC. Fig 3.4.4 shows KYSE30 cells cultured on nanoporous alumina membranes for different days. Fig 3.4.4 (a) shows the cells on day 3, many of the cells have already spread and covered on the surface. Fig 3.4.4 (b) shows the cells on day 5, there are more cells at the same sizes of surface and they also spread very well. Fig 3.4.4 (c) shows the cells on day 7, the concentration of cells are higher than before, but the difference between day 7 and day 5

is not as large as that between day 3 and day 5. Fig 3.4.4 (d) shows cells cultured on the surface for 9 days, the concentration is very high and cells have already form monolayer on the surface. Though the nanopores were not observed directly by fluorescence, it can be concluded that most of the nanopores were covered and blocked, to make the ions not pass through them. The images of cells at different stages show they exhibiting normal phenotype and morphology.

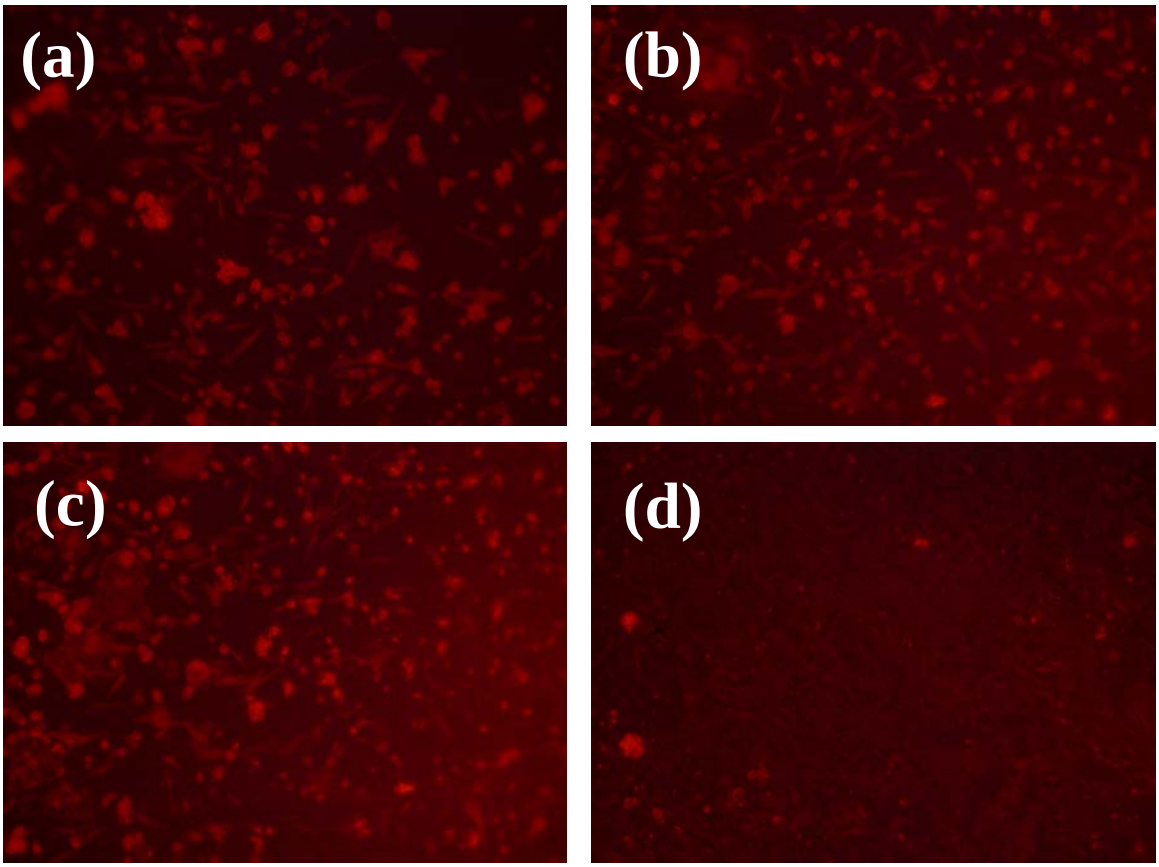

Fig.3.4.4. Fluorescence images of KYSE30 cells cultured on nanoporous alumina membranes surfaces for different days (a) Day3 (b) Day5 (c) Day7 (d) Day 9

The numbers of cells were counted from the fluorescence images and calculated. Fig 3.4.5 shows the concentrations of KYSE30 cells cultured on different surfaces for 3~9

days. On nanoporous alumina membranes, the concentration of cells has increased while the culture time lasted. At day 3, the concentration is around 1.90×10^5, at day 5 the concentration has increased to 2.68×10^5, which is 41% higher than day 3. At day 7, the concentration is around 3.71×10^5 and it is around 38% higher than day 5. At day 9, the concentration is around 4.23×10^5, which is around 9% higher than day 7. The increasing speed is smaller than before, which indicates the cells may have already formed confluent layer on the surfaces. Comparing day 9 to day 3, the concentration of cells has already increased by 213%.

On glass surfaces, the concentration is around 1.85×10^5 at day 3 and is around 3.87×10^5 at day 9, which is less than nanoporous alumina membranes. Glass surface could be considered as a control, and the membranes should have better biocompatibility than it. On pure aluminum surface, the concentration is around 1.82×10^5 at day 3 and is around 2.32×10^5 at day 9, it indicate this surface has negative impact on KYSE30 cells though other references reported alumina also supported cell growth and did not negatively affect cell viability (Popat et al. 2005). Among these three surfaces, nanoporous alumina membrane supports the highest cell proliferation and it has better biocompatibility than the other two.

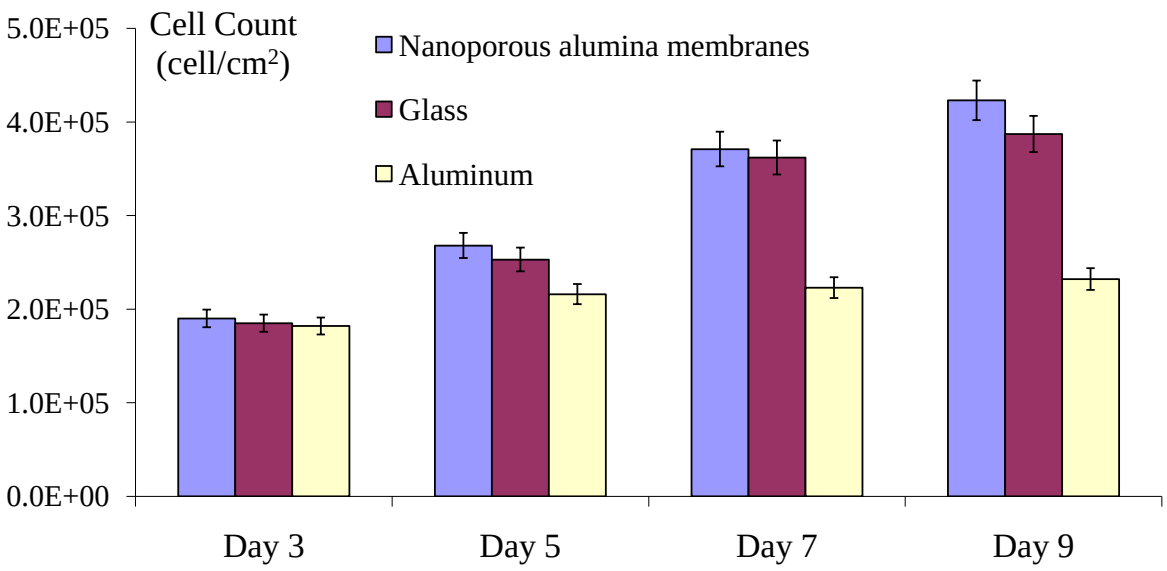

Fig 3.4.5 KYSE30 cells cultured on different membranes

Different cell were applied to study the biocompatibility of nanoporous alumina membranes. Cancer cells were used for apoptosis study, and other cells were used only to prove the biocompatibility of the membrane. Using different cells open the door for other potential applications. The results show that the membranes can provide a biocompatible nanoscale environment which is suitable for cell culture. The reason for the better biocompatibility is the surface property. After silane treatment, the surface can adsorb more protein, which will increase the adsorption effect of cells cultured on the surface, finally result in better spreading and proliferation. SEM images showed that the cells not only covered on the nanopores, but also inserted parts of cell cytoskeleton into the nanopores. These findings suggested the ions would be blocked when they wanted to go through the nanopores, which would induce the increase of impedance finally during impedance spectra measurement.

3.5 Impedance spectrum with electrolyte

After successful fabrication of nanoporous alumina membranes and incorporation of them with PDMS device, electrical impedance analysis was performed to ensure that the nanopores are completely open. A series of conducting solutions in different concentrations, which are made by adding an ionic salt to an appropriate solvent, are required for performing the impedance analysis. NaCl solutions with different concentrations were chosen as the electrolyte solutions to perform impedance measurement and analysis.

3.5.1 Impedance measurements of nanoporous alumina membrane

Impedance spectra of the chamber incorporated with nanoporous alumina membrane were measured. Fig. 3.5.1 shows the impedance spectra of sodium chloride solutions with different concentration from 0.001 M to 1 M, the nanopore size is 100 nm here. It can be seen that the impedance spectra of solutions respond different with sodium chloride concentrations in the frequency from 0.1 Hz to 10 KHz. It is obvious that the magnitude of the impedance decrease with increasing electrolyte solutions concentrations. When the concentration is 0.001M, the impedance is nearly as high as that of distilled water, which indicates there was even no ions transport from the nanopores. When the concentration is 0.01M, the impedance decreased dramatically and it shows that there were some ions transporting through the nanopores. Solutions with higher concentrations such as 0.2 M, 0.5 M and 1 M contain more ions in them and there are more ions transporting through the nanopores at the same time, which are make the

impedance data lower at any specific frequency. However, the magnitude of the impedance was not inversely proportional to the concentration of the solutions, probably because of the slightly variation of other conditions such as positions of electrodes, existing of small bubbles under the nanoporous membranes. This relationship suggested us the flow of electric current, which are carried by ions such as sodium (Na^+), chloride (Cl^-) originated from electrolyte solutions, can go through the nanopores freely when nothing is on the surface blocking the nanopores.

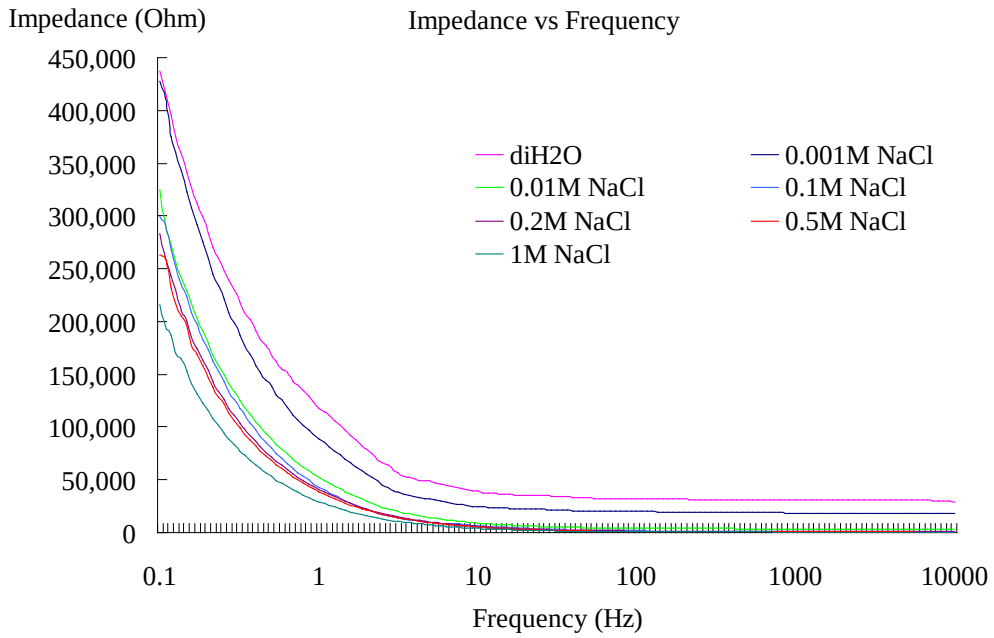

Fig 3.5.1 Impedance spectra of nanoporous alumina membrane in frequency domain

To find out the best frequency to take analysis, impedance data at different frequencies was normalized by setting the impedance of deionized water as 1. Fig 3.5.2 shows differences between NaCl solutions at different frequencies. At higher frequencies such as 10000 Hz, the differences between solutions with different concentrations are very large and obvious. At frequencies as low as 0.1 Hz, the differences is not so large but also obvious enough to be observed. It indicates that even at low frequency, the electric

currents which are due to the ions transporting through nanopores are also detectable and correlated with the concentrations of ions in the electrolytes.

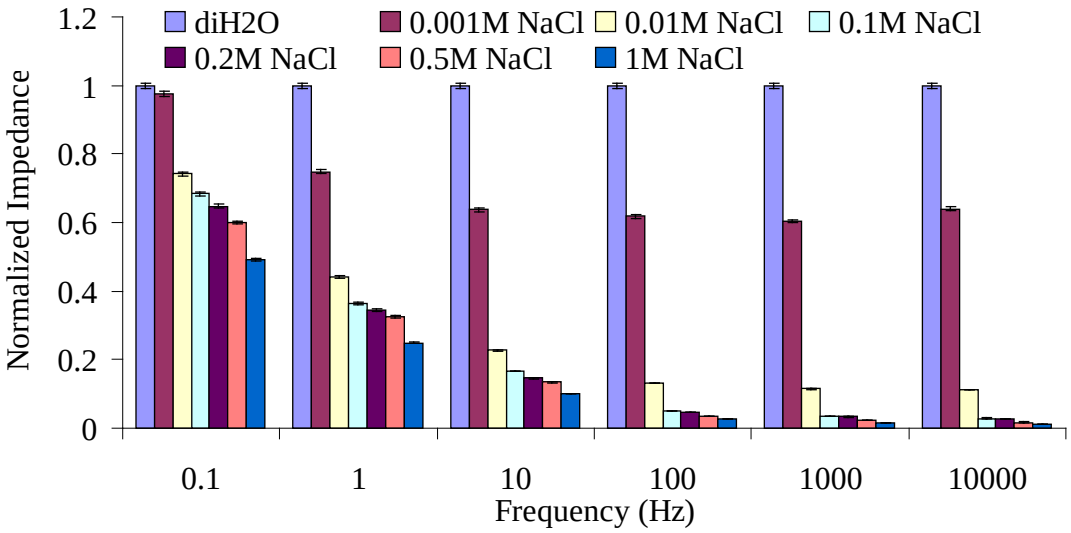

Fig 3.5.2 Relative impedance differences between solutions at different frequencies

3.5.2 Equivalent circuit model analysis of impedance spectra

For analysis of the measured impedance spectra through the nanoporous membrane, the impedance data must be modeled. Fig 3.5.3 shows the equivalent circuit model of the device incorporated with nanoporous alumina membrane. The equivalent impedance of a nanochannel is modeled as a RC circuit, which is widely used for simulating of porous membranes. The electrical double layer capacitance of the device is represented aracterized using a capacitor Q, which is an imperfect capacitor since it could not be considered as a pure capacitor. The capacitance Q is consisted of two elements, Q-n and Q-Yo. The resistance of the nanopores is modeled by a resistor Rp.

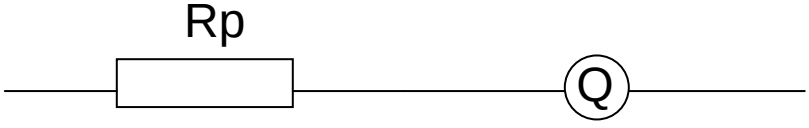

Fig 3.5.3 Equivalent circuit model of nanoporous alumina membrane incorporated device

Q is also known as constant phase element (CPE), which contains Q-Yo and Q-n. Q-Yo represents the dielectric properties of the membrane/ electrolyte and the effect of surface morphology. Here, $Y = Yo (j\omega)^n$. If the n-value of a Q is a little less than 1.0, then the Q behavior is close to that of a pure capacitance. The imperfect capacitor Q has two parameters. The parameter Q-Yo is similar as a capacitor and another parameter n is between 0 and 1. Since the surface property of the nanoporous structure is complex, it should not be defined as a simple capacitor.

ZSimpWin (EChem Software), a software for circuit modeling and data fitting, was adopted to calculate the resistance Rp and capacitance Q of the nanoporous membrane from the Bode plot of device for different electrolyte concentrations. The parameters of every element for the impedance spectrum for each concentration were fitted. Curves of the values for different concentrations were plotted.

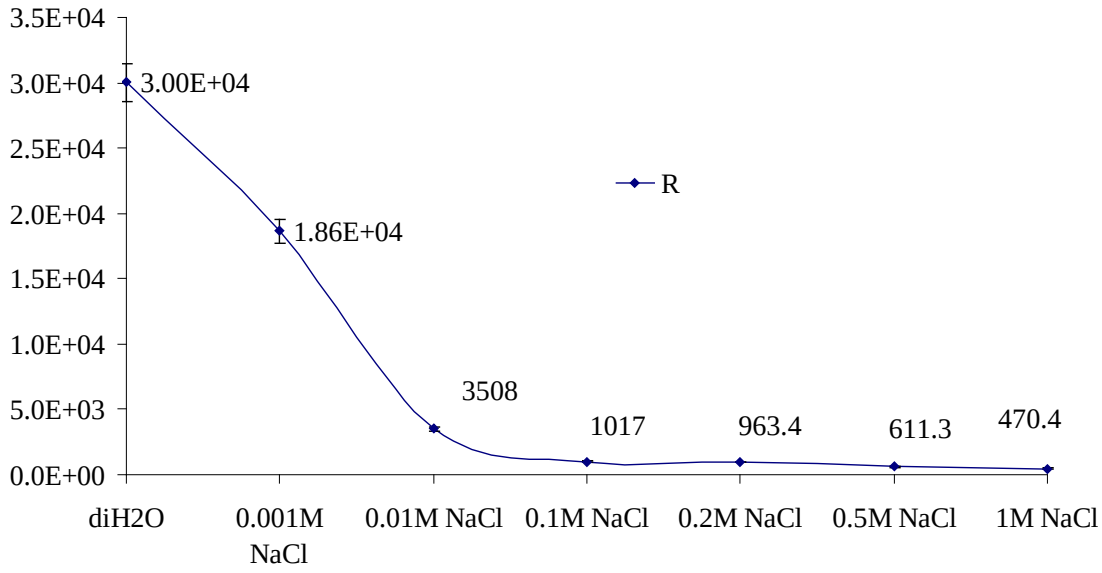

Fig 3.5.4 Resistance of nanopores decreases while concentrations increases (frequency 100 Hz)

Fig 3.5.4 show the resistance of nanoporous alumina membranes, when frequency was set at 100 Hz. When use distilled water, the resistance is around 3.00×10^4 Ω, and the resistance is around 1.86×10^4 Ω when use sodium chloride solution with concentration 0.001M, it is about 38% less than the distilled water. It indicates more ions are transporting through the nanopores when using 0.001 M solution than that of distilled water. The resistances of higher concentrations solutions lead to lower resistances. For the 1M NaCl, the resistance is around 470.4, which is around 97.5% less than that of 0.001M solution. R decrease while the concentration of electrolyte solution increase significantly, which conclude the resistance changes are an important part of the impedance changes. There are more ions in the higher concentration solutions to go through the nanopores, which make the current higher and impedance lower.

Fig 3.5.5 shows Q-Yo and Q-n of the nanopores. Q-Yo and Q-n are two parameters of the imperfect capacitor Q. Q-Yo is the double layer capacitor. When used distilled water, the Q-Yo is around 3.06×10^{-6} F, and it is 3.29×10^{-6} F when using 0.001M NaCl, which is around 7% than that of distilled water. Q-Yo slightly increases while the concentration increases. When using 1 M NaCl, the Q-Yo is 7.26×10^{-6} F, which is only less than 2 times as that of 0.001 M NaCl. Comparing with the differences of resistance between high concentration solutions and low concentration ones, the capacitance of the double layer is also part of the impedance, but it is not the mainly factors of the measured impedance. Q-n is another parameter for the imperfect capacitor Q, which is used to show the degree of imperfection for the capacitor. If n=1, it is a pure capacitor. The fitted Q-n is around 0.7~0.85 and increase slightly. The smallest one is 0.6931 for distilled water and the biggest one is 0.8546 for the 1 MNaCl. It means the double layer is a relatively pure capacitor and its property remain unchanged while the concentration of the electrolyte solutions changes.

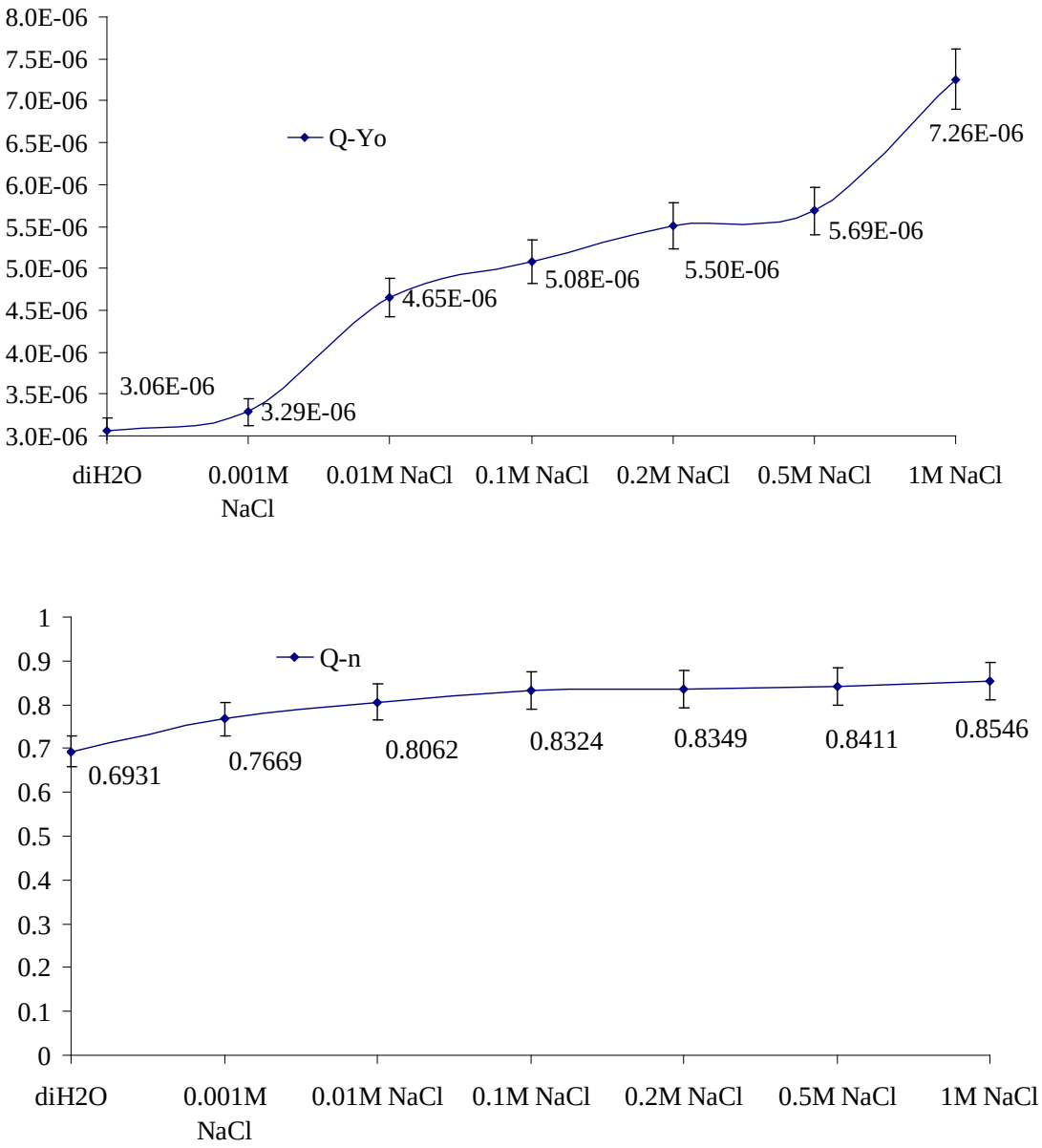

Fig 3.5.5 Q of nanopores increases while concentrations increase

The equivalent circuit model suggests us the system consisted of two main parts: nanoporous alumina membranes membrane and electrolyte solutions, the impedance changes can be caused mainly by the changes of circuit current through the nanoporous alumina membranes. It can be concluded that if the surface of the nanoporous alumina

membrane has been covered and the nanopores were blocked by cells or other samples, the impedance will change because of the blockage.

3.6 Patterning of cells in the microwells

In order to define sensing area, cell micropatterning is required for confine cultured cells within specific microwells.

3.6.1 Single microwell for cell culture

Single well experiments were explored to verify the patterning effects. Protein/cell repelling hydrogel layer with 500 μm microwell was fabricated on the silane modified nanoporous alumina membranes with the nanopore size of around 75 nm. Fig 3.6.1 (a) shows the fluorescence image of the microwell before cell seeding. The round shaped microwell could be observed by mixing with green dye. The PEG hydrogel micropatterns on the silane modified nanoporous alumina surface created controlled spatial distribution of hydrophobic and hydrophilic regions, which interacted differently with cells. The PEG patterned substrates were incubated with KYSE30 cells for 1 day. After incubation, the chip with adhered cells was removed from cell culture media followed by washing. Then the cells were stained with propidium iodide (Invitrogen) and observed using fluorescence microscopy. Fig 3.6.1 (b) shows the fluorescence image of the nanoporous surface after cells seeding. The fluorescence labeled KYSE30 cells are captured within the microwell after cell seeding. There’re no cells adhered on the PEG surface. The difference of cell adhesion between PEG and modified nanoporous

alumina membrane surface enabled the spatial control of cells. The modified nanoporous alumina membrane was more capable of cell adhesion than PEG surface.

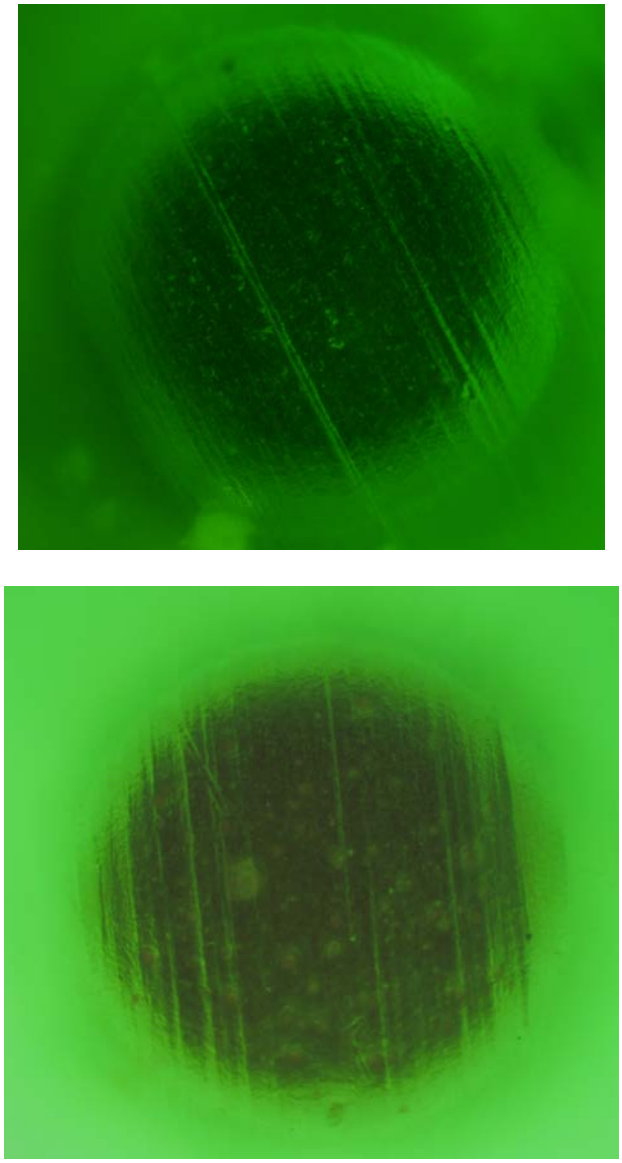

Fig 3.6.1 Fluorescence images before (a) and after (b) cell seeding

3.6.2 Array of microwells for cell culture

An array with 10 X 10 microwells was fabricated with PEG on silane modified nanoporous alumina membrane. The diameter of every microwell is 200 μm. After seeding and culture for three days, cells were stained with phalloidin-TRITC. Fig 3.6.2 shows part of the array with 2 X 3 microwells, and background color has already been subtracted. Cells could be observed clearly from the image. In some of the microwells, several cells can be found. But in others of them, only one or two cells can be found within one microwell. Most of the cells are spreading very well in the microwells.

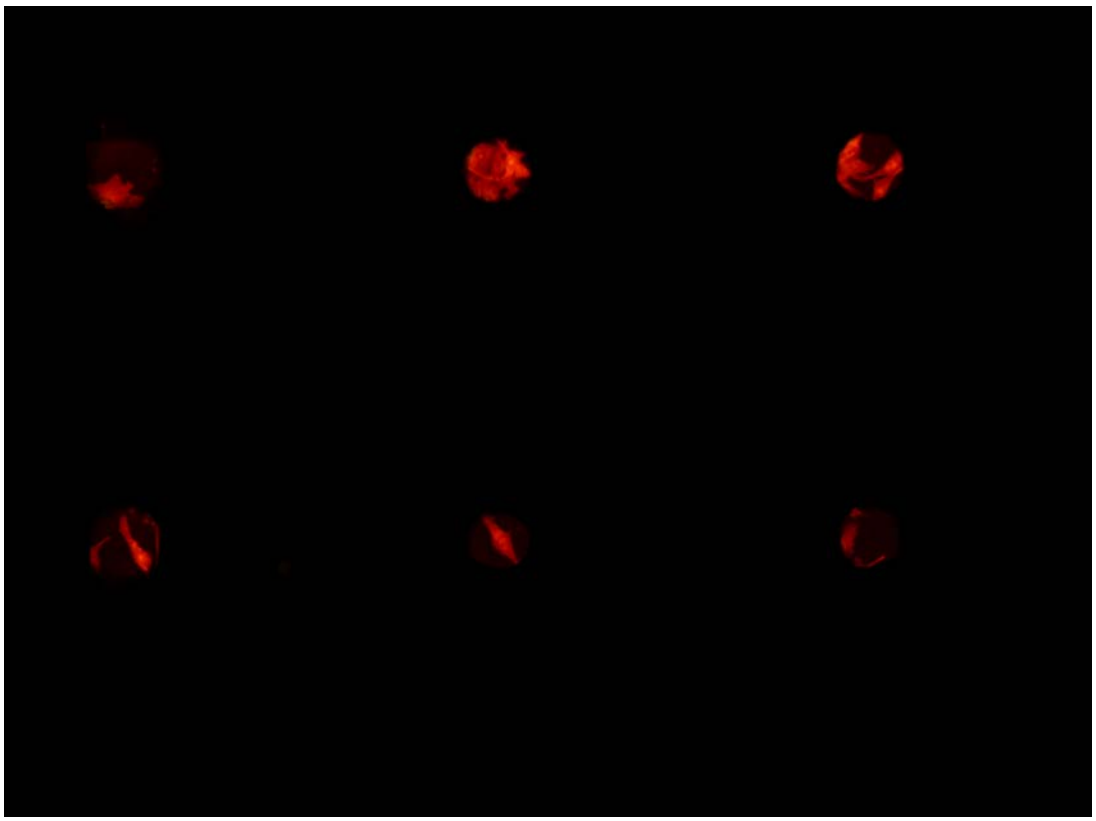

Fig 3.6.2 Array of microwells with cells cultured within them

For the 100 microwells, cells per microwell were counted using MetaMorph.

The numbers of cells within each microwell was plotted. Fig 3.6.3 shows the numbers of microwells which has specific numbers of cells within them. X axis means the numbers

of cells within each microwell, and Y axis means the numbers of microwells. There're 6 microwells which has no cells within them while 4 microwells has 8 cells within them. Among the 100 microwells, 20 of them have 2 cells within them and 26 of them have 3 cells within them. The average numbers of cells within each microwell is 3.5, which means around 3~4 cells were cultured within every microwell with the diameter 200 μm.

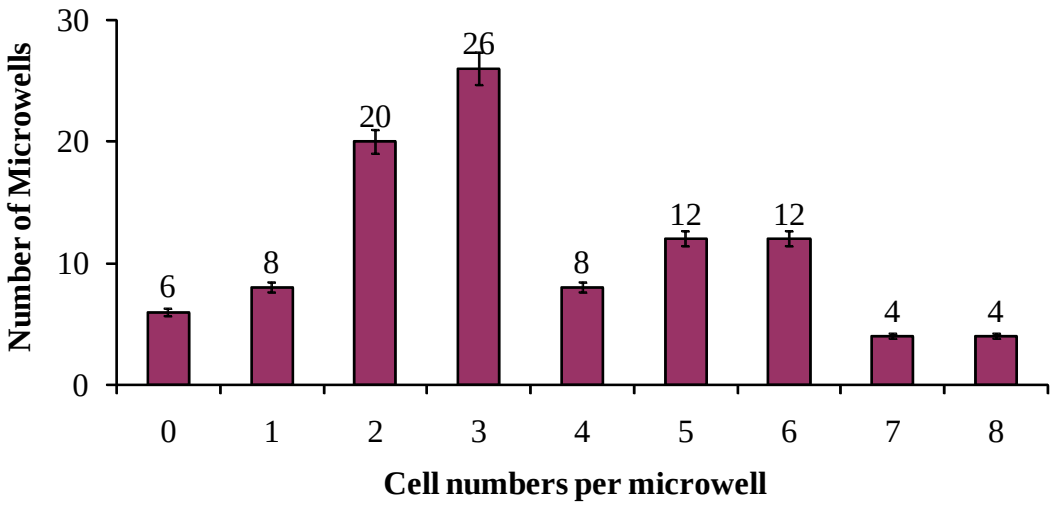

Fig 3.6.3 Numbers of Microwells have specific numbers of cells within them

The results showed that PEG hydrogen microwell was successfully fabricated on the nanoporous alumina membranes, and the cells were cultured and patterned within the microwells, which define the sensing area in these microwells.

3.7 Impedance spectrum for cancer cell adhesion

Cell adhesion and cell spreading are fundamental processes of adherent cancer cells. Because of the complexity of cell adhesion and cell spreading processes, these cellular processes were studied at many levels including the tissue, individual cell, and molecular levels (Seriburi et al. 2008). Cell morphology changes when cells adhere and spread, so the dynamics of cell spreading and cell adhesion can be monitored by recording cell morphology changes. The cell morphology changes are measured using different conventional optical methods. Electrochemical methods offer a non-invasive and cost-effective technique compared to optical methods for measurement of cell morphology changes. Some electrochemical methods such as a transistor probe and impedance sensing using microelectrodes were previously used to study attachment, adhesion and spreading of cells. As we described in the background area, electrical cell-substrate impedance sensing (ECIS) was used as a tool to study properties of monolayer of cells for many years.

But, this method has some limitation and restrictions. In many situations, the size of electrode should be fabricated less than 100 μm. The electrode impedance caused by the electrode polarization is increased at the low frequency range when the size of electrode decreases. If the impedance related with the cell morphology changes is too much smaller than the high electrode impedance caused by the polarization, it is hard to extract the impedance data of cells from the total measured impedance data. Micro hole-based cell chip can be applied to avoid the problem of electrode polarization. When the micro holes or even nanopores are on the insulating membrane and when the electric fields are

applied in the electrolyte, the current density nearby the holes should be high but no electric double layer existed. The electrical current flowing through the hole or the measured impedance should be changed sensitively according to the state and morphology of the cell covered on the hole. Using the micro holes based impedance sensor, the impedance of a small amount of cells or even single cell can be measured at the low frequency range but not be affected by the electrode polarization. Sungbo have fabricated a micro hole-based chip for fast positioning of a single cell on the hole. Using the micro hole-based chip, the electrode polarization or viability of single cell can be detected. The micro hole-based cell chip also can be utilized for the impedance monitoring of cell cultivation on the chip. Comparing the electrode-based cell chip, the micro hole-based cell chip can be used to measure the impedance of even single cell in the low frequency range, due to avoiding the effect of electrode polarization. Further, the micro hole-based cell chip can be utilized to position the cell on the required location of the micro holes quickly by using micro fluid controller. It possible to do a fast bio-sensing using this micro hole based cell chip (Cho and Thielecke 2007).

The electrical property of the micro hole-based chip is determined by the sizes of holes and the insulating membrane. In order to increase the sensitivity of the micro-hole based chip, we developed a novel nano-hole based chip with impedance spectroscopy. It is a new morphology-sensitive electrochemical micro-system with nanoporous alumina membrane which can detect the small cancer cell morphology changes, not only during the processes of cell adhesion and cell spreading, but also the changes induced by anti-cancer drugs even in trace quantities. Increasing surface area of the nanoporous material

leads to the increasing of the surface chemical reaction rate of the electron transfer through the solid-liquid interface.

The fabrication process of the device and cell biocompatibility have already been demonstrated before, we have measured the impedance of nanoporous alumina membrane according to the different culture periods of cells on the nanopores by impedance spectroscopy. The electrical properties of different components were separated and the influence of cell adhesion or spread on the total measured impedance was calculated.

In our experimental setup, cancer cells were cultured on the modified nanoporous alumina membranes, which were covered by ECM protein before cell culture. The impedance spectra were recorded before and adding of cells, so that the characteristics of the cell-free and cell-covered impedance-sensing system could be determined and described with equivalent circuit models.

3.7.1 Impedance spectra for cells cultured on nanoporous membranes

For cells cultured on the nanoporous membrane for different days, the impedance spectra were also recorded, which can be used to determine the components of the whole system.

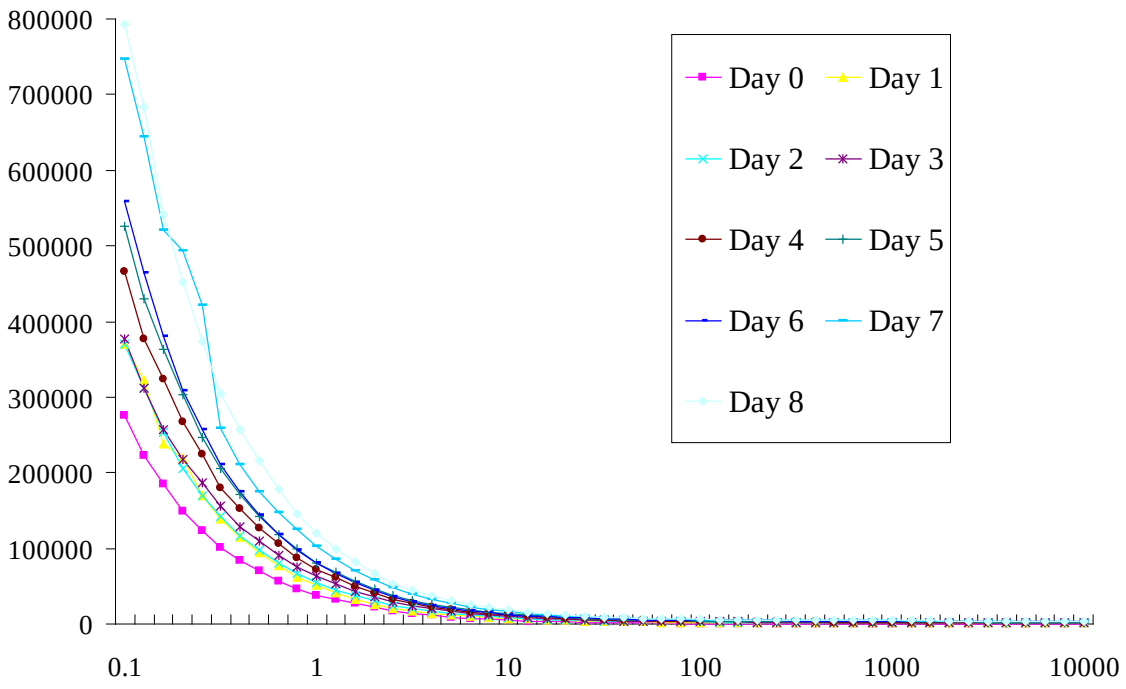

Fig 3.7.1 Impedance spectra of cell growth for different days

Fig 3.7.1 shows the measured impedance spectra of KYSE30 cells with different cultivation days on nanoporous alumina membrane. The impedance spectra were measured in the low frequency of 0.1 Hz to 10,000 Hz from day 1 to day 8. It can be seen that the impedance magnitude increase while the cells were cultured on the surface. When the cells were just seeded on the nanoporous alumina membrane on day 0, the average impedance amplitude was 276.2 ± 7.8 KΩ at 0.1 Hz. At day 1, the impedance spectra increase a lot, and the average impedance amplitude was 370.2 ± 9.3 KΩ at 0.1 Hz, which indicate the cell adhesion on the nanoporous alumina membrane. During this process, the cell morphology changes dramatically and causes large impedance changes. In the following days, impedance also increases but the speed is not so high, which indicates the normal cell proliferation and spreading on the surface. For day7 and day 8, the impedance remains nearly the same, it can be seen that the cells have already form

monolayer on the surface and the morphology changes is very small. When cancer cells achieved confluence on the nanoporous alumina membrane after 8 days of cultivation, the average impedance amplitude was increased to 793.5 ± 14.3 KΩ at 0.1 Hz. No significant difference of impedance amplitude could be observed when the frequency was above 10 Hz.

3.7.2 Equivalent circuit modeling for cells cultured on membranes

In order to correlate the variation of impedance of cells behavior, the impedance spectra were fitted with the equivalent circuit. The cell-membrane interface is modeled for coverage of the nanoporous alumina membrane by the cells. The impedance-sensing system with cells can be represented by the equivalent circuit model shown in Fig 3.7.2. Similar like the model we used before to simulate the membranes, the resistance of the nanopores is represented by R_p. While the electrical double layer capacitance of the device is characterized using a imperfect capacitor Q. The resistance and capacitance of the cell layer on the nanoporous membrane were characterized using a resistor R_c and a capacitor C_c. This is the equivalent circuit model of the impedance-sensing system with cells, which means cells have already cultured on the nanoporous alumina membranes. So a new part with cells should be considered in the circuit model.

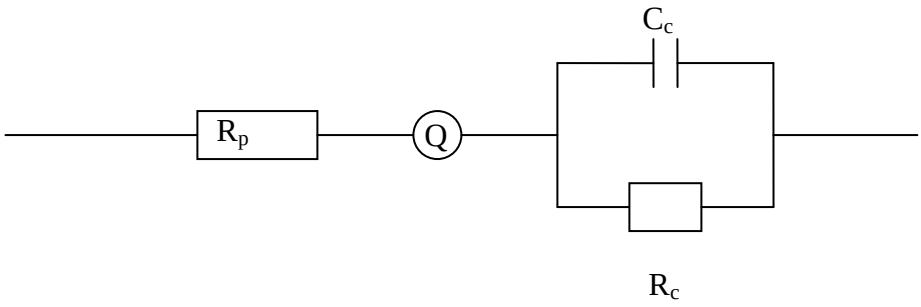

Fig 3.7.2 Equivalent circuit model of the impedance-sensing system with cells

In order to evaluate the changes caused by the cells cultured on the nanoporous alumina membrane, during the whole process, because the system is the same as that without cells covering, Rp represented the resistance of the nanoporous alumina membrane, and it should be kept unchanged when we culture cells on the surface. Before cell culture, impedance signal with cell culture medium was measured and set at the fixed value Rp =470 Ohm. Changes of circuit parameters can be read out by comparing different impedance spectroscopy acquired at different time points. Then, the cell-membrane connection can be monitored, and the cause of the impedance changes can be evaluated based on physical meanings of different circuit parameters.

Q is also known as CPE, it contains Q-Yo and Q-n. If the n-value of a Q is a little less than 1.0, then the Q behavior is close to that of a pure capacitance. As we described before, it contains two parameters:.

Q (CPE) $1/Z=Y= Yo (j\omega)^n$

Capacitor $1/Z=Y=Yo(j\omega)^1= C (j\omega)$

Where Yo is numerically equal to the admittance (1/|Z|) at ω = 1 rad/s. The value of Yo could be associated for a Q with the capacitance value, C, for an equivalent capacitor.

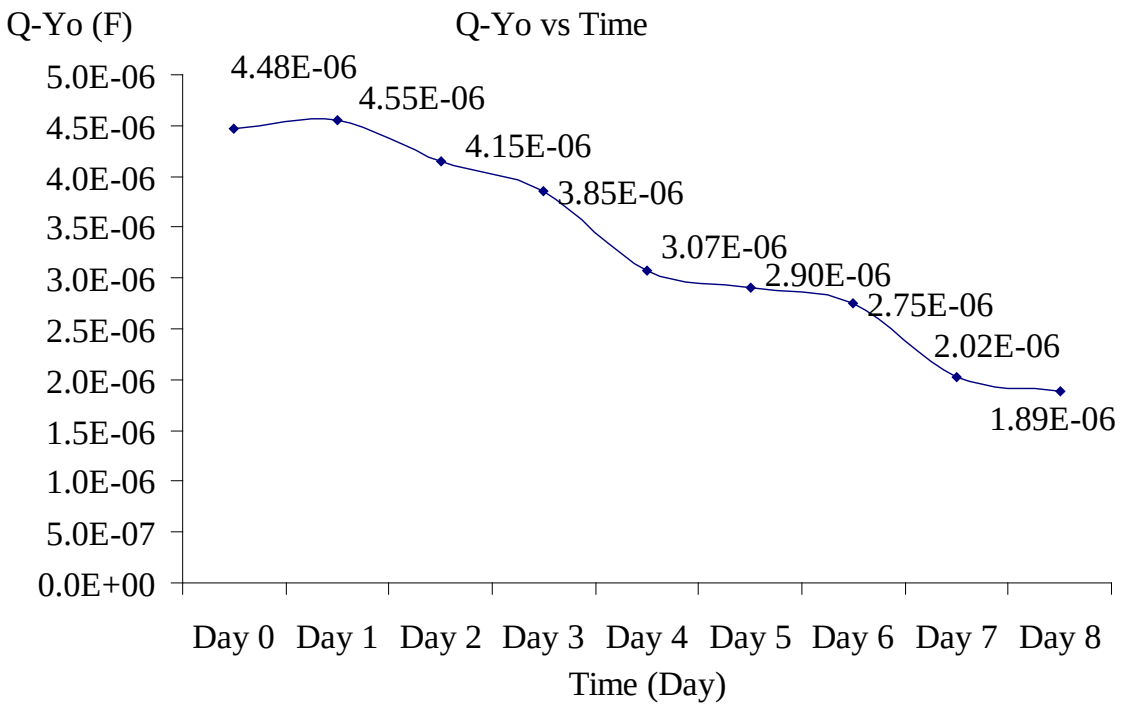

Fig 3.7.3 Circuit model parameters Q-Yo versus cell cultivation days

Q-Yo represents the dielectric properties of the membrane/ electrolyte and surface morphological information. The capacitance of the nanoporous alumina membrane decreases from day 0 to day 8. At the first day the value of Q-Yo is around 4.48×10^6, after a little increase on day 2, it decreased in the following days. At day 8, the value decreased to 1.89×10^6, which is around 42% of the first day.

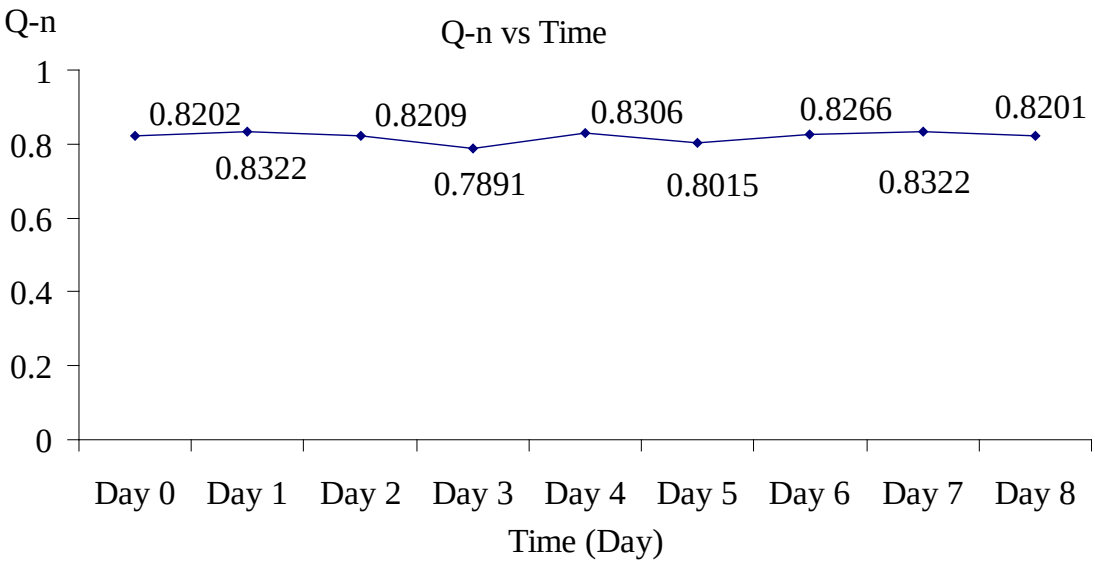

Fig 3.7.4 Circuit model parameters Q-n versus cell cultivation days

The Q-n remains nearly unchanged during the whole process. The smallest value of Q-n was fitted for the data of day 3, which is 0.7891. And the biggest value of Q-n was fitted at day 1 and day 7, which are both 0.8322. The average value of Q-n is Q-n = 0.8193 ± 0.01478. The standard deviation is very small and indicates that the Q-n is nearly a constant for all the days. It can be concluded that the property of the nanoporous alumina membrane kept unchanged during the days when cells cultured on the surface for around 8 days, till they form monolayer.

The cellular circuit is modeled with the parallel-serial of a capacitor for cell layer capacitance (Cc) and a resistor for cell layer resistance (Rc). These two parameters are also can be contracted from the impedance spectra.

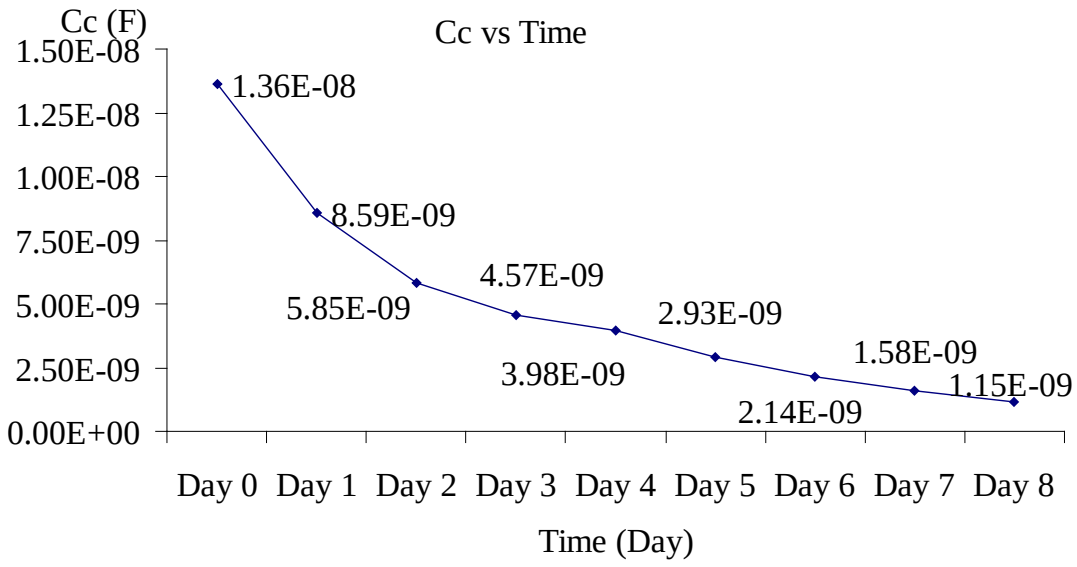

Fig 3.7.5 Circuit model parameters Cc versus cell cultivation days

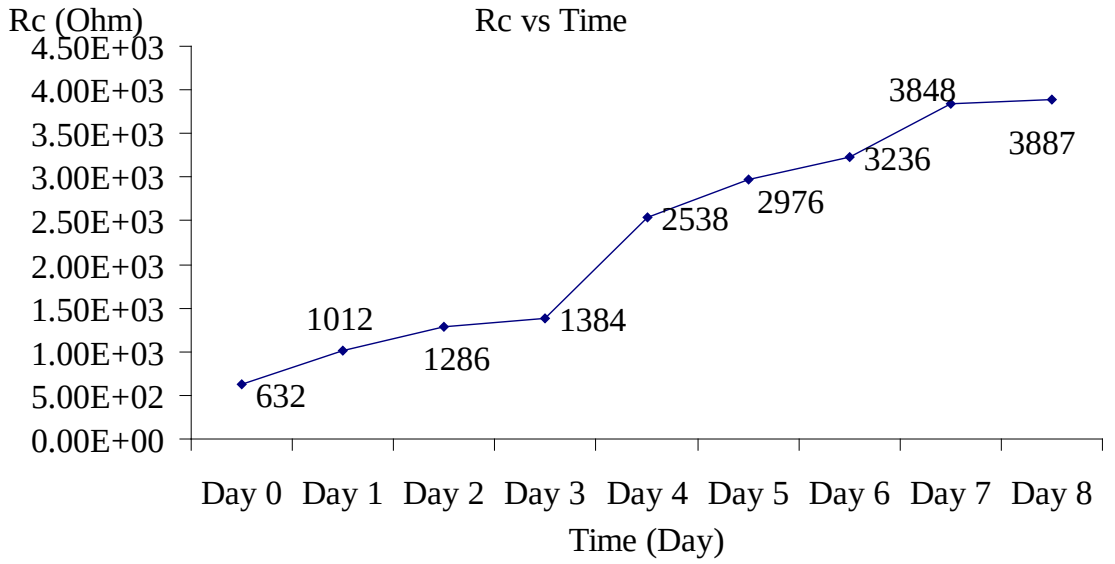

Fig 3.7.6 Circuit model parameters Rc versus cell cultivation days

From the above two images, it is clear that Cc decreased and Rc increased when cell were cultured and spread on nanoporous alumina membrane for 8 days. On the first day,

the value of Cc is around 1.36×10^{-8}F, it decreased everyday when cells cultured on the nanoporous alumina membrane, and the value on day 8 is around 1.15×10^{-9}, which is less than 10% of the first day. At the first day, Rc is around 632 Ohm, and it increased a lot when cell cultured on the membrane. From day 1 to day 3, the resistance increase not very much, but it increased a lot from day 3 to day 7, and it reach nearly unchanged at day 7 and day 8.

The Cc decrease more than 80% from day 0 to day 8, at the same time Rc increase around 6 times. It can be conclude that the impedance changes are mainly caused by cell capacitance changes and cell resistance changes, which was related with cell morphology changes. The change of Rc and Cc may be related to the increase of blocked nanoporous area by cell adhesion, cell spreading and cell proliferation, and also the gap decrease between cells and the nanopores during the cell culture process. Other properties may also change the values of Rc and Cc, such as membrane integrity, membrane potential, adhesion strength, extra-cellular ionic distributions, and also number and surface area coverage of cells above the nanoporous area. The above analysis shows that cellular adhesion, spreading, proliferation, and morphology changes can be monitored with this nanoporous alumina membrane based impedance sensor.

3.8 Impedance spectrum for drug effects

When cells are cultured on nanoporous alumina membranes for many days and form a cell monolayer, the impedance spectrum will reach a stable value. This stable impedance value could be used as the base line for the following drug testing.

3.8.1 Impedance measurement for cells treated by different chemicals

Retinoic acid (RA, Sigma-Aldrich) is both an immunomodulator and a preventive and chemotherapeutic anticancer agent and its derivatives were used to treat many cancer and tumor types. Retinoic acid can specifically change the morphology of cells by suppressing the synthesis of intermediate filament protein. The anti-cancer effects of retinoic acid are in part due to its ability to inhibit proliferation of cancer cells and it can interfere with the growth and development of cells. RA inhibits the cell-substrate adhesion and motility and also induces morphological and functional terminal differentiation of a cell line. It is reported that the modulation of proliferation and adhesion in epithelial cells and fibroblasts of human skin by RA is associated with changes in the extracellular matrix production of Ca^{2+} metabolism. The anti-cancer effect of retinoic acid is in part due to their ability to inhibit proliferation of cancer cells. RA inhibits cancer cell-substrate adhesion and motility and also induces morphological and functional terminal differentiation of a cell line.

In our experiment, RA is dissolved in absolute ethanol at the concentration of 0.01M (3 mg/mL). After 8 days' culture, the impedance amplitude was stable around a constant value and was normalized as 1 at 0.1 Hz. Then, retinoic acid with 0.01 M concentration was added for the anti-cancer drug experiment. Fig 3.8.1 shows impedance amplitude change with time under the effect of 0.01M RA. After the addition of RA with 0.01 M concentration to the cell chip, the impedance magnitude decreased with time. After taking effects for 12 hours, the impedance magnitude decreased to a stable value which was close to the initial impedance base line of chips without cells.

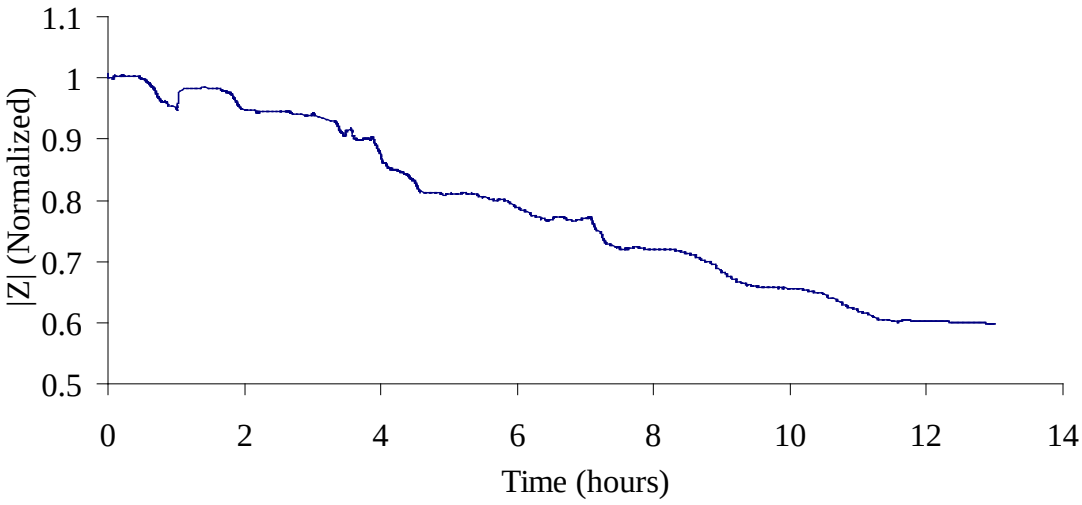

Fig 3.8.1 Impedance amplitude change with time under the effect of retinoic acid (0.01M) at 0.1 Hz

5-Fluorouridine (5-FU, Sigma-Aldrich) can also be used for chemotherapeutic treatment of certain cancers because it is a potent inhibitor of the incorporation of formate into DNA thymine both *in vitro* and *in vivo*. 5-FU is dissolved in cell culture medium and the final concentration is 0.1mg/mL. Fig 3.8.2 shows impedance amplitude change with time under the effect of 5-Fu. After addition of 5-Fu, the amplitude of magnification decreased around 55% after 400 minutes. After that, the impedance amplitude was kept unchanged. It indicates the effect of 5-Fu on impedance amplitude is very quick.

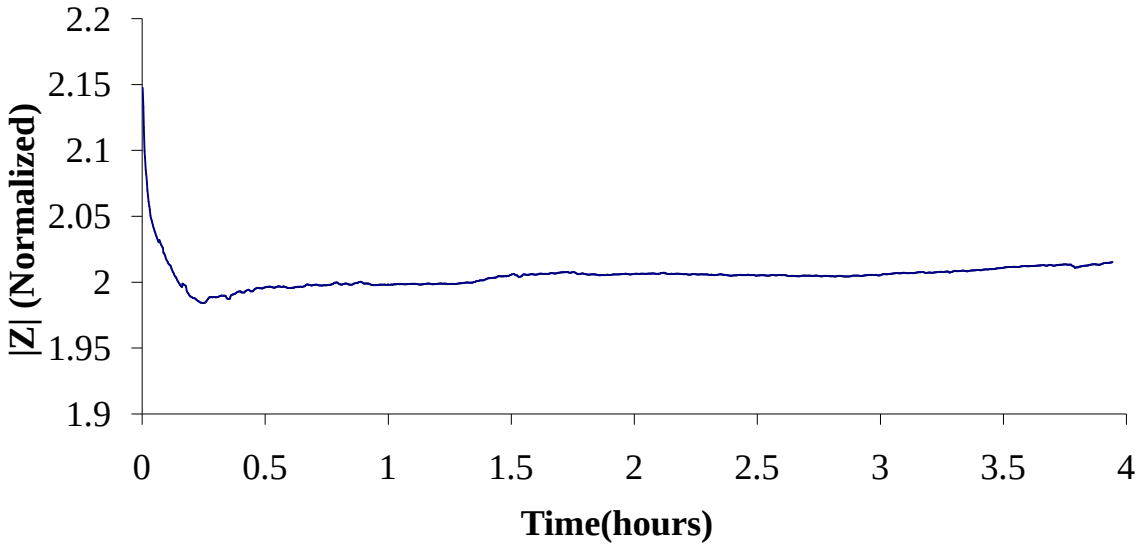

Fig 3.8.2 Impedance amplitude change with time under the effect of 5-Fu (0.1mg/mL) at 0.1 Hz

Cisplatin (CDDP, Sigma-Aldrich) is a platinum-based chemotherapy drug which is used to treat various types of cancers and it can induce morphological changes of cancer cell lines. In this experiment, CDDP was dissolved in cell culture medium and the final concentration of 0.5mg/ml was applied.

Fig 3.8.3 shows the relative impedance amplitude change with time under the effect of CDDP with 0.5mg/ml concentration. After the addition of CDDP with 0.5 mg/ml, the impedance decreased around 2.7% at the early 180 minutes. After that the impedance did not decrease any longer.

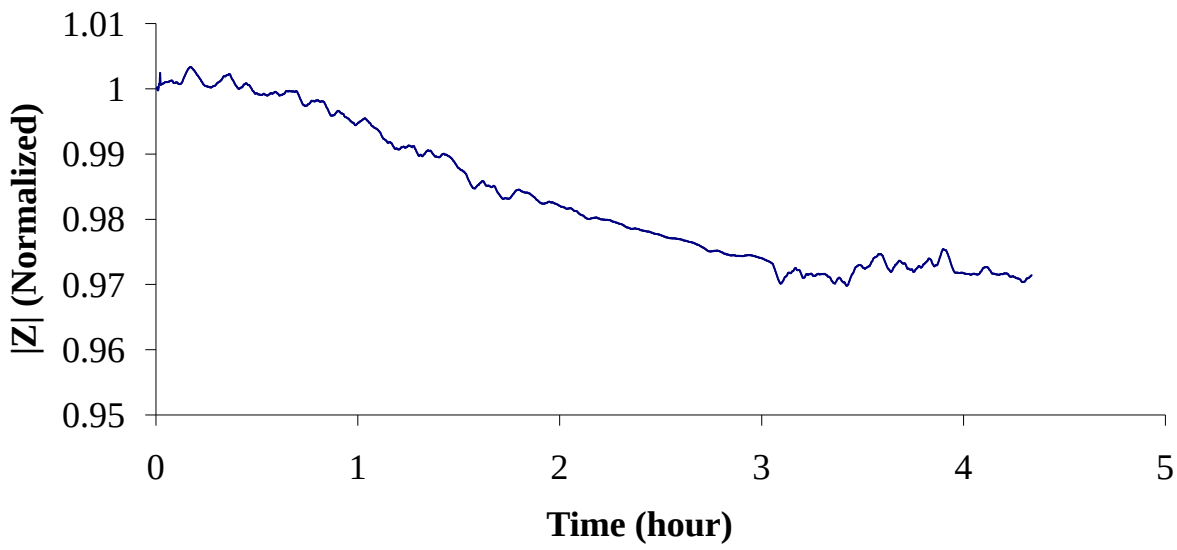

Fig 3.8.3 Impedance amplitude change with time under the effect of CDDP (0.5mg/mL) at 0.1 Hz

3.8.2 Impedance for cells treated by 5-Fu with different concentrations

The concentration effect of drug on impedance amplitude change was also tested with 5-Fu. Different concentrations of 5-Fu (0.1mg/mL, 0.2 mg/mL, and 0.5mg/mL) were used. Fig 3.8.4 shows the impedance amplitude change with time under the effect of 5-Fu at 0.1 Hz for different concentrations. After addition of 0.1 mg/mL 5-Fu, the amplitude of magnification decreased 55% after 400 minutes. The relative impedance amplitude decreased 60% after the addition of 0.2 mg/mL at the same time. However, 0.5 mg/mL addition changed the impedance amplitude much faster after 400 minutes and the value decreased around 65%. After 400 minutes, impedance amplitudes of all the three cases were kept nearly unchanged.

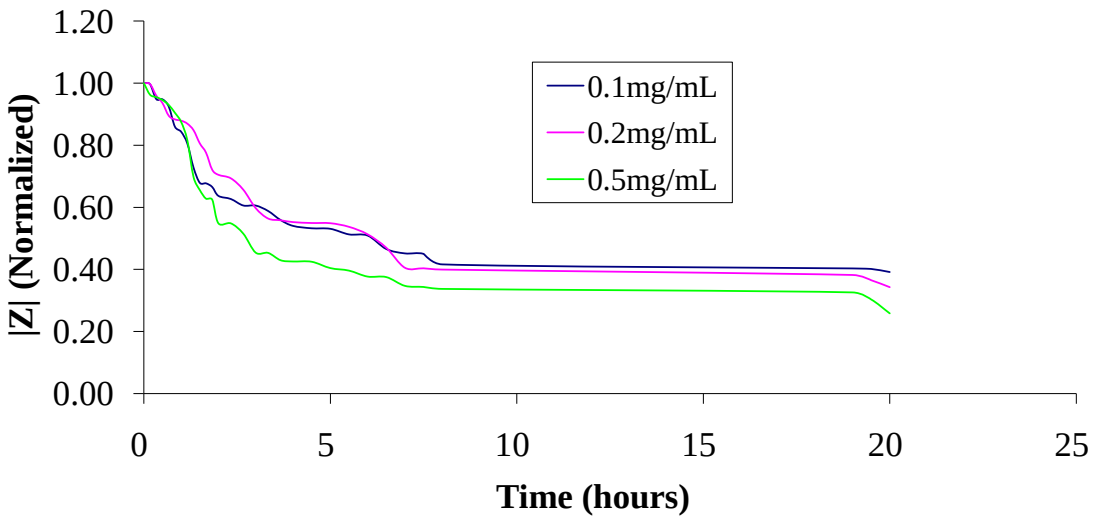

Fig 3.8.4 Impedance amplitude change with time under the effect of 5-Fu at 0.1 Hz for different concentrations

It is concluded that 5-Fu with higher concentrations could decreased the impedance amplitude larger than the ones with lower concentrations. But the effect of 0.1 mg/mL 5-Fu is also strong enough to make impedance changes detectable by our biosensor.

3.8.3 Equivalent circuit modeling for cells treated with 0.1 mg/mL 5-Fu

In order to correlate the variation of impedance spectra with cells behavior during 5-Fu treatment, the impedance spectra were fitted with the equivalent circuit which is described before. During the whole process, the resistance and capacitance Q-Yo of the nanoporous alumina membrane were set at fixed values, which were fitted from the measured impedance spectra without cells. Changes of the parameters of the circuit model were read out by comparing different impedance spectroscopy acquired at

different time points. Then, the cell-substrate adhesion could be monitored, and the mechanism of the impedance changes could be evaluated based on physical meanings of different circuit parameters from the fitted model. Fig 3.8.5 shows the circuit model parameters Cc versus 5-Fu (0.1mg/mL) treatment time. C_c represented the capacitance of cell monolayer. In Fig 3.8.5, initially, C_c is around 4.3 $\times 10^{-8}$F and increased with the drug treatment time. After 400 minutes, it reached around 2.5 $\times 10^{-7}$ F, which was around 6 times of the value at the initial stage. After 400 minutes, C_c kept nearly unchanged.

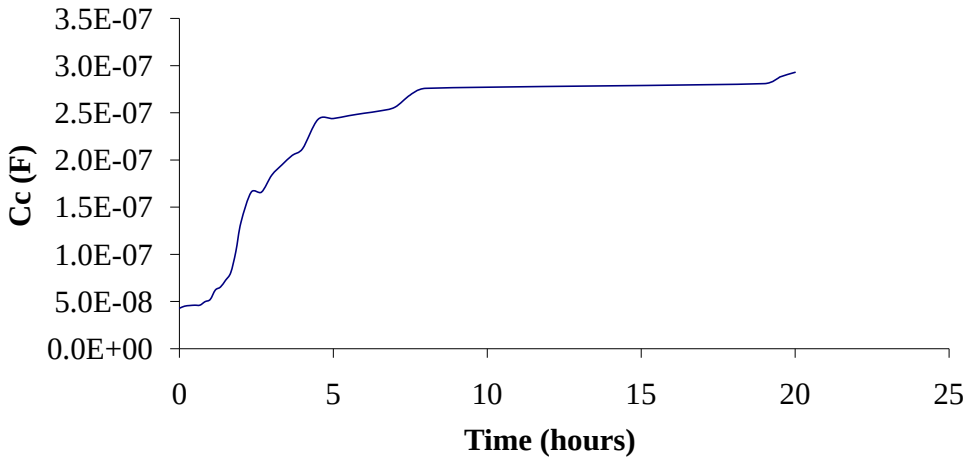

Fig 3.8.5 Circuit model parameter Cc versus 5-Fu treatment time

Fig 3.8.6 shows the circuit model parameter Rc versus 5-Fu (0.1mg/mL) treatment time. Rc represents the resistance value of the cell monolayer, and it decreased with the treatment time until 400 minutes. At first it was around 8.0 $\times 10^{4}$ Ohm, and it reached around 3.2 $\times 10^{4}$ Ohm at 400 minute, which was just around 40% of the value at the initial stage.

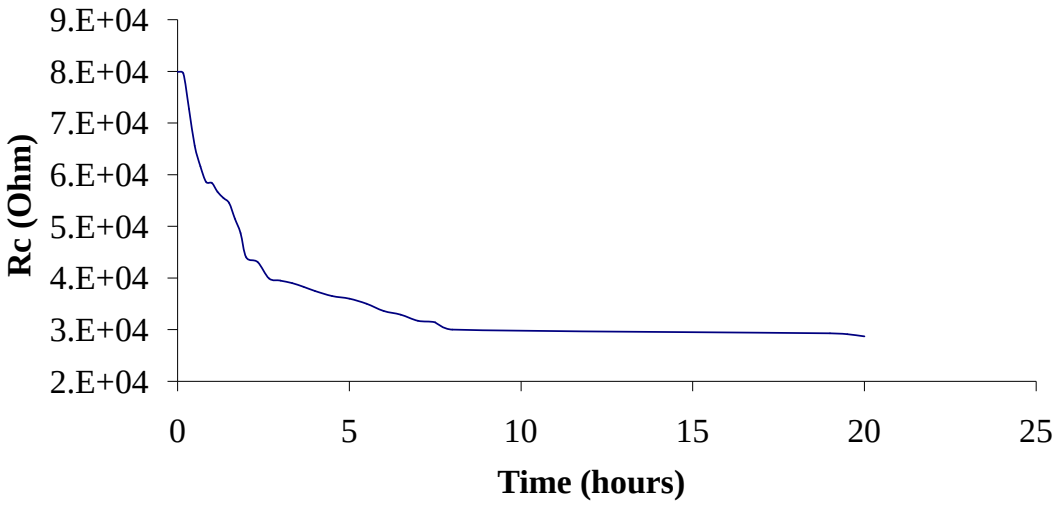

Fig 3.8.6 Circuit model parameters Rc versus 5-Fu treatment time

From the above results, we could conclude that the changes for amplitude of impedance during the drug experiments are mainly from the C_c and R_c. The C_c and R_c are properties of cell monolayer on the nanoporous alumina membranes. The changes of values of C_c and R_c are mainly caused by the changes of cells, including cell morphology changes, cell adhesion, cell spreading, cell proliferation, cell apoptosis etc.

3.8.4 Relationship between apoptosis and cell morphology changes

Apoptosis was evaluated at different time points with cell death detection ELISA. Rate of apoptosis is reflected by the enrichment of nucleosomes in the cytoplasm, which was shown of four samples. Fig 3.8.7 shows the apoptosis induced by 0.1 mg/mL 5-Fu at different time points. The enrichment factors increase with treatment time. After treatment for 2 hours, the enrichment factor is around 3.17, and the enrichment factor increases to 4.65 after 4 hours of treatment. After 6 hours treatment, it increases to 7.89

and finally reaches 10.24 after 8 hours treatment. It is shown that the enrichment factors which represent apoptosis degree increase with treatment time.

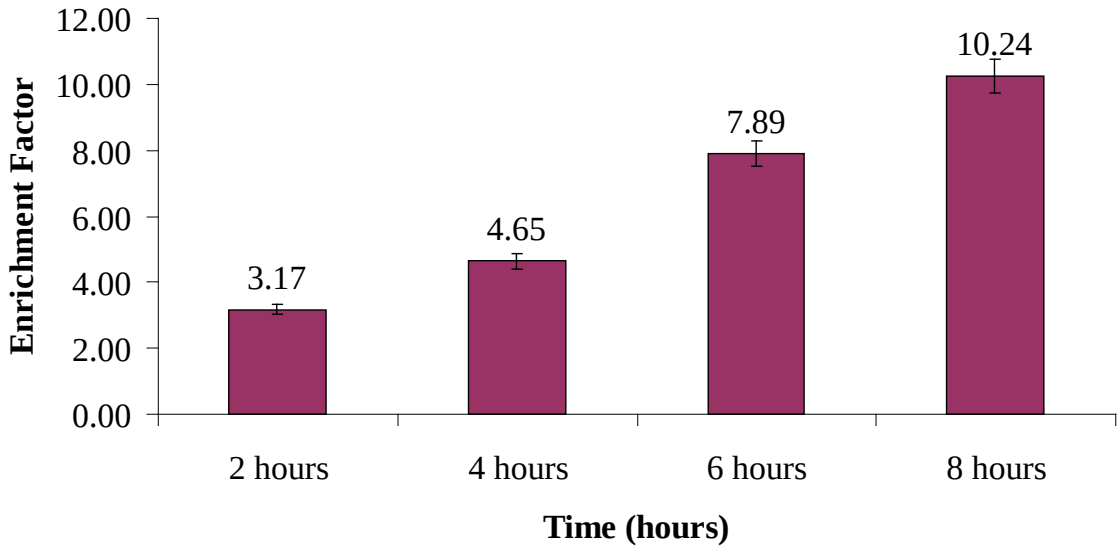

Fig 3.8.7 Apoptosis induced by 5-Fu (0.1mg/mL) treatment for different time

In order to find out the relationship between the impedance changes and morphology changes, fluorescence images after 0.1mg/mL 5-Fu treatment for different time were captured. The average covered area per cell was analyzed by MetaMorph. Fig 3.8.8 shows the average covered area per cell after 0.1 mg/mL 5-Fu treatment for different time. The average covered area was around 237.72 μm^2 per cell without treatment of drug. After 2 hours treatment, the covered area decreased to around 222.05 μm^2, this was about 6.6% decrease of that without treatment. After 4 hours treatment, the area decreased to around 200.08 μm^2, which had a 9.9% decrease of that at 2 hours. After 6 hours treatment, the area decreased to 177.40 μm^2, which had an 11.3% decreased of that at 4 hours. After 8 hours treatment, the area deceased to 166.69 μm^2, which has around 6.0% decrease of the value at 6 hours. The change between 6 hours and 8 hours

was less than the changes during other time interval, which may indicate that the effect of 5-Fu after 6 hours was not as effective as that before. Comparing with the average covered area per cell without drug treatment, the area after 8 hour treatment has a 29.9% decrease.

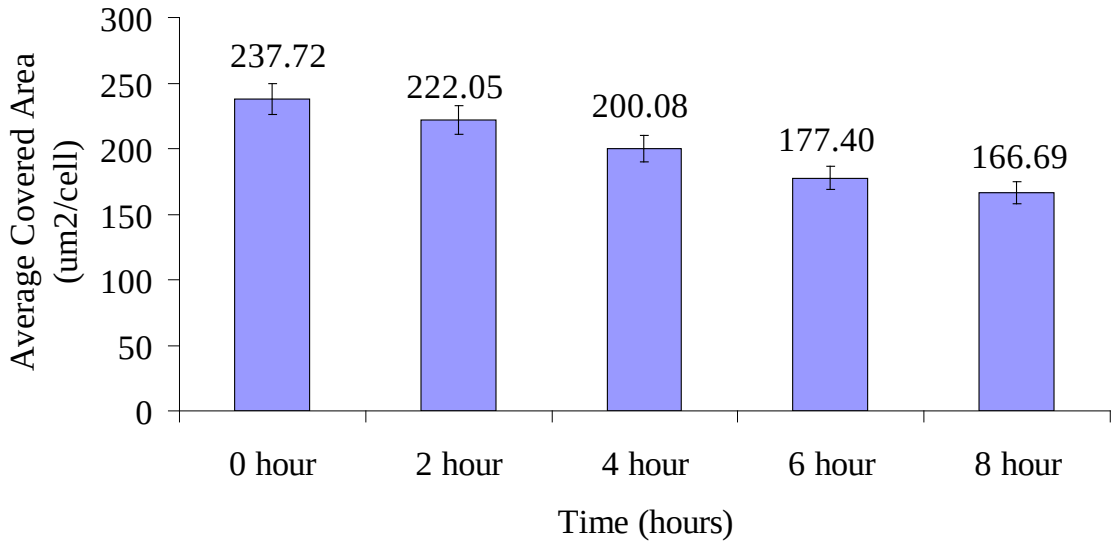

Fig 3.8.8 Average covered area per cell after 0.1 mg/mL 5-Fu treatment for different time

As described, enrichment factor is a parameter to reflect cell apoptosis by determination of mono- and oligonucleosomes in the cytoplasmic fraction of cell lysates and average covered area per cell is a parameter to reflect the cell morphology change by directly measuring of cell covered areas during apoptosis procedure. So the relationship between these two parameters is able to confirm the relationship between cell morphology changes and apoptosis degree. Fig 3.8.9 shows trends of enrichment factor measured by ELISA and average covered area per cell calculated by fluorescence image analysis versus time. After 2 hours' treatment of 0.1 mg/mL 5-Fu solution, enrichment factor is 3.17 while the average cell covered area is 222.05 μm^2. After 4 hours' treatment,

enrichment factor increased to 4.65 while average covered area decreased to 200.08 μm^2. After 6 hours' treatment, enrichment factor increased to 7.89 while covered area decreased to 177.40 μm^2. Finally after 8 hours' treatment, enrichment factor increased to 10.24 while covered area per cell decreased to 166.69 μm^2. From this analysis, the average cell covered area decreased while the enrichment factor increased with drug treatment time. A linear relationship was calculated as y = -7.5579x + 240.59, while correlation coefficient R^2= 0.9544. The R^2 is close to 1 and it indicates that the average covered area should be a good parameter to reflect apoptosis due to its relationship with enrichment factor.

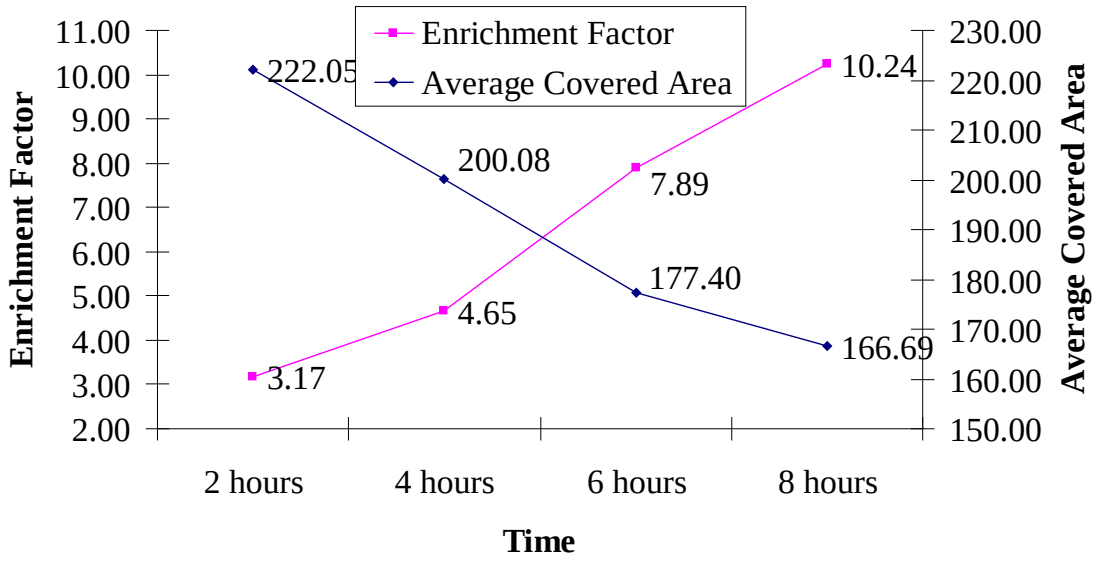

Fig 3.8.9 Trends of enrichment factor and average covered area versus time

3.8.5 Apoptosis determination by impedance analysis

After equivalent circuit modeling analysis, it is concluded R_c could be used to monitor the changes of cell monolayer cultured on nanoporous alumina membrane during the

drug treatment process. From the ELISA data and the images taken by fluorescence microscopy, it is concluded that average single cell covered area which described cell morphology changes could be used to reflect apoptosis after drug treatment. So, it is important for us to find the relationship between R_c and average single cell covered area, to determine the effectiveness of our biosensor. Fig 3.8.10 shows the relationship between resistance of cell monolayer (R_c), and average single cell covered area. After 2 hours' treatment of 0.1mg/mL 5-Fu, average single cell covered area was 222.05 μm^2 while R_c is 44000 Ohm. After 4 hours' treatment, average covered area was 200.08 μm^2 while R_c is 37500 Ohm. After 6 hours' treatment, average single cell covered area was 177.40μm^2 while R_c is 33600 Ohm. Finally after 8 hours' treatment, average covered area per cell was 166.69 μm^2 while R_c is 30000 Ohm. It is obviously that R_c increased while average cell covered area increased. A linear relationship is calculated as $y = 0.0041x + 43.393$ while $R^2 = 0.9865$. R^2 is very close to 1, which indicates that there is a highly linear relationship between R_c and average covered area per cell.

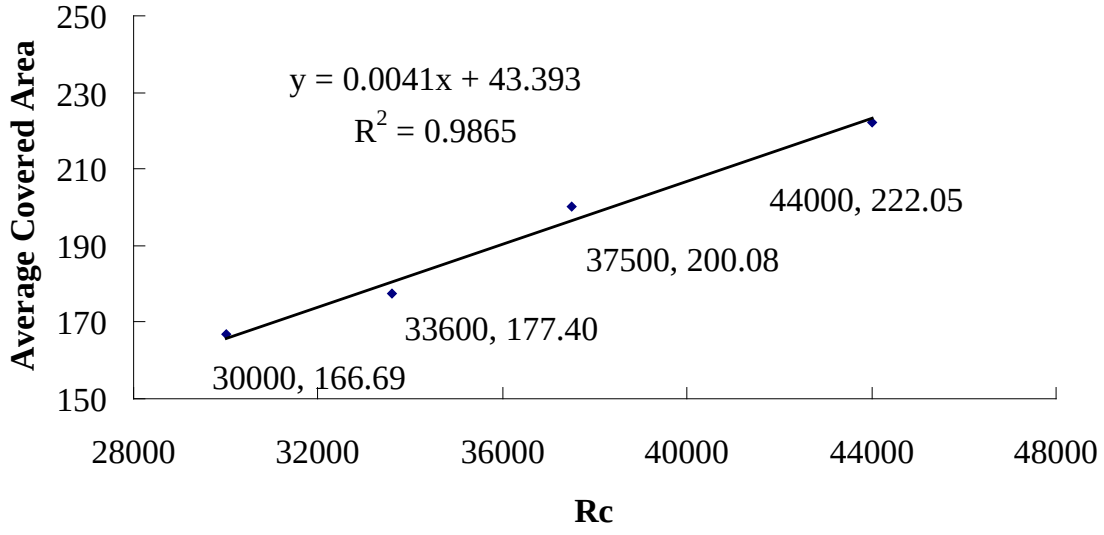

Fig 3.8.10 Relationship between R_c and average covered area per cell

After the positive linear relationship was found, the Rc could be used to reflect average covered area, and thus apoptosis could be monitored by the Rc. It could be concluded that our biosensor is effective to monitor cell apoptosis by measuring impedance of cells cultured on nanoporous alumina membrane.

Chapter 4 Discussion and Future Work

4.1 Fabrication of Nanoporous Alumina Membranes

We utilized two-step anodization technique to obtain highly ordered nanoporous alumina membranes from pure aluminum foil, different conditions were optimized to achieve best results. It is one of the most widely used techniques to obtain this nanoporous structure while other methods were also applied and investigated. We also tried a method called one-step anodization, which had similar anodization conditions but only one step was required. This one-step anodization method was investigated before the establishment of the two-step anodization method by Masuda (Masuda et al. 1997). From our experiences, this method can save experimental time and decrease the cost of materials after optimization while problems existed. For the two-step anodization method, the purpose of the first anodization is making ripples where the second anodization can take place. But for the one-step anodization, the development of the nanopores is initialized and guided by the appropriate texture of the aluminum surface at the initial stage of anodization. When we applied anodization voltage 60 V and anodization time 4 hours, nanopores were achieved, but only on parts of the surface, not the whole surface. The sizes of different nanopores are not uniform but varied, even on some parts pores in micro scales were found, which indicated the dissolution of aluminum happened heavily along these sites and formed micro-pores finally. But in other sites without ripples at the initial stage, there's no pores formed. So the one-step

anodization is not the best way to fabricate nanopores but two-step anodization is required. The fabrication process is relatively easy; the physical properties of the nanopores could be controlled by changing some parameter during the fabrication process.

Before fabrication, the aluminum surfaces were pre-treated to make it clean and smooth. Acetone is a highly evaporative chemical and it removed soluble impurities and contaminants on the surface of aluminum during the 5 minutes washing, after that acetone was evaporated and removed by thorough washing in water. An additional electro-polishing step was taken when we found some of the aluminum surfaces are not clean and smooth even after acetone wash. The step used 5% H_3PO_4 (wt/wt), 5% H_2SO_4 (wt/wt), and 0.2 M CrO_3 at 20 V for around 15 minutes. The electro-polishing using these high acid solutions made the surface extremely smooth and clean. We carefully controlled the time of this electro-polishing since the acid solutions also made the aluminum thinner. It was totally dissolved and disappeared once when the electro-polishing time was longer than 1 hour during that experiment process.

We investigated on the principle happened during the anodization procedure of the two step anodization. The method was relatively simple, but the principles that taken place were complex. The structure of aluminum/alumina/electrolyte interface during anodization in acidic electrolytes is well established. The interface consists of three distinct layers: metallic aluminum, a thin barrier oxide layer, and a relatively thick nanoporous oxide layer. Understanding the anodization process and monitoring the barrier oxide layer thickness can help us fabricate nanoporous alumina membranes with

the regular nanopore arrays. To remove the barrier oxide layer, the anodization voltage and current were optimized and kept constant. Fig 3.1.2 showed that the barrier oxide layer was removed by using our anodization conditions, comparing with the membranes purchased. The oxidation reaction of aluminum to produce alumina happens at the metallic aluminum/barrier oxide layer interface. The thickness of the barrier oxide layer has linearly relationship with the anodization voltage. If the anodization voltage is kept at a constant value during the whole process, the rate of alumina dissolution on the electrolyte side is equal to the rate of alumina production on the metallic side, and then the thickness of the barrier oxide layer remains constant.

To achieve better result and find out relationships, all the conditions for the method were monitored very well, and the conditions used every time were recorded and optimized. Conditions were kept constant for the self-ordering nanoporous architecture can be grown spontaneously, not only for each nanopore but for all the nanoporous patterns on the whole surface. Among these conditions, voltage, current, time and temperature were discussed below. The morphology, topography, sizes and other properties of the membranes can be effectively modified by optimizing the anodizing conditions such as electrolyte, temperature, voltage or time.

Anodization voltage is one of the most important factors to control the sizes and patterns of nanopores. The effect of the anodization voltage can be correlated with a voltage dependence of the volume expansion of the aluminum during oxidation and also the current efficiency for oxide formation It affected the growth rate of nanopores and the inter-pore distance. Optimizing different anodization voltages and temperatures leads to

highly ordered nanoporous membranes. Higher voltage increases the dissolution rate of the aluminum to form pattern, which finally induce the widening of the nanopores, so higher voltages lead larger nanopore sizes. And high voltages lead to wider pore size distribution and low voltages made the size distribution more uniform. During our projects, voltages were applied between 60 V and 120 V. The theoretical linear relationship between anodization voltages and pore diameter is 1.2625 nm/V, as shown in Fig 3.1.5. If the voltage was less than 40 V, it was too low to initial the formation of ripples, so the fabrication process didn't happen and no patter was formed. The distribution of the nanopore sizes were shown in Fig 3.1.6. We also noticed when the voltage was higher than 200 V, regular nanopores could not be formed but only mountain and valley like pattern. It was because of the too high voltages made the dissolution rate too quick and the pores were widened too much to form patterns in micro scale.

Electrical current is another condition which has important effect on the pattern of nanopores. The current increased when higher anodization voltage was applied, and it also increased very quickly if the temperature was higher than 25 ℃. The main driving force in the formation of the channel in the anodic alumina is the electric field and it allowed the fabrication of the initiation point by a mechanical deformation process and continuous growth of the ordered nanoporous channels. When the current is too high, nanopores were not formed and even the sheet of aluminum was broken. Mountain and valley like patterns were found in Fig 3.1.7 when high electrical current were applied. The principle is similar like the voltage, higher current lead faster dissolution rate and made the pores widen. Anyway, there was no linear relationship found for the nanopore

sizes and electrical current. To obtain nanopores with better hexagonal shape, current should be kept less than 200 mA by controlling the temperature low.

The anodization time will also affect the formation of nanopores during the anodization process. The procedure consisted of two different steps, so anodization times were monitored separately. The first anodization time mainly affects the pore arrangement, while the second anodization time only influences the pore length. The primary relationship between parameters of fabricated nanopores and the anodization time was investigated. For the first step, the anodization time was kept shorter than 4 hour. The first step was used to prepare the initial points and holes on the aluminum surface. The step introduced the development of nanopores and also guided the growth of channels. Too less time was not enough to form ripples on the surface of aluminum, but only made tiny dots. But longer time made the surface roughly because of the dissolution happened too much. After careful optimization, we also found that 2 hours were good for the second step. If the total anodization time is too long such as longer than 8 hours, it makes the patter non-uniform and even break into pieces. If the anodization time is shorter than 2 hours, only ripples were found but nanopores were not formed.

We also found that lower temperature was better for the formation of nanopores pattern. When the temperature was higher than 40 ℃, the solution became hot and the ion current became extremely high, which induced the nanopores widen and destroy the formed pattern. Without temperature control, the acid solution will become hot and the diffusion rate increase quickly to form uncontrollable larger pores, and even dissolve all the aluminum within one hour. In order to keep the oxalic acid solution cool, an ice bag

was pasted on the outer wall of the container where fabrication procedure happened. A magnetic stirrer was put into the solutions to make the solution homogeneous while it also helped the solution to keep cool. The temperature of the solution was kept around 5 °C after optimization, and we found it could make the pattern more uniform to achieve regular arrangement of nanopores. As we mentioned, magnetic stirring is important to keep acid concentration distribution uniform in the anodization process. Without stirring, the concentrations of the solutions were not uniform and only parts of the surface could form nanoporous structures.

The two-step anodization was taken in different acid solutions, such as oxalic acid solution, sulfuric acid solution, or phosphoric acid solutions. We found that both 0.3 M oxalic acid and sulfuric acid are suitable for obtain highly ordered nanopore arrays when other conditions are similar. But since sulfuric acid is strong acid, it also etch the aluminum very quickly and made the final product too thin, so we decided to use oxalic acid as anodization solutions.

Thickness of the most widely used aluminum foil is around 50 nm, which is easily to fabricate, researchers are also interested in fabricating the nanoporous membranes with ultra-thin aluminum sheet and on the support of other materials. But for the aluminum foils which were thicker than 200 nm, the fabrication time required was too long. It was better to use aluminum foil thinner than 50 nm to achieve better result in relatively short time.

4.2 Surface modification and micro-patterning

We used silane to make surface modification and PEG to form micro-patterning on the surface. These patterned membranes can be used as substrates for define sensing areas. As we described before, PEG is has excellent chemical properties. The PEG molecular with different chemical groups was used in our lab and the binding efficiency of them were tested and optimized. Fig 3.2.7 showed the SEM image of microwell on nanoporous alumina membrane. The micro-patterns are attractive platforms for a number of biological and biomedical applications including basic investigation of cell adhesion, apoptosis, cell differentiation, phenotype expression. PEG also can be used to fabricate a cellular microenvironment for co-culture for different cells, or three-dimensional (3D) microenvironments with controlled spatiotemporal patterning physical and biochemical factors. Control of the surface function for different areas of surfaces by micro-pattern immobilization of different biomolecules were useful either for investigating the mechanism of cellular signal transduction or for precise control of cell behavior on biomaterial matrices used in tissue engineering. The biomaterials with surface micro-patterning had the ability to regulate cell functions such as proliferation, differentiation, and apoptosis. It is not only an essential tool to investigate the fundamental roles of cell geometry in growth and apoptosis, but also means by which to control cell function in specific areas. Combination of nanoporous membrane and micro-pattern is of highly interests for many biomedical scientists who want to confine cells into specific areas.

After testing PEG with different groups, we found that chemical bonding between PEG layer and nanoporous membrane is better than physical adsorption, since PEG layer can firmly bond with membrane and not easy to detach. The basic chemical structure was showed on Fig 3.2.1. Silane was used as a coupling agent for self-assembly on surfaces with oxide layers, such as Al_2O_3, SiO_2, and glass, for covalent grafting of PEG on these surfaces. The incorporation of a hydrophobic link between PEG and silane could be used to generate extra stabilization of the grafted polymer chains through hydrophobic interactions between them. Different functional groups on silane have distinct properties when binding with PEG and nanoporous surfaces. The silanated polymers can be used to graft on various substrate with oxide layers, including silicates, silicon wafer, ceramic, aluminum, stainless steel, and NiTi alloy. Because these materials are widely used as biomaterials, PEG grafting with silane treatment could be a new method for surface modification for improved biocompatibility.

We investigated on the approach of combining PEG with silane, especially for the grafting efficiency of PEG with different molecular weights ranging from 200 Da to 800 Da. For the lower molecular weights, the grafting efficiency is relatively low. The reason for this problem is the lack of contact between the end hydroxyl (-OH) groups of PEG and the surface. In bulk solution, PEG with high molecular weight is a random coil shape and the hydroxyl groups do not have any driving force to adsorb to the surface. Consequently the density of the grafted chains is usually low when molecular weight is high. Using of smaller PEG monomer with molecular weight less than 500 Da can increase the grafting efficiency significantly. Thus, in many cases PEG less than 800 Da

is applied to increase the effect of PEG grafting on the surfaces. We used PEG with smaller molecular weight in our research because of this.

We also found another factor which should be considered: PEG molecule weight has an important effect on the stability of hydrogel layer and the shape formation of micro-pattern by UV curing. PEG with large molecular weight (MW=3400 or 800 Da) is easy to swell in the solution, which will break into pieces. And also, high molecular weight PEG has less sensitivity to UV light and difficult to be cured. So irregular micro-patterns were formed When PEG with high molecular weight were applied. PEG with smaller molecular weight (MW=300) can form uniform and stable micro-patterns for long term recording.

We noticed several tricks during the fabrication procedure of PEG micro-pattern. The ratio between PEG molecule solution and photo-initiator is important for the PEG hydrogel UV curing. The optimal weight ratio in this experiment is 5:1. More photo-initiator makes the curing process too fast to be controlled while less photo-initiator requires relatively long exposure time which will decrease the resolution of the micro-patterns.

After surface modification with PEG, study was carried out to investigate the relationships between surface properties, protein adsorption and the activity of cells on the modified surfaces treated with media containing serum. Fig 3.2.1 to Fig 3.2.6 showed the results monitored by three different techniques: XPS, water contact angle, and fluorescence imaging. PEG is very widely used for micro-patterning. PEG micro-

patterning could be incorporated with other techniques to fabricate stable, precise, well-controlled patterns for cells. In our project, surface modification and protein adsorption were both taken and the microenvironments were formed by micro-patterning of silane and PEG, which were useful for controlling of cells distribution and co-culture for different cells.

The designed cell patterning to control cell position and function on a substrate is a fundamental focus for the development of cell biosensor technology and tissue engineering applications. The micro-patterning technology is useful for construction of biosensor devices and also for the investigation of the fundamental biology of cell-ECM interactions. The surface modification we used is also very effective to change the properties of the nanoporous membranes and also increase the protein adsorption, which result in higher cell biocompatibility through the better adhesion effect of cells.

4.3 Cell culture and cell biocompatibility of the membranes

Behaviors of different cells cultured on nanoporous alumina membrane were studied.

We studied the impact of the nanopores on cell response by evaluating cell adhesion, morphology, cell proliferation. Both short-term adhesion and long-term proliferation of cells on nanoporous alumina membrane surfaces were investigated. As in Fig 3.4.1, SEM images of cells fixed on the surface showed that the cells had extended their processes into the nanopores and were indeed able to respond to the nanoscale features. Analysis of fluorescence images of the cells at different culture days showed that the cells exhibiting normal phenotype and morphology and the cell can respond to both the

substrate topography and surface chemistry. The images were showed in Fig 3.4.4. The cells performance can be significantly improved using nanoporous alumina membrane as a culture substrate. Anyway, the surface properties may be different when the materials were from different lab, and the cell lines are also different, so we need to do biocompatibility experiments by ourselves.

In our project, because the properties of the culture device incorporated with nanoporous alumina membranes were not the same as common culture dish, there were several tips should be mentioned and noticed. We use UV sterilization instead of high temperatures sterilization. Before cell culture, sterilization is required, but the only method could be applied is UV curing, avoid using high temperature. The temperature above 80 ℃ will make the PEG hydrogel broken and destroy the micro-pattern. The PEG monomer could be cured using UV light, but cured PEG hydrogel will not be affected by UV, so UV light can be used for sterilization.

In order to get subtle pattern of cells on the surface, we controlled the cell numbers within PEG hydrogel microwells, to get low concentration of cells or even single cells in every microwell. Fig 3.6.2 showed the array of microwells with cells cultured within them, fig 3.6.3 counted the number of cells within each microwell. The size of microwells is very important to contol the numbers. Smaller microwell size can achieve a few of cells within it, while the larger microwell size can achieve more cells. After optimization of microwell sizes, a 50 μm microwell can even achieve single cell patterning with appropriate initial cell concentration. Anyway, the concentration of initial cells is another important factor to achieve single cell within each microwell.

High concentration will make too many cells within each microwell, while too low concentration will make most of the microwells empty.

Three types of surfaces were used to culture cells, in order to compare the effects and find which one are most suitable for the proliferation of cells. From the results we acquired, which were shown in Fig 3.4.5, among nanoporous alumina membrane, pure aluminum, and glass, nanoporous alumina membranes we fabricated has the highest biocompatibility. It indicates that the cells like the surface with nanostructures, which is even better than the microstructures. The surface roughness and porosity also has positive impacts on cell activity on it. The results showed that nanoporous alumina membrane is an excellent biomaterial to culture cells. Overall, the results showed that nanoporous alumina membrane is an excellent biomaterial for cell culture, and good for the impedance measurements and analysis.

From the results we acquired from section 3.4, we found the conclusion that surface topographical cues of biomaterials may have significant effects upon cellular behavior *in vivo* and *in vitro*. The topography of different substrates plays an important role in regulating cellular behavior, which could finally reflect as different biocompatibility of the substrates.

Alumina has already been used extensively, in various forms, as a scaffold for bone tissue engineering applications. And the alumina surface show significant biointegration and cell ingrowth. When using nanoporous alumina, which has features on the nano-scale, the surface topography has been shown to influence cell orientation, migration,

and attachment. Nanoporous alumina surfaces demonstrated high cell adhesion and promoted cell proliferation, when compared with amorphous alumina surfaces or traditional micro-scale topography. The adhesion and proliferation phases are extremely important because these factors will govern the long-term functionality of the cells cultured on the surfaces. Thus, the nano-architectures on surface can facilitate the cell culture and provide long-term cell viability and functionality. So, the topographical properties make those alumina nanopores relatively more biocompatible than other substrates, tested in our studies.

4.4 Impedance Analysis of our nanopore-based impedance biosensor

We used the non-conductive nanoporous alumina membrane as substrate to culture cells, it has less polarization effect compared with metal electrode. Comparing with the electrode-based impedance biosensor, nanopore-based impedance biosensors have many advantages. In this project, the diameters of the nanopores are between 20 nm ~200 nm which can be controlled by adjusting the anodization voltages. The impedance spectra with different nanopore sizes were shown in chapter 3.5. While the diameters of common ions in the electrolytes are less than 20 nm, the ions can go through the nanopores freely when the electrical fields are applied in the electrolyte. Because alumina is an oxide of aluminum, it is an electrical insulator which can resist the flow of electric current, nanoporous alumina membrane is an insulated membrane which doesn’t allow electrical current to flow through. That means when the electrical fields are applied, the electrical current can only go through the nanopores but not other areas. So

the current density nearby the nanopores is relatively high while the current density in other areas is relatively low.

From Fig 3.7.1, we investigated the impedance spectra of cell growth for different days when frequency ranging from 0.1 Hz to 10 KHz. For metal electrode, the working frequency is between 10 KHz and 100 KHz due to the high surface polarization effect. But for the nanoporous alumina membranes, the working frequency is between 1 Hz and 100 Hz, which is much less than the traditional metal electrode. For cell culture and monitoring purpose, the best frequency range is within low frequency range, since most cell activities are within this range. So the nanoporous alumina membranes are suitable for cell activity monitoring.

When cells are cultured on the nanoporous alumina membranes, some of the nanopores are covered and blocked by the cells. As shown in Chapter 3.1, the nanopore density of fabricated membranes was calculated and the values were around 50 pores/μm^2. Generally, the sizes of mammalian cells are between 10 μm and 50 μm, so a normal cell can cover more than 20,000 nanopores. The current flowing through the nanopores should be changed sensitively according to the cell morphology changes since states of large numbers of nanopores will be changed. The measured impedance should also be changed according to the electrical current change. In this configuration and setup, if there are only a few numbers of cells or even single cell cultured on the membrane or within the sensing area, it also can be measured and the morphology changes can be detected. There are several possible factors which may have influence on the sensitivity

of this nanopore based impedance biosensor, such as average diameter of nanopore and frequency of electrical current.

The first factor is nanopore size diameter. The diffusion rates of drugs were monitored and shown in chapter 3.3. If the average value of nanopore diameters increase, the nanopore density will decrease per unit area, then the number of nanopores covered per cells will decrease. The same morphology changes altered status of fewer nanopores, and finally the change of measured impedance was not as large as that of smaller nanopore sizes. From this point, smaller nanopore diameters increased sensitivity while larger nanopore diameters decreased sensitivity of this impedance biosensor. But if the diameters are too small, the nanostructures could not perform their positive impact on the cells. So, the nanopores which have the diameter near the scales of subcellular is best suitable for the experiments.

The frequency of the electrical current is also an important factor to the sensitivity. Fig 3.7.1 showed the impedance data for different frequency. Because nanoporous alumina membrane is insulating and the low frequency current should be blocked well because of its low conductivity, and therefore the low frequency current tends to flow through the nanopores, the sensitivity will be increased since most of the electrical field lines are going through the nanopores. On the other hand, since a high frequency current can penetrate the insulated membrane, the electrical field lines not only go through the nanopores but also go through other areas of the insulated membrane. This will lead higher electrical current and lower impedance data and the sensitivity about the measured impedance will be decreased.

As mentioned before, one advantage of this nanopore-based impedance biosensor is high sensitivity which can be used for low concentrations of cells detection. It has the potential for even single cell impedance sensing. To combine with the PEG surface modification, it is possible to define sensing area, the area of which can be controlled. After the first step of silane treatment, photoresist masks with different patterns can be used to fabricate micro-pattern on the surface. The final PEG micro-patterns on the nanoporous alumina membranes are defined by the patterns on the masks. If the diameter of every microhole is less than 50 μm, it is relatively easy to just culture only a few cells or even single cell within one microhole. At the same time, if there's only one microhole in the pattern or the distances between microholes are very large, most of the surface area would be covered with PEG, and the cells could not be cultured on these area. Finally the number of cells cultured on the nanoporous alumina membranes with PEG micro-patterns would be very low. This PEG modified membranes are very suitable to monitoring cells with low concentration or even single cell.

4.5 Future Work

Furthermore, the drug delivery function will be added to this nanoporous membrane based cell impedance sensing platform. The nanoporous alumina membrane will be integrated with PDMS channel and micro-tubes which connected with micro-pumps will be used to deliver and inject drug into the chamber. Different drug delivery patterns will be designed and the cancer cell response under these patterns will be studied.

More anti-cancer drug testing will be explored to improve the measuring accuracy of this device. Since the system contains microwells which can have low concentration cells or even single cell, it is possible for us to observe the single cell response under the effect of several drugs at the same time.

The nanoporous alumina membranes will be integrated with silicon microfluidic chips to add other functions. A layer of aluminum with thickness of 50 um will be deposited on silicon wafer. Then two step anodization happened on the surface could make nanoporous aluminum membrane on it. Traditional micro-fabrication methods will be applied on the Si wafer to achieve different chips or devices. More functions will be introduced by these steps.

This nanopore-based impedance biosensor also can be used to monitoring and detection for other samples such as bacteria, DNA. Before silane treatment procedure, special groups can be introduced on silane. After the silane treatment, bacteria antibody can binding on the group and to be captured. Then the changes of concentrations or morphology can be detected by measuring impedance of nanoporous alumina membranes. Impedance amplitude could be used to monitor the biological sample behavior study, and phase base sensing can be another potential area to explorer.

4.6 Conclusion

The main contribution of this thesis is the fabrication and demonstration of a novel non-conductive nanoporous membrane based cellular impedance biosensor with high sensitivity in the low frequency range.

Nanoporous alumina membranes were fabricated by two-step anodization techniques, and investigated by SEM. The method is straightforward and the nanoporous structure can be fabricated either from bulk aluminum foil or on solid supports such as silicon wafers with aluminum films. We also tried to combine many different techniques including photolithography, plasma etching to fabricate the patterned nanoporous arrays. All of these fabrication steps can be integrated into a easily controlled fabrication line, and the advantages of the combination of these techniques will facilitate the incorporation of patterned nanoporous alumina arrays into micro- and nanodevices, or even fabricate nanopores on the solid base material like Si wafer.

The unique properties of the nanoporous alumina membranes, such as extremely high aspect ration features, make them increasingly attractive and to be suitable candidates for many applications in physical, chemical, electrical and other research fields. The nanoporous membranes provided a wide range of potential applications in various fields, such as filtration, duplication matrixes, evaporation masks, the high-density recording media, rechargeable batteries, optoelectronic devices and template for the growth of metal or semiconductor nanowire. The membranes were also used in biomedical applications or tissue engineering applications, including fabrication of implantable

device or artificial bone structures. The biocompatibility of nanoporous alumina membranes should be studied and some surface modifications should be taken for adhesion and spreading of cells when cultured on the nanoporous alumina membranes. Our research also gave contribution to the usage of nanoporous alumina membranes in biomedical fields, which will be discussed later.

The PEG hydrogel layer with micro-pattern was fabricated on the silane modified membranes, and analyzed by XPS, water contact angle measurement and protein adsorption. The micro-pattern controlled the spatial distribution of hydrophobic and hydrophilic areas on the surface. This PEG microwell based cell patterning technique can achieve low number or even single cell within microwells. A microfluidic chip integrated with nanoporous membranes was developed for low concentration of cells study. KYSE30 cancer cells were patterned within the microwells but not outside of them. Impedance spectra of the nanoporous alumina membrane with cell cultured on it were explored. It could be used to detect cell morphology changes by monitoring impedance spectroscopy. Described in my thesis, impedance spectra of the nanoporous alumina membrane with cell cultured on it were explored. Some biometric parameters related with both cell growth and drug induced changes such as sizes, numbers, spreading areas, or even concentrations of ECM were detected with impedance spectroscopy. This new morphology-sensitive electrochemical micro-system was tested by detecting the impedance change for both cell growth and drug induced changes. The technique was also testified by detecting the impedance change for different anti-cancer drugs induced apoptosis. ELISA and fluorescence images are utilized to confirm the effectiveness of the impendence changes.

Combined with traditional biochemical methods, nanoporous membrane based cell impedance sensing platform can be a valid tool for study drug effects on cancer cell apoptosis. This platform is also very useful for other cells and other biological species sensing including bacteria, DNA, and protein.

Reference

Akeson, M., D. Branton, J. J. Kasianowicz, E. Brandin, and D. W. Deamer. 1999. Microsecond time-scale discrimination among polycytidylic acid, polyadenylic acid, and polyuridylic acid as homopolymers or as segments within single RNA molecules. *Biophysical Journal* 77: 3227-3233.

Alivisatos, A. P. 1999. Semiconductor nanocrystals as fluorescent biological labels. *Abstracts of Papers of the American Chemical Society* 218: U296-U296.

Arndt, S., J. Seebach, K. Psathaki, H. J. Galla, and J. Wegener. 2004. Bioelectrical impedance assay to monitor changes in cell shape during apoptosis. *Biosensors & Bioelectronics* 19: 583-594.

Bauer, L. A., N. S. Birenbaum, and G. J. Meyer. 2004. Biological applications of high aspect ratio nanoparticles. *Journal of Materials Chemistry* 14: 517-526.

Baughman, R. H., C. X. Cui, A. A. Zakhidov, Z. Iqbal, J. N. Barisci, G. M. Spinks, G. G. Wallace, A. Mazzoldi, D. De Rossi, A. G. Rinzler, O. Jaschinski, S. Roth, and M. Kertesz. 1999. Carbon nanotube actuators. *Science* 284: 1340-1344.

Bayley, H., and P. S. Cremer. 2001. Stochastic sensors inspired by biology. *Nature* 413: 226-230.

Brevnov, D. A., M. Barela, M. E. Piyasena, G. P. Lopez, and P. B. Atanassov. 2004. Patterning of nanoporous anodic aluminum oxide arrays by using sol-gel processing, photolithography, and plasma etching. *Chemistry of Materials* 16: 682-687.

Campbell, C. E., M. M. Laane, E. Haugarvoll, and I. Giaever. 2007. Monitoring viral-induced cell death using electric cell-substrate impedance sensing. *Biosensors & Bioelectronics* 23: 536-542.

Cao, R. G., B. Zhu, J. J. Li, and D. S. Xu. 2009. Oligonucleotides-based biosensors with high sensitivity and selectivity for mercury using electrochemical impedance spectroscopy. *Electrochemistry Communications* 11: 1815-1818.

Chen, C. S., M. Mrksich, S. Huang, G. M. Whitesides, and D. E. Ingber. 1998. Micropatterned surfaces for control of cell shape, position, and function. *Biotechnology Progress* 14: 356-363.

Cho, S. B., and H. Thielecke. 2007. Micro hole-based cell chip with impedance spectroscopy. *Biosensors & Bioelectronics* 22: 1764-1768.

Chong, M. A. S., Y. B. Zheng, H. Gao, and L. K. Tan. 2006. Combinational template-assisted fabrication of hierarchically ordered nanowire arrays on substrates for device applications. *Applied Physics Letters* 89: -.

Chui, C. H., R. Gambari, F. Y. Lau, G. Y. M. Cheng, R. S. M. Wong, S. H. L. Kok, J. C. O. Tang, I. T. N. Teo, F. Cheung, C. H. Cheng, K. P. Ho, A. S. C. Chan, and A. Wong. 2006. *In vitro* anti-cancer activity of a novel microbial fermentation product on human carcinomas. *International Journal of Molecular Medicine* 17: 675-679.

Chung, C. K., R. X. Zhou, T. Y. Liu, and W. T. Chang. 2009. Hybrid pulse anodization for the fabrication of porous anodic alumina films from commercial purity (99%) aluminum at room temperature. *Nanotechnology* 20: -.

Connolly, P., P. Clark, A. S. G. Curtis, J. A. T. Dow, and C. D. W. Wilkinson. 1990. An Extracellular Microelectrode Array for Monitoring Electrogenic Cells in Culture. *Biosensors & Bioelectronics* 5: 223-234.

Cui, D. X. 2007. Advances and prospects on biomolecules functionalized carbon nanotubes. *Journal of Nanoscience and Nanotechnology* 7: 1298-1314.

Daniels, J. S., and N. Pourmand. 2007. Label-free impedance biosensors: Opportunities and challenges. *Electroanalysis* 19: 1239-1257.

Dean, D. A., T. Ramanathan, D. Machado, and R. Sundararajan. 2008. Electrical impedance spectroscopy study of biological tissues. *Journal of Electrostatics* 66: 165-177.

Ding, G. Q., M. J. Zheng, W. L. Xu, and W. Z. Shen. 2005. Fabrication of controllable free-standing ultrathin porous alumina membranes. *Nanotechnology* 16: 1285-1289.

Ehret, R., W. Baumann, M. Brischwein, A. Schwinde, K. Stegbauer, and B. Wolf. 1997. Monitoring of cellular behaviour by impedance measurements on interdigitated electrode structures. *Biosensors & Bioelectronics* 12: 29-41.

Ehret, R., W. Baumann, M. Brischwein, A. Schwinde, and B. Wolf. 1998. On-line control of cellular adhesion with impedance measurements using interdigitated electrode structures. *Medical & Biological Engineering & Computing* 36: 365-370.

Faucheux, N., R. Schweiss, K. Lutzow, C. Werner, and T. Groth. 2004. Self-assembled monolayers with different terminating groups as model substrates for cell adhesion studies. *Biomaterials* 25: 2721-2730.

Fissell, W. H., H. D. Humes, A. J. Fleischman, and S. Roy. 2007. Dialysis and nanotechnology: Now, 10 years, or never? *Blood Purification* 25: 12-17.

Flemming, R. G., C. J. Murphy, G. A. Abrams, S. L. Goodman, and P. F. Nealey. 1999. Effects of synthetic micro- and nano-structured surfaces on cell behavior. *Biomaterials* 20: 573-588.

Fodor, P. S., G. M. Tsoi, and L. E. Wenger. 2002. Fabrication and characterization of Co1-xFex alloy nanowires. *Journal of Applied Physics* 91: 8186-8188.

Fulda, S., and K. M. Debatin. 2004. Apoptosis signaling in tumor therapy. *Signal Transduction and Communication in Cancer Cells* 1028: 150-156.

Giaever, I., and C. R. Keese. 1993. A Morphological Biosensor for Mammalian-Cells. *Nature* 366: 591-592.

Glamann, J., and A. J. Hansen. 2006. Dynamic detection of natural killer cell-mediated cytotoxicity and cell adhesion by electrical impedance measurements. *Assay and Drug Development Technologies* 4: 555-563.

Hacker, G. 2000. The morphology of apoptosis. *Cell and Tissue Research* 301: 5-17.

Han, K. H., A. Han, and A. B. Frazier. 2006. Microsystems for isolation and electrophysiological analysis of breast cancer cells from blood. *Biosensors & Bioelectronics* 21: 1907-1914.

Hanahan, D., and R. A. Weinberg. 2000. The hallmarks of cancer. *Cell* 100: 57-70.

Hennessey, H., N. Afara, S. Omanovic, and A. L. Padjen. 2009. Electrochemical investigations of the interaction of C-reactive protein (CRP) with a CRP antibody chemically immobilized on a gold surface. *Analytica Chimica Acta* 643: 45-53.

HKACS. http://www.hkacs.org.hk/tc/agm2004_01.html. *Hong Kong Anti-Cancer Society*.

Hoess, A., N. Teuscher, A. Thormann, H. Aurich, and A. Heilmann. 2007. Cultivation of hepatoma cell line HepG2 on nanoporous aluminum oxide membranes. *Acta Biomaterialia* 3: 43-50.

Huang, Y., M. C. Bell, and I. I. Suni. 2008. Impedance Biosensor for Peanut Protein Ara h 1. *Analytical Chemistry* 80: 9157-9161.

Hwang, S. K., S. H. Jeong, H. Y. Hwang, O. J. Lee, and K. H. Lee. 2002. Fabrication of highly ordered pore array in anodic aluminum oxide. *Korean Journal of Chemical Engineering* 19: 467-473.

Ito, Y. 1999. Surface micropatterning to regulate cell functions. *Biomaterials* 20: 2333-2342.

Jager, E. W. H., C. Immerstrand, K. H. Peterson, K. E. Magnusson, I. Lundstrom, and O. Inganas. 2002. The cell clinic: Closable microvials for single cell studies. *Biomedical Microdevices* 4: 177-187.

Jessensky, O., F. Muller, and U. Gosele. 1998. Self-organized formation of hexagonal pore arrays in anodic alumina. *Applied Physics Letters* 72: 1173-1175.

Jie, G. F., B. Liu, H. C. Pan, J. J. Zhu, and H. Y. Chen. 2007. CdS nanocrystal-based electrochemiluminescence biosensor for the detection of low-density lipoprotein by increasing sensitivity with gold nanoparticle amplification. *Analytical Chemistry* 79: 5574-5581.

Jo, S., and K. Park. 2000. Surface modification using silanated poly(ethylene glycol)s. *Biomaterials* 21: 605-616.

Jung, D. R., D. S. Cuttino, J. J. Pancrazio, P. Manos, T. Cluster, R. S. Sathanoori, L. E. Aloi, M. G. Coulombe, M. A. Czamaski, D. A. Borkholder, G. T. A. Kovacs, P. Bey, D. A. Stenger, and J. J. Hickman. 1998. Cell-based sensor microelectrode

array characterized by imaging x-ray photoelectron spectroscopy, scanning electron microscopy, impedance measurements, and extracellular recordings. *Journal of Vacuum Science & Technology a-Vacuum Surfaces and Films* 16: 1183-1188.

K'Owino, I. O., and O. A. Sadik. 2005. Impedance spectroscopy: A powerful tool for rapid biomolecular screening and cell culture monitoring. *Electroanalysis* 17: 2101-2113.

Kang, X. H., Z. B. Mai, X. Y. Zou, P. X. Cai, and J. Y. Mo. 2008. Glucose biosensors based on platinum nanoparticles-deposited carbon nanotubes in sol-gel chitosan/silica hybrid. *Talanta* 74: 879-886.

Katz, E., O. Lioubashevski, and I. Willner. 2004. Magnetic field effects on cytochrome c-mediated bioelectrocatalytic transformations. *Journal of the American Chemical Society* 126: 11088-11092.

Keese, C. R., J. Wegener, S. R. Walker, and L. Giaever. 2004. Electrical wound-healing assay for cells *in vitro*. *Proceedings of the National Academy of Sciences of the United States of America* 101: 1554-1559.

Kelley, S. O., J. K. Barton, N. M. Jackson, L. D. McPherson, A. B. Potter, E. M. Spain, M. J. Allen, and M. G. Hill. 1998. Orienting DNA helices on gold using applied electric fields. *Langmuir* 14: 6781-6784.

La Flamme, K. E., K. C. Popat, L. Leoni, E. Markiewicz, T. J. La Tempa, B. B. Roman, C. A. Grimes, and T. A. Desai. 2007. Biocompatibility of nanoporous alumina membranes for immunoisolation. *Biomaterials* 28: 2638-2645.

Lee, S. W., H. Shang, R. T. Haasch, V. Petrova, and G. U. Lee. 2005. Transport and functional behaviour of poly(ethylene glycol)-modified nanoporous alumina membranes. *Nanotechnology* 16: 1335-1340.

Li, Q. W., G. A. Luo, J. Feng, Q. Zhou, L. Zhang, and Y. F. Zhu. 2001. Amperometric detection of glucose with glucose oxidase absorbed on porous nanocrystalline TiO2 film. *Electroanalysis* 13: 413-416.

Li, X. M., H. Gao, M. Uo, Y. Sato, T. Akasaka, Q. L. Feng, F. Z. Cui, X. H. Liu, and F. Watari. 2009. Effect of carbon nanotubes on cellular functions *in vitro*. *Journal of Biomedical Materials Research Part A* 91A: 132-139.

Li, Y. B., M. J. Zheng, L. Ma, and W. Z. Shen. 2006. Fabrication of highly ordered nanoporous alumina films by stable high-field anodization. *Nanotechnology* 17: 5101-5105.

Liu, B., A. J. Bard, C. Z. Li, and H. B. Kraatz. 2005. Scanning electrochemical microscopy. 51. Studies of self-assembled monolayers of DNA in the absence and presence of metal ions. *J Phys Chem B* 109: 5193-8.

Liu, W. T. 2006. Nanoparticles and their biological and environmental applications. *Journal of Bioscience and Bioengineering* 102: 1-7.

Liu, Y. T., W. Zhao, Z. Y. Huang, Y. F. Gao, X. M. Xie, X. H. Wang, and X. Y. Ye. 2006. Noncovalent surface modification of carbon nanotubes for solubility in organic solvents. *Carbon* 44: 1613-1616.

Lo, C. M., C. R. Keese, and I. Giaever. 1994. Ph Changes in Pulsed Co2 Incubators Cause Periodic Changes in Cell Morphology. *Experimental Cell Research* 213: 391-397.

Long, Y. T., C. Z. Li, H. B. Kraatz, and J. S. Lee. 2003. AC impedance spectroscopy of native DNA and M-DNA. *Biophys J* 84: 3218-25.

Losic, D., and S. Simovic. 2009. Self-ordered nanopore and nanotube platforms for drug delivery applications. *Expert Opinion on Drug Delivery* 6: 1363-1381.

Luong, J. H. T., M. Habibi-Rezaei, J. Meghrous, C. Xiao, K. B. Male, and A. Kamen. 2001. Monitoring motility, spreading, and mortality of adherent insect cells using an impedance sensor. *Analytical Chemistry* 73: 1844-1848.

Mapili, G., Y. Lu, S. C. Chen, and K. Roy. 2005. Laser-layered microfabrication of spatially patterned functionalized tissue-engineering scaffolds. *Journal of Biomedical Materials Research Part B-Applied Biomaterials* 75B: 414-424.

Marquis, M. E., E. Lord, E. Bergeron, O. Drevelle, H. Park, F. Cabana, H. Senta, and N. Faucheux. 2009. Bone cells-biomaterials interactions. *Frontiers in Bioscience* 14: 1023-1067.

Marsal, L. F., L. Vojkuvka, P. Formentin, J. Pallares, and J. Ferre-Borrull. 2009. Fabrication and optical characterization of nanoporous alumina films annealed at different temperatures. *Optical Materials* 31: 860-864.

Martin, J. I., J. Nogues, K. Liu, J. L. Vicent, and I. K. Schuller. 2003. Ordered magnetic nanostructures: fabrication and properties. *Journal of Magnetism and Magnetic Materials* 256: 449-501.

Masuda, H., H. Yamada, M. Satoh, H. Asoh, M. Nakao, and T. Tamamura. 1997. Highly ordered nanochannel-array architecture in anodic alumina. *Applied Physics Letters* 71: 2770-2772.

McBain, S. C., H. H. P. Yiu, and J. Dobson. 2008. Magnetic nanoparticles for gene and drug delivery. *International Journal of Nanomedicine* 3: 169-180.

Mearns, F. J., E. L. S. Wong, K. Short, D. B. Hibbert, and J. J. Gooding. 2006. DNA biosensor concepts based on a change in the DNA persistence length upon hybridization. *Electroanalysis* 18: 1971-1981.

Miyawaki, J., M. Yudasaka, T. Azami, Y. Kubo, and S. Iijima. 2008. Toxicity of single-walled carbon nanohorns. *Acs Nano* 2: 213-226.

Murray, C. B., C. R. Kagan, and M. G. Bawendi. 2000. Synthesis and characterization of monodisperse nanocrystals and close-packed nanocrystal assemblies. *Annual Review of Materials Science* 30: 545-610.

Ozao, R., H. Yoshida, T. Inada, and M. Ochiai. 2003. Sulfur concentration in nanoporous alumina membrane - Studied by TA and XPS. *Journal of Thermal Analysis and Calorimetry* 72: 113-118.

Pan, S. L., and L. J. Rothberg. 2003. Interferometric sensing of biomolecular binding using nanoporous aluminum oxide templates. *Nano Letters* 3: 811-814.

Patolsky, F., G. Zheng, and C. M. Lieber. 2006. Nanowire sensors for medicine and the life sciences. *Nanomedicine* 1: 51-65.

Paulus, P. M., F. Luis, M. Kroll, G. Schmid, and L. J. de Jongh. 2001. Low-temperature study of the magnetization reversal and magnetic anisotropy of Fe, Ni, and Co nanowires. *Journal of Magnetism and Magnetic Materials* 224: 180-196.

Popat, K. C., K. I. Chatvanichkul, G. L. Barnes, T. J. Latempa, C. A. Grimes, and T. A. Desai. 2007. Osteogenic differentiation of marrow stromal cells cultured on nanoporous alumina surfaces. *Journal of Biomedical Materials Research Part A* 80A: 955-964.

Popat, K. C., E. E. L. Swan, V. Mukhatyar, K. I. Chatvanichkul, G. K. Mor, C. A. Grimes, and T. A. Desai. 2005. Influence of nanoporous alumina membranes on long-term osteoblast response. *Biomaterials* 26: 4516-4522.

Ran, C. B., G. Q. Ding, W. C. Liu, Y. Deng, and W. T. Hou. 2008. Wetting on nanoporous alumina surface: Transition between Wenzel and Cassie states controlled by surface structure. *Langmuir* 24: 9952-9955.

Reddy, L., H. S. Wang, C. R. Keese, I. Giaever, and T. J. Smith. 1998. Assessment of rapid morphological changes associated with elevated cAMP levels in human orbital fibroblasts. *Experimental Cell Research* 245: 360-367.

Reich, D. H., M. Tanase, A. Hultgren, L. A. Bauer, C. S. Chen, and G. J. Meyer. 2003. Biological applications of multifunctional magnetic nanowires (invited). *Journal of Applied Physics* 93: 7275-7280.

Rodriguez, M., and J. Schaper. 2005. Apoptosis: measurement and technical issues. *Journal of Molecular and Cellular Cardiology* 38: 15-20.

Romer, W., and C. Steinem. 2004. Impedance analysis and single-channel recordings on nano-black lipid membranes based on porous alumina. *Biophysical Journal* 86: 955-965.

Sackmann, E. 1996. Supported membranes: Scientific and practical applications. *Science* 271: 43-48.

Sadik, O. A., H. Xu, E. Gheorghiu, D. Andreescu, C. Balut, M. Gheorghiu, and D. Bratu. 2002. Differential impedance Spectroscopy for monitoring protein immobilization and antibody-antigen reactions. *Analytical Chemistry* 74: 3142-3150.

Sellers, W. R., and D. E. Fisher. 1999. Apoptosis and cancer drug targeting. *Journal of Clinical Investigation* 104: 1655-1661.

Seriburi, P., S. McGuire, A. Shastry, K. F. Bohringer, and D. R. Meldruim. 2008. Measurement of the cell-substrate separation and the projected area of an individual adherent cell using electric cell-substrate impedance sensing. *Analytical Chemistry* 80: 3677-3683.

Sharma, G., M. V. Pishko, and C. A. Grimes. 2007. Fabrication of metallic nanowire arrays by electrodeposition into nanoporous alumina membranes: effect of barrier layer. *Journal of Materials Science* 42: 4738-4744.

Singh, S. P., S. K. Arya, P. Pandey, B. D. Malhotra, S. Saha, K. Sreenivas, and V. Gupta. 2007. Cholesterol biosensor based on rf sputtered zinc oxide nanoporous thin film. *Applied Physics Letters* 91: -.

Steinem, C., A. Janshoff, W. P. Ulrich, M. Sieber, and H. J. Galla. 1996. Impedance analysis of supported lipid bilayer membranes: A scrutiny of different preparation techniques. *Biochimica Et Biophysica Acta-Biomembranes* 1279: 169-180.

Sun, S. S., C. Z. Li, L. Zhang, H. L. Du, and J. S. Burnell-Gray. 2006. Effects of surface modification of fumed silica on interfacial structures and mechanical properties of poly(vinyl chloride) composites. *European Polymer Journal* 42: 1643-1652.

Swan, E. E. L., K. C. Popat, and T. A. Desai. 2005a. Peptide-immobilized nanoporous alumina membranes for enhanced osteoblast adhesion. *Biomaterials* 26: 1969-1976.

Swan, E. E. L., K. C. Popat, C. A. Grimes, and T. A. Desai. 2005b. Fabrication and evaluation of nanoporous alumina membranes for osteoblast culture. *Journal of Biomedical Materials Research Part A* 72A: 288-295.

Takmakov, P., I. Vlassiouk, and S. Smirnov. 2006. Application of anodized aluminum in fluorescence detection of biological species. *Analytical and Bioanalytical Chemistry* 385: 954-958.

Tan, J., and W. M. Saltzman. 2002. Topographical control of human neutrophil motility on micropatterned materials with various surface chemistry. *Biomaterials* 23: 3215-3225.

Tiruppathi, C., A. B. Malik, P. J. Delvecchio, C. R. Keese, and I. Giaever. 1992. Electrical Method for Detection of Endothelial-Cell Shape Change in Real-Time - Assessment of Endothelial Barrier Function. *Proceedings of the National Academy of Sciences of the United States of America* 89: 7919-7923.

Tlili, C., N. Jaffrezic-Renault, C. Martelet, J. P. Mahy, S. Lecomte, M. M. Chehimi, and H. Korri-Youssoufi. 2008. A new method of immobilization of proteins on activated ester terminated alkanethiol monolayers towards the label free impedancemetric detection. *Materials Science & Engineering C-Biomimetic and Supramolecular Systems* 28: 861-868.

Tsujino, I., J. Ako, Y. Honda, and P. J. Fitzgerald. 2007. Drug delivery via nano-, micro and macroporous coronary stent surfaces. *Expert Opinion on Drug Delivery* 4: 287-295.

Usui, Y., K. Aoki, N. Narita, N. Murakami, I. Nakamura, K. Nakamura, N. Ishigaki, H. Yamazaki, H. Horiuchi, H. Kato, S. Taruta, Y. A. Kim, M. Endo, and N. Saito.

2008. Carbon nanotubes with high bone-tissue compatibility and bone-formation acceleration effects. *Small* 4: 240-246.

Vestergaard, M., K. Kerman, and E. Tamiya. 2007. An overview of label-free electrochemical protein sensors. *Sensors* 7: 3442-3458.

Vlassiouk, I., A. Krasnoslobodtsev, S. Smirnov, and M. Germann. 2004. "Direct" detection and separation of DNA using nanoporous alumina filters. *Langmuir* 20: 9913-9915.

Wang, J. 2005. Carbon-nanotube based electrochemical biosensors: A review. *Electroanalysis* 17: 7-14.

Wang, J. L., D. K. Xu, and H. Y. Chen. 2009a. A novel protein analytical method based on hybrid-aptamer and DNA-arrayed electrodes. *Electrochemistry Communications* 11: 1627-1630.

Wang, P., and Q. Liu. 2009. *Cell-Based Biosensors: Principles and Applications*.

Wang, R. H., Y. Wang, K. Lassiter, Y. B. Li, B. Hargis, S. Tung, L. Berghman, and W. Bottje. 2009b. Interdigitated array microelectrode based impedance immunosensor for detection of avian influenza virus H5N1. *Talanta* 79: 159-164.

Wegener, J., C. R. Keese, and I. Giaever. 2000. Electric cell-substrate impedance sensing (ECIS) as a noninvasive means to monitor the kinetics of cell spreading to artificial surfaces. *Experimental Cell Research* 259: 158-166.

Wikipedia. http://en.wikipedia.org/wiki/Cancer.

Wu, M. T., I. C. Leu, J. H. Yen, and A. H. Hon. 2005. Novel electrodeposition behavior of ni on porous anodic alumina templates without a conductive interlayer. *Journal of Physical Chemistry B* 109: 9575-9580.

Xiao, C., B. Lachance, G. Sunahara, and J. H. T. Luong. 2002a. An in-depth analysis of electric cell-substrate impedance sensing to study the attachment and spreading mammalian cells. *Analytical Chemistry* 74: 1333-1339.

Xiao, C., and J. H. T. Luong. 2003. On-line monitoring of cell growth and cytotoxicity using electric cell-substrate impedance sensing (ECIS). *Biotechnology Progress* 19: 1000-1005.

Xiao, C. D., B. Lachance, G. Sunahara, and J. H. T. Luong. 2002b. Assessment of cytotoxicity using electric cell-substrate impedance sensing: Concentration and time response function approach. *Analytical Chemistry* 74: 5748-5753.

Yang, L. J. 2008. Electrical impedance spectroscopy for detection of bacterial cells in suspensions using interdigitated microelectrodes. *Talanta* 74: 1621-1629.

Yang, L. J., Y. B. Li, C. L. Griffis, and M. G. Johnson. 2004. Interdigitated microelectrode (IME) impedance sensor for the detection of viable Salmonella typhimurium. *Biosensors & Bioelectronics* 19: 1139-1147.

Yang, W. R., P. Thordarson, J. J. Gooding, S. P. Ringer, and F. Braet. 2007. Carbon nanotubes for biological and biomedical applications. *Nanotechnology* 18: -.

Yin, A., M. Tzolov, D. Cardimona, L. Guo, and J. Xu. 2007a. Fabrication of highly ordered anodic aluminium oxide templates on silicon substrates. *Iet Circuits Devices & Systems* 1: 205-209.

Yin, H. Y., F. L. Wang, A. L. Wang, J. Cheng, and Y. X. Zhou. 2007b. Bioelectrical impedance assay to monitor changes in aspirin-treated human colon cancer HT-29 cell shape during apoptosis. *Analytical Letters* 40: 85-94.

Zhang, K. I., H. Y. Ma, L. P. Zhang, and Y. Z. Zhang. 2008. Fabrication of a Sensitive Impedance Biosensor of DNA Hybridization Based on Gold Nanoparticles Modified Gold Electrode. *Electroanalysis* 20: 2127-2133.

Zhang, W., T. Yang, X. Li, D. B. Wang, and K. Jiao. 2009. Conductive architecture of Fe2O3 microspheres/self-doped polyaniline nanofibers on carbon ionic liquid electrode for impedance sensing of DNA hybridization. *Biosensors & Bioelectronics* 25: 428-434.

List of Publications

Journal Papers (Total 7, First Author 3/7, Second Author 1/7, Third Author 3/7) :

1. **Yu JJ**, Liu ZB, Yang M*, Mak, A.F.T., "Nanoporous Membrane based Cell Chip for the Study of Anti-Cancer Drug Effect of Retinoic Acid with Impedance Spectroscopy," Talanta, 80(1), 189-194 (2009) (IF: 3.374).

2. **Yu JJ**, Liu ZB, Liu QJ, Wang P, Yang M*, and Polly Leung and., "A Polyethylene glycol (PEG) Microfluidic Chip with Nanostructures for Bacteria Rapid Patterning and Detection." Sensors and Actuators A-Physical ， 154(2), 288-294 (2009) (IF: 1.434).

3. **Yu JJ,** Jha KS, Xiao LD, Liu QJ, Wang P, S C, Yang M*, "AlGaN/GaN Heterostructures for Non-Invasive Cell Electrophysiological Measurements", Biosensors and Bioelectronics, 23, 513-519 (2007) (IF: 5.061).

4. Liu QJ, **Yu JJ**, Xiao LD, Tang J. C. O. Zhang Y, Wang, P., Yang M*. "Impedance studies of bio-behavior and chemosensitivity of cancer cells by micro-electrode arrays," Biosens Bioelectron 24(5), 1305-1310. (2009) (IF: 5.061).

5. Yan. F., Mok. S. M., **Yu JJ**., Chan, Helen L.W., Choy, C.L. Yang M*, “Label-free DNA sensor based on organic thin film transistor”, Biosens Bioelectron (In revision) (IF: 5.061**).**

6. Liu ZB., Zhang Y., **Yu JJ.**, Mak AFT., Li Y., Yang M*., “A microfluidic chip with poly(ethylene glycol) hydrogel microarray on nanoporous alumina membrane for cell patterning and drug testing” : Sensors And Actuators B-Chemical, 143(2), 776-783. (2010)(IF:3.083).

7. Lin P, Yan F, **Yu JJ**, Chan H.L.W, Yang M*, “The application of organic electrochemical transistors in cell-based biosensors” (Accepted), Advanced materials, (IF: 8.191).

Conference Proceedings (Total 9, First Author 4/9, Second Author 4/9, Third Author 1/9) :

1. **Yu JJ**, Liu QJ, Xiao LD and Yang M " Micro Chip with Nanostructured Membranes for Anti Cancer Drug Screening using Impedance Spectroscopy," Proceedings of 10th World Congress on Biosensors, Shanghai, China, May 14-16, 2008.

2. **Yu JJ**, Liu QJ, Xiao LD and Yang M "A PDMS Microfluidic chip with Nanostructures for Bacteria Concentration and Fast Detection," Proceeding of the 21st IEEE International Conference on Micro Electro Mechanical Systems (MEMS '08), Tucson, Arizona, USA, January 13-17, 2008.

3. **Yu JJ**, Liu QJ, Xiao LD and Yang M "Micro Chip with Nanostructured Membranes for Cell Morphology Monitoring," Proceedings of 7th International Conference on Nanotechnology, Hong Kong., Page 304-307, August 2-5, 2007.

4. **Yu JJ**, Liu QJ, Xiao LD and Yang M "Nanostructured biomedical micro cell chip with impedance spectroscopy for anti-cancer drug screening," World Congress on Bioengineering 2007 Bangkok, THAILAND

5. Liu QJ, **Yu JJ**, Liu ZB, Zhang W, Wang P and Yang M, "Impedance Monitoring of Behaviour and Chemosensitivity of Cancer Cells by Micro-electrode Arrays,"

IFMBE Proceedings, 7th Asian-Pacific Conference on Medical and Biological Engineering, vol. 19, pp. 309-312, 2008.

6. Liu QJ, **Yu JJ**, Yu H, Xiao LD, Wang P and Yang M, "A Novel Taste Sensor Based on Ion Channels Incorporated in Nano-lipid Bilayer Membranes,"IFMBE Proceedings, 7th Asian-Pacific Conference on Medical and Biological Engineering, vol. 19, 306-308, 2008.

7. Liu QJ, **Yu JJ**, and Yang M, "Impedance Monitoring of Behavior and Chemosensitivity of Cancer Cells by Micro-electrode Arrays," Proceedings of 10th World Congress on Biosensors, Shanghai, China, May 14-16, 2008.

8. Xiao LD, **Yu JJ,** and Yang M "Integration of Insulator-based Dielectrophoresis manipulator with planar patch clamp on a single PDMS substrate" World Congress on Bioengineering 2007 Bangkok, THAILAND

9. Xu BJ, Liu ZB, **Yu JJ**, Lee, YK, and Yang M, "A PDMS planar patch-clamp array chip with Poly(Ethylene Glycol)/SU-8 cell-patch interface", Proceeding of the 22nd IEEE International Conference on Micro Electro Mechanical Systems (MEMS '09), Sorrento, Italy, January 25-29, 2009.